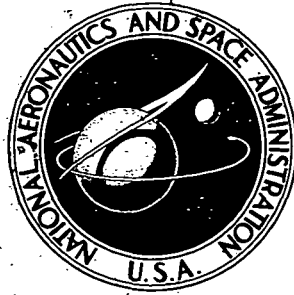


**NASA CONTRACTOR
REPORT**



NASA CR-2202

NASA CR-2202

**EVALUATION OF EFFECTIVENESS
OF VARIOUS DEVICES FOR ATTENUATION
OF TRAILING VORTICES BASED ON
MODEL TESTS IN A LARGE TOWING BASIN**

*by Karl L. Kirkman, Clinton E. Brown,
and Alex Goodman*

Prepared by

HYDRONAUTICS, Inc.

Laurel, Md. 20810

for Langley Research Center

NATIONAL AERONAUTICS AND SPACE ADMINISTRATION • WASHINGTON, D. C. • DECEMBER 1973

1. Report No. NASA CR-2202	2. Government Accession No.	3. Recipient's Catalog No.	
4. Title and Subtitle Evaluation of Effectiveness of Various Devices for Attenuation of Trailing Vortices Based on Model Tests in a Large Towing Basin		5. Report Date December 1973	
		6. Performing Organization Code	
7. Author(s) Karl L. Kirkman, Clinton E. Brown, and Alex Goodman		8. Performing Organization Report No.	
		10. Work Unit No.	
9. Performing Organization Name and Address HYDRONAUTICS, Incorporated 7210 Pindell School Road Laurel, Maryland 20810		11. Contract or Grant No. NAS1-11389	
		13. Type of Report and Period Covered Contractor Report	
12. Sponsoring Agency Name and Address National Aeronautics and Space Administration Washington, D.C. 20546		14. Sponsoring Agency Code	
		15. Supplementary Notes This is a final report.	
16. Abstract The effectiveness of various candidate aircraft-wing devices for attenuation of trailing vortices generated by large aircraft is evaluated on basis of results of experiments conducted with a 0.03-scale model of a Boeing 747 transport aircraft using a technique developed at the HYDRONAUTICS Ship Model Basin. Emphasis is on the effects produced by these devices in the far-field (up to 8 kilometers downstream of full-scale generating aircraft) where the unaltered vortex wakes could still be hazardous to small following aircraft. The evaluation is based primarily on quantitative measurements of the respective vortex velocity distributions made by means of hot-film probe traverses in a transverse plane at selected stations downstream. The effects of these altered wakes on rolling moment induced on a small following aircraft are also studied using a modified lifting-surface theory with a synthesized Gates Learjet as a typical example. Lift and drag measurements concurrently obtained in the model tests are used to appraise the effects of each device investigated on the performance characteristics of the generating aircraft			
17. Key Words (Suggested by Author(s)) Trailing Vortices Vortex Velocities Vortex Attenuation Induced Rolling Moments		18. Distribution Statement Distribution of this report is provided in the interest of information exchange. Responsibility for the contents resides in the author or organization that prepared it.	
19. Security Classif. (of this report) Unclassified	20. Security Classif. (of this page) Unclassified	21. No. of Pages 115	22. Price* Domestic, \$4.25 Foreign, \$6.75

TABLE OF CONTENTS

	Page
SUMMARY.....	1
INTRODUCTION.....	1
DESCRIPTION OF BASIC AIRCRAFT AND MODEL.....	3
DESCRIPTION OF VORTEX-ATTENUATION DEVICES.....	7
Active Devices.....	7
Passive Devices.....	16
TEST PROGRAM AND PROCEDURES.....	22
REDUCTION AND PRESENTATION OF DATA.....	25
DISCUSSION OF RESULTS.....	33
Effect on Vortex Velocity.....	34
Effect on Performance of Generating Aircraft.....	36
CONCLUSIONS.....	42
APPENDIX A - DISCUSSION OF SCALING LAWS PERTINENT TO EXPERIMENTS.....	43
APPENDIX B - DESCRIPTION OF FACILITIES AND TEST APPARATUS.....	49
APPENDIX C - TEST DATA SHOWING EFFECTIVENESS OF VORTEX- ATTENUATION DEVICES ON BOEING 747 AIRCRAFT IN CRUISE CONDITION.....	65
APPENDIX D - TEST DATA SHOWING EFFECTIVENESS OF VORTEX- ATTENUATION DEVICES ON BOEING 747 AIRCRAFT IN FLAPS-30 CONDITION.....	79
APPENDIX E - TYPICAL TIME-HISTORY RECORDS OF HOT-FILM VELOCITY MEASUREMENTS FROM TESTS WITH VARIOUS VORTEX-ATTENUATION DEVICES.....	85
APPENDIX F - CALCULATED ROLLING MOMENTS AND ROLLING VELOCITIES INDUCED ON A SMALL FOLLOWING AIRCRAFT BY ALTERED TRAILING VORTICES.....	91
REFERENCES.....	103

LIST OF FIGURES

		Page
Figure 1 -	Basic Model of Boeing 747 Aircraft.....	5
Figure 2 -	Leading Edge Devices and Flaps for Flaps-30 Configuration.....	6
Figure 3 -	Sketch and Close-Up Views Showing Device A (Forward Blowing Jet) on Wing Tip.....	10
Figure 4 -	Sketch and Close-Up Views Showing Device B (Downward Blowing Jet) on Wing Tip.....	11
Figure 5 -	Sketch and Close-Up Views Showing Device C (Rearward Blowing Jet) on Wing Tip.....	12
Figure 6 -	Sketch and Close-Up Views Showing Device D (Deflected Jet) on Wing Tip.....	13
Figure 7 -	Sketch and Close-Up Views Showing Device E (Jet Flap) on Wing Tip.....	14
Figure 8 -	Sketch and Close-Up Views Showing Device F (Blown Flap) on Wing Tip.....	15
Figure 9 -	Sketch and Close-Up View Showing Device G (Cabled Drogue Cone) and Its Location Relative to Wing.....	17
Figure 10 -	Sketch and Close-Up View Showing Devices H-1, H-2, and H-3 (Splines) with Wing Tip Mounting Sting.....	18
Figure 11 -	Sketch and Close-Up Views Showing Device I (Vortex Generator) on Wing Tip.....	19
Figure 12 -	Sketch and Close-Up Views Showing Device J (Spoiler Dissipator) on Wing Tip.....	20
Figure 13 -	Sketch and Close-Up Views Showing Device K (Trailing Edge Flap) on Wing Tip.....	21

	Page
Figure 14 - Typical Time-Sequence Photographs of Trailing Vortices from Basic Aircraft at Cruise Condition.....	26
Figure 15 - Typical Trajectory of Vortex Pair for Basic Aircraft in Cruise Mode Derived from Time-Sequence Photographs.....	27
Figure 16 - Sketches Showing Interpretation of Velocity Data.....	28
Figure 17 - Sample Time Histories of Probe Output Voltage for Basic Aircraft in Cruise Configuration.....	31
Figure 18 - Sample Hot Film Anemometer Voltage-Velocity Calibration Curves.....	32
Figure 19 - Comparison of Effects of Active Vortex-Attenuation Devices on Downwash Velocity Distributions for Cruise Condition.....	35
Figure 20 - Comparison of Effects of Passive Vortex-Attenuation Devices on Downwash Velocity Distributions for Cruise Condition.....	37
Figure 21 - Lift, Drag, and Pitching Moment Coefficients for Basic Aircraft.....	38
APPENDIX B - DESCRIPTION OF FACILITIES AND TEST APPARATUS.....	49
Figure 22 - View of HYDRONAUTICS Ship Model Basin.....	52
Figure 23 - HSMB Towing Carriage with 747 Aircraft Model Installed for Testing.....	53
Figure 24 - Aircraft Model Support System	54
Figure 25 - Schematic Sketch of Force Measurement System.....	56
Figure 26 - Block Gage Assemblies in Model.....	56
Figure 27 - Close-Up of Block Gages.....	57

	Page
Figure 28 - Signal Conditioning and DVM Units.....	59
Figure 29 - Dye-Ejection Nozzles Installed on 747 Model.....	60
Figure 30 - Dye Tanks and Control Manifolds.....	61
Figure 31 - Cross Section of Test Area Showing Arrange- ment of Photographic Equipment.....	62
Figure 32 - Test Area with Insert Showing Close-Up View of Hot Film Anemometer Probes.....	63
APPENDIX C - TEST DATA SHOWING EFFECTIVENESS OF VORTEX- ATTENUATION DEVICES ON BOEING 747 AIRCRAFT IN CRUISE CONDITION.....	65
Figure 33 - Vortex Velocity Distribution for Basic Aircraft.....	67
Figure 34 - Effect of Device A (Forward Blowing Jet) on Vortex Velocity Distribution.....	68
Figure 35 - Effect of Device B (Downward Blowing Jet) on Vortex Velocity Distribution.....	69
Figure 36 - Effect of Device C (Rearward Blowing Jet) on Vortex Velocity Distribution.....	70
Figure 37 - Effect of Device D (Deflected Jet) on Vortex Velocity Distribution.....	71
Figure 38 - Effect of Device E (Jet Flap) on Vortex Velocity Distribution.....	72
Figure 39 - Effect of Device F (Blown Flap) on Vortex Velocity Distribution	73
Figure 40 - Effect of Device G (Cabled Drogue Cone) on Vortex Velocity Distribution.....	74
Figure 41 - Effect of Device H (Splines) on Vortex Velocity Distribution.....	75

Figure 42 -	Effect of Device I (Vortex Generator) on Vortex Velocity Distribution.....	76
Figure 43 -	Effect of Device J (Spoiler Dissipator) on Vortex Velocity Distribution.....	77
Figure 44 -	Effect of Device K (Trailing Edge Flap) on Vortex Velocity Distribution.....	78
APPENDIX D -	TEST DATA SHOWING EFFECTIVENESS OF VORTEX ATTENUATION DEVICES ON BOEING 747 AIRCRAFT IN FLAPS-30 CONDITION.....	79
Figure 45 -	Vortex Velocity Distribution for Basic Aircraft.....	81
Figure 46 -	Effect of Device H (Splines) on Vortex Velocity Distribution.....	82
Figure 47 -	Effect of Device I (Vortex Generator) on Vortex Velocity Distribution.....	83
Figure 48 -	Effect of Device J (Spoiler Dissipator) on Vortex Velocity Distribution.....	84
APPENDIX E -	TYPICAL TIME HISTORY RECORDS OF HOT-FILM VELOCITY MEASUREMENTS FROM TESTS WITH VARIOUS VORTEX-ATTENUATION DEVICES.....	85
Figure 49 -	Cruise Condition with Device A.....	87
Figure 50 -	Cruise Condition with Device B.....	87
Figure 51 -	Cruise Condition with Device C.....	87
Figure 52 -	Cruise Condition with Device D.....	88
Figure 53 -	Cruise Condition with Device E.....	88
Figure 54 -	Cruise Condition with Device F.....	88
Figure 55 -	Cruise Condition with Device G.....	89
Figure 56 -	Cruise Condition with Device H.....	89

	Page
Figure 57 - Cruise Condition with Device I.....	90
Figure 58 - Cruise Condition with Device J.....	90
Figure 59 - Cruise Condition with Device K.....	90
APPENDIX F - CALCULATED ROLLING MOMENTS AND ROLLING VELOCITIES INDUCED ON A SMALL FOLLOWING AIRCRAFT BY ALTERED TRAILING VORTICES.....	91
Figure 60 - Vortex Pattern, System of Axes, and Subscripts Used in Calculation of Span Loading by Modi- fied Lifting-Surface Method.....	94
Figure 61 - Orientation of Gates Learjet Wing and Dis- tribution of Downwash Velocities Used in Calculation.....	99
Figure 62 - Effects of Various Devices on the Calculated Induced Span Loading Coefficient for the Gates Learjet Wing.....	100

LIST OF TABLES

	Page
Table 1 - Principal Geometric Characteristics of Prototype and 0.03 - Scale Model of Boeing 747 Transport Aircraft.....	4
Table 2 - Designation and Classification of Vortex-Attenuation Devices.....	7
Table 3 - Jet Momentum Characteristics for Active Vortex-Attenuation Devices.....	9
Table 4 - Program of Test Runs Made with Basic Aircraft Model (Boeing 747) with and without Vortex-Attenuation Devices.....	23
Table 5 - Changes in Lift, Drag, and Pitching Moment Coefficients Due to Addition of Vortex-Attenuation Devices to Basic Aircraft in Cruise Condition.....	40
Table 6 - Changes in Lift, Drag, and Pitching Moment Coefficients Due to Addition of Vortex-Attenuation Devices to Basic Aircraft in Flaps-30 Condition.....	41
APPENDIX F - CALCULATED ROLLING MOMENTS AND ROLLING VELOCITIES INDUCED ON A SMALL FOLLOWING AIRCRAFT BY ALTERED TRAILING VORTICES.....	91
Table 7 - Principal Geometric Characteristics of Gates Learjet Used in Calculations to Represent Small Following Aircraft.....	98
Table 8 - Calculated Effects of Vortex Wakes of Generating Aircraft on Induced Rolling Moment and Rolling Velocity of Small Following Aircraft.....	101

Page Intentionally Left Blank

NOTATION

The results are presented in the form of standard NASA coefficients of forces and moments, which are referred in all cases to the body axes with the origin at the quarter-chord point of the mean aerodynamic chord. The coefficients and symbols used herein are defined as follows:

C_L	Lift coefficient (Lift/qS)
C_D	Drag coefficient (Drag/qS)
$(C_m)_{\bar{c}/4}$	Pitching-moment coefficient (pitching moment/qS \bar{c})
C_ℓ	Rolling-moment coefficient (Rolling moment/qSb)
D	Drag
X	Longitudinal force
Z	Normal force
$(M)_{\bar{c}/4}$	Pitching moment about $\bar{c}/4$
q	Dynamic pressure ($\frac{1}{2}\rho V^2$)
ρ	Mass density of medium
V	Free-stream velocity or towing speed
S	Wing area
S_j	Jet area
b	Span of wing, measured perpendicular to plane of symmetry
c	Chord of wing, measured parallel to plane of symmetry
\bar{c}	Mean aerodynamic chord $\left(\frac{2}{S} \int_0^{b/2} c^2 dy \right)$
A	Aspect ratio (b^2/S)
λ	Taper ratio (tip chord/root chord)
x_o, y_o	Coordinates of a point on the wing surface with respect to axes of a given horseshoe vortex
y	Spanwise distance
y_c	Lateral distance of vortex core from plane of symmetry

N	Number of horseshoe vortices across total wing span (b/2s)
s	Semiwidth of horseshoe vortex
w(x,y)	Downwash velocity at any point (x,y) in the plane of a horseshoe vortex, positive downward
F(x,y)	Downwash velocity at any point (x,y) caused by a rectangular horseshoe vortex of unit semiwidth and circulation strength equal to 4π
Γ	Circulation strength
$\Gamma' = \frac{2\Gamma}{bV}$	
c_l	Section lift coefficient ($2\Gamma/Vc$)
a_o	Section lift-curve slope ($dc_l/d\alpha$)
α	Angle of attack, radians
δa	Aileron deflection, degrees
Λ	Angle of sweep, degrees
$pb/2V$	Wing-tip helix angle, radians
p	Rolling angular velocity, radians per second
$C_{L\alpha} = \frac{\partial c_L}{\partial \alpha}$	Lift curve slope, per degree
$C_{l_{\delta a}} = \frac{\partial c_l}{\partial \delta a}$	Aileron effectiveness, per radian
$C_{l_p} = \frac{\partial c_l}{\partial \frac{pb}{2V}}$	Damping in roll, per radian

Subscripts and abbreviations:

n	Number designating a particular horseshoe vortex; starting from left wing tip
LE	Leading edge
TE	Trailing edge
i	Inboard
o	Outboard
m	Model
fs	Full scale

EVALUATION OF EFFECTIVENESS
OF VARIOUS DEVICES FOR
ATTENUATION OF TRAILING VORTICES
BASED ON MODEL TESTS IN
A LARGE TOWING BASIN

By Karl L. Kirkman, Clinton E. Brown
and Alex Goodman
HYDRONAUTICS, Incorporated

SUMMARY

The effectiveness of various candidate aircraft-wing devices for attenuation of trailing vortices generated by large aircraft is evaluated on basis of results of experiments conducted with a 0.03-scale model of a Boeing 747 transport aircraft using a technique developed at the HYDRONAUTICS Ship Model Basin. Emphasis is on the effects produced by these devices in the far-field (up to 8 kilometers downstream of full-scale generating aircraft) where the unaltered vortex wakes could still be hazardous to small following aircraft. The evaluation is based primarily on quantitative measurements of the respective vortex velocity distributions made by means of hot-film probe traverses in a transverse plane at selected stations downstream. The effects of these altered wakes on rolling moment induced on a small following aircraft are also studied using a modified lifting-surface theory with a synthesized Gates Learjet as a typical example. Lift and drag measurements concurrently obtained in the model tests are used to appraise the effects of each device investigated on the performance characteristics of the generating aircraft.

INTRODUCTION

A comprehensive program was conducted to investigate the feasibility of various auxiliary devices proposed for installation on the wings of large aircraft. The primary objective of this program was to evaluate the effectiveness of these devices from the standpoint of their ability to attenuate the trailing vortices in the "far field" where the vortices could still produce hazardous effects when encountered by smaller aircraft. As an integral part of the evaluation, it was considered necessary also to determine the extent to which each of the proposed devices would affect the performance characteristics (lift, drag and pitching moment) of the generating aircraft.

The problem of trailing vortices generated by large aircraft, and their associated adverse effects on following aircraft, has been the subject of growing concern in recent years. The problem has become particularly acute because of the abundance of large commercial transport planes such as the Boeing 747 which are currently operating in and out of airports that must be shared with numerous smaller aircraft.

Due to the urgency of the problem a considerable effort has been devoted to theoretical (Refs. 1 and 2) and experimental studies of the growth and decay of trailing vortex systems as well as means for speeding up the decay of such systems. The earliest experimental studies along these lines were based either on full-scale flight tests or wind-tunnel tests on scale models (Refs. 3,4,5, and 6). The use of full-scale flight tests to obtain measurements of vortex decay in presence of atmospheric turbulence and ground-wing boundary layer constitutes a difficult task due to the vagaries of nature. This is further complicated by the difficulty of obtaining the repeatable conditions required for a systematic study. Unfortunately, the existing large wind-tunnel facilities cannot be used for this purpose owing to the great distances behind the generating aircraft required to permit vortex development, decay, and breakup. Thus, vortex-attenuation devices shown by recent wind-tunnel experiments to cause marked modifications to the vortex pattern near the wing tip (Refs. 7,8,9,10) still remain to be properly evaluated on basis of their effects on the trailing vortex system far downstream in the area of primary interest.

In view of the foregoing, NASA Langley Research Center sponsored a program to develop experimental techniques involving the use of a large towing basin that would permit the detailed study of trailing vortex wakes at far distances behind aircraft. As a result, the capability for performing the desired studies with large models (relatively high Reynolds numbers) at simulated distances behind aircraft of up to about 8 kilometers was developed at the HYDRONAUTICS Ship Model Basin (Ref. 11).

To fulfill the specific objectives of the present investigation, runs using the techniques of Reference 11, were made first for the basic aircraft, represented by the existing 0.03-scale model of the Boeing 747 transport aircraft, and then with each of several vortex-attenuation devices installed on the model wings. Measurements were taken to determine the vortex velocity distributions at selected far-field distances downstream as well as the lift and drag characteristics of the aircraft (both without and with the devices installed). A total of eleven different vortex-attenuation devices were investigated.

This report describes the basic aircraft model and models of the various vortex-attenuation devices investigated; outlines the program and procedures used in the tests; explains the methods used to reduce and analyze the data; presents and discusses the results of the investigation in terms of the effects of the vortex attenuation devices on magnitude and distribution of vortex velocity and on the performance characteristics of the generating aircraft; compares the experimentally determined vortex velocity distribution for the basic aircraft with that obtained from existing theory; and draws conclusions concerning the various findings of the investigation. Detailed information is presented in the appendixes including: a discussion of the scaling laws pertinent to the modeling technique used; a description of the facilities, test apparatus, and instrumentation employed; test data for the various conditions investigated; and calculations of induced rolling moments and rolling velocities based on a modified lifting-surface method.

DESCRIPTION OF BASIC AIRCRAFT AND MODEL

The Boeing 747 Transport Aircraft, a 0.03-scale model of which was available as the result of the investigation of Reference 11, was used as the basic aircraft for purposes of the subject experimental program. The principal geometric characteristics of the basic aircraft are presented in terms of prototype and model dimensions in Table 1.

The basic model was built by the Boeing Company using existing wind-tunnel model molds. It is of composite aluminum, stainless steel, and plastic construction designed for a maximum measured lift force of 1800 kilograms. Included internally were mounting plates and dye tubes which were constructed to be compatible with the model support, force measurement, and flow visualization systems described in Appendix B. The orifices of the dye tubes were located at the wing tips, the outboard engine nacelles and at two intermediate spanwise stations at the trailing edge of each wing. As is the usual practice for Boeing wind-tunnel models, the Flaps-30 configuration does not simulate exactly the corresponding full-scale arrangement. For simplicity, the trailing edge flaps are appended to the complete wing rather than the integral double-slotted movable flap arrangement used on the actual aircraft.

Figure 1 shows the basic model in a configuration representing the Cruise Condition and Figure 2 shows the leading edge devices and flaps which are attached to the model to represent the Flaps-30 Condition.

TABLE 1

Principal Geometric Characteristics of Prototype and
0.03-Scale Model of Boeing 747 Transport Aircraft

	Prototype	Model
Wing		
Span, m	59.64	1.79
Mean aerodynamic chord, m	8.32	0.25
Root chord, m	16.6	0.497
Tip chord, m	4.05	0.121
Sweepback at quarter chord, deg	37.5	37.5
Area, m ²	511.0	0.460
Aspect ratio	6.96	6.96
Fuselage		
Length, m	68.64	2.06
Tailplane		
Span, m	22.19	0.664
Area, m ²	136.6	0.123
Aspect ratio	3.6	3.6
<p>Note: For other physical characteristics see "Janes All the World's Aircraft 1971-72", pp. 260-262.</p>		

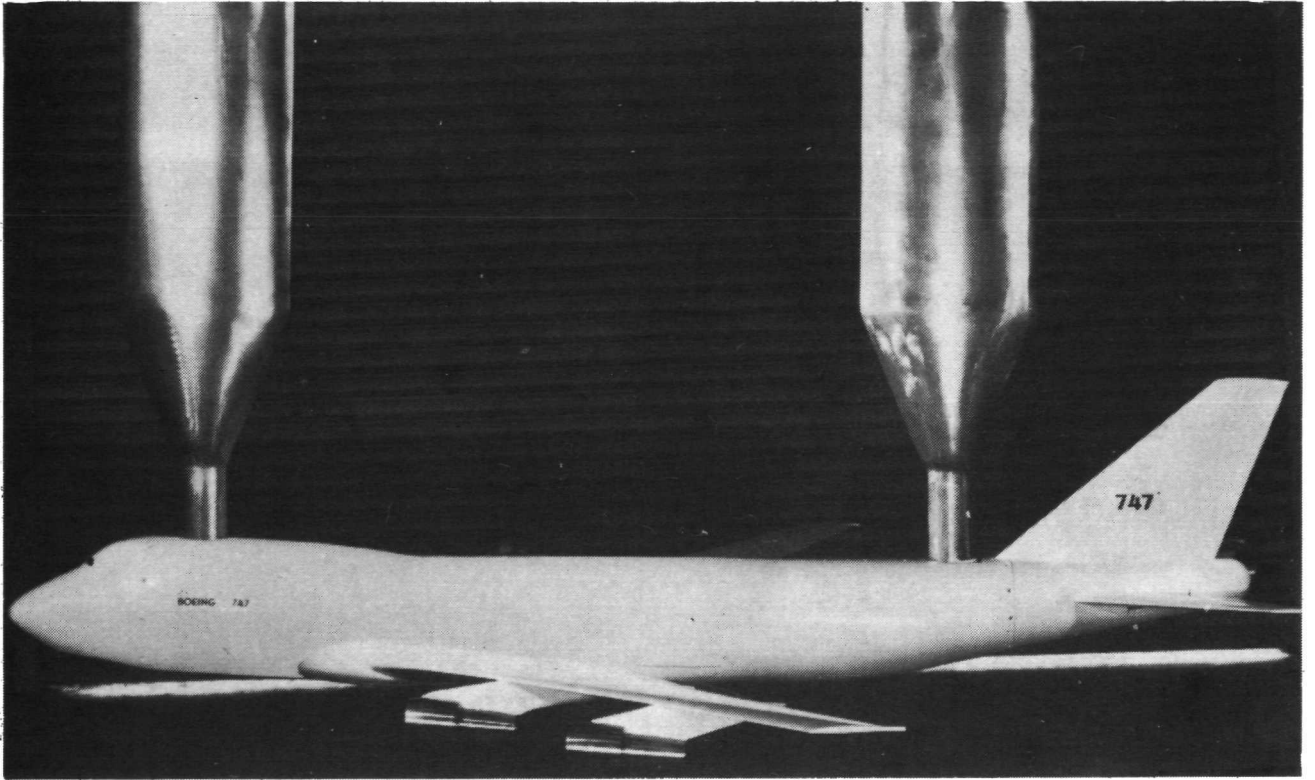
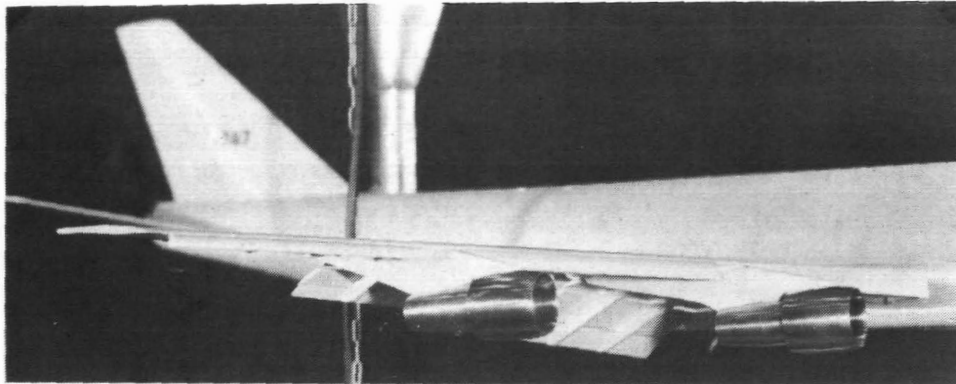
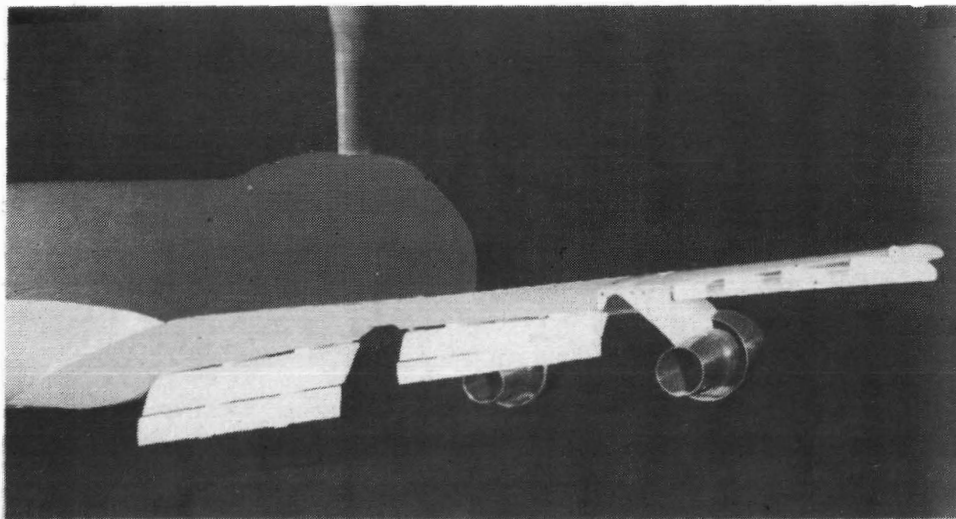


FIGURE 1 - BASIC MODEL OF BOEING 747 AIRCRAFT



LEADING EDGE DEVICES



FLAPS

FIGURE 2 - LEADING EDGE DEVICES AND FLAPS FOR FLAPS-30 CONFIGURATION

DESCRIPTION OF VORTEX-ATTENUATION DEVICES

The various vortex-attenuation devices which were evaluated in conjunction with the basic aircraft in the present program are listed and identified in Table 2. The devices are classified into two general categories "Active" and "Passive" and are described separately in the following sections.

TABLE 2

Designations of Vortex-Attenuation Devices

Designation	Description	Classification	Fig. No.
A	Forward Blowing Jet	Active	3
B	Downward Blowing Jet	Active	4
C	Rearward Blowing Jet	Active	5
D	Deflected Jet	Active	6
E	Jet Flap	Active	7
F	Blown Flap	Active	8
G	Cabled Drogue Cone	Passive	9
H	Spline	Passive	10
I	Vortex Generator	Passive	11
J	Spoiler Dissipator	Passive	12
K	Trailing Edge Flap	Passive	13

Note: H-1, H-2, and H-3 denote model splines of 10.16-, 15.24-, and 20.32-cm diameter, respectively.

Active Devices

All of the active vortex-attenuation devices involved variations of a blowing jet which was intended to directly diffuse the tip vortex or to provide a change in local angle of attack close to the wing tip. Conceptually, it was assumed for each of these devices that the necessary flow would be provided by air bled from a propulsion engine. In the model experiments, however, these devices were simulated by using water jets to provide the same fluid

density as the "atmosphere" which also was being represented by the water in the towing basin. Table 3 lists the jet momentum characteristics that were simulated in the experiments along with the water jet velocity and jet area for each model of the active devices investigated. The models of the individual active devices are shown both by photographs and sketches in Figures 3 through 8, and are briefly described as follows:

Forward blowing jet (Device A). - Figure 3 shows the details and arrangement of Device A mounted on the leading edge and near the wing tip of the basic aircraft model. The jet passage was faired into the wing tip with epoxy cement and connected (through the wing, fuselage and support struts) to an external water supply system mounted on the towing carriage. The supply system was pressurized and could be controlled to provide a range of constant flow rates to the jet.

Downward blowing jet (Device B). - Figure 4 shows Device B installed in the underside of the wing tip of the basic aircraft model. The fluid passes through a narrow slit to form a jet sheet which is directed downward. The supply system is the same as that used for Device A.

Rearward blowing jet (Device C). - Figure 5 shows the arrangement of Device C mounted on the trailing edge and near the wing tip of the basic aircraft model. The jet is supplied through a tube in the same manner as for Device A.

Deflected jet (Device D). - Figure 6 shows the details and arrangement of Device D. This device was intended to represent a rudimentary jet flap with the expectation that further exploration of refined versions of the jet flap concept would be made later. The device was formed by adding a nozzle (with a rectangular orifice) to Device C.

Jet flap (Device E). - Figure 7 shows Device E installed near the trailing edge of the wing tip of the basic aircraft model. This device is a more refined version of the jet flap concept which was investigated after the preliminary tests with Device D had shown promising results. The jet flap is formed by a rectangular slit which was machined to direct the jet upward at an angle of 70 degrees to the chordline at the wing tip. The supply system used for the jet is the same as that used for Device A.

TABLE 3

Jet Momentum Characteristics for Active
Vortex-Attenuation Devices

Device	Model Jet Velocity V_j , m per sec	Model Jet Area S_j , m^2	Momentum Coefficient C_μ
Forward Blowing Jet	7.3	2.87×10^{-5}	4.60×10^{-4}
Downward Blowing Jet	6.7	1.29×10^{-5}	1.74×10^{-4}
Rearward Blowing Jet	10.4	1.66×10^{-5}	8.36×10^{-4}
Deflected Jet	10.7	1.30×10^{-5}	4.43×10^{-4}
Jet Flap	9.9	1.68×10^{-5}	4.94×10^{-4}
Blown Flap	9.9	1.68×10^{-5}	4.94×10^{-4}

where

$$C_\mu = \frac{\rho_j V_j^2 S_j}{\frac{1}{2} \rho V^2 S}$$

- C_μ is the jet momentum coefficient,
 ρ_j is the mass density of jet fluid,
 V_j is the jet velocity,
 S_j is the jet area,
 ρ is the mass density of medium,
 V is the forward velocity, and
 S is the wing area.

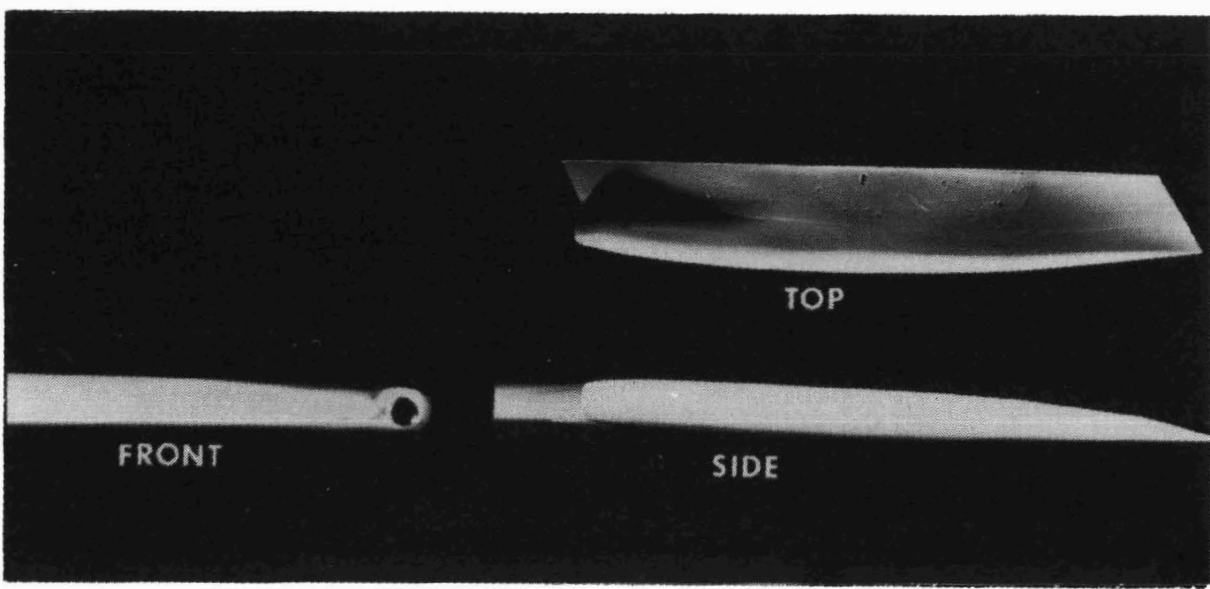
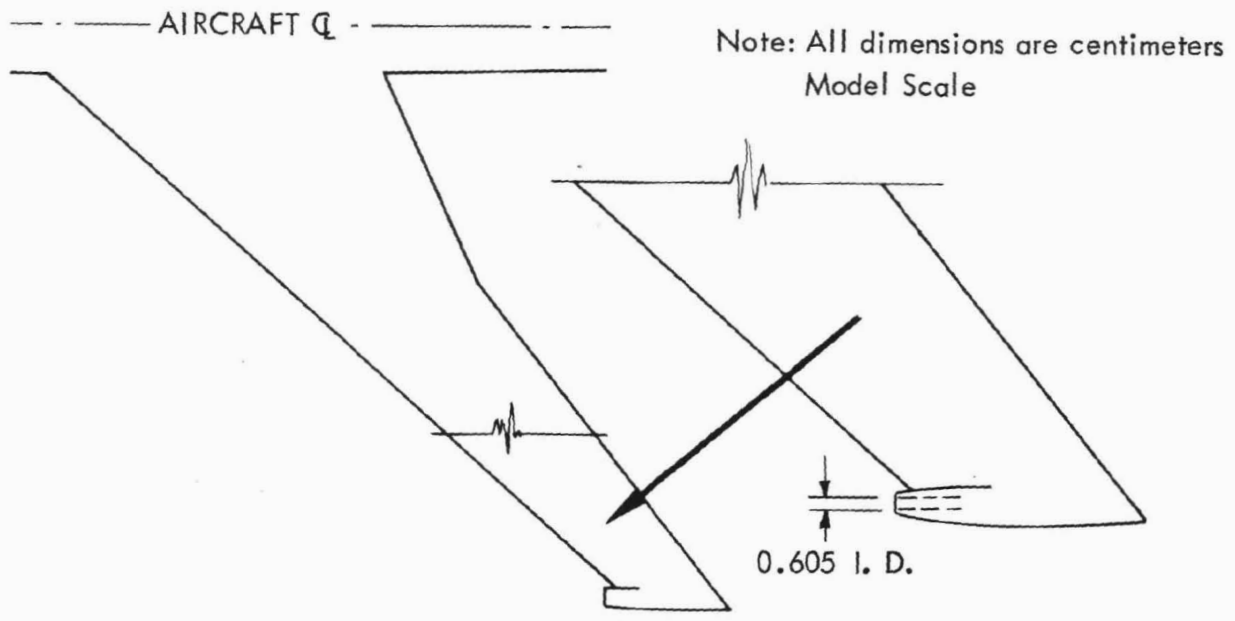


FIGURE 3 - SKETCH AND CLOSE-UP VIEWS SHOWING DEVICE A (FORWARD BLOWING JET) ON WING TIP

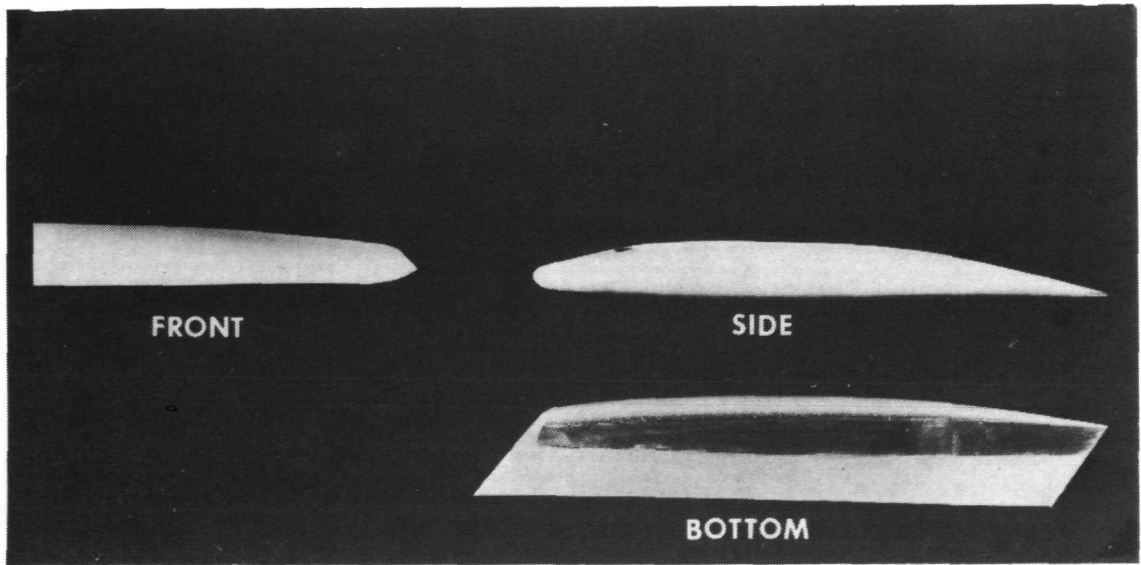
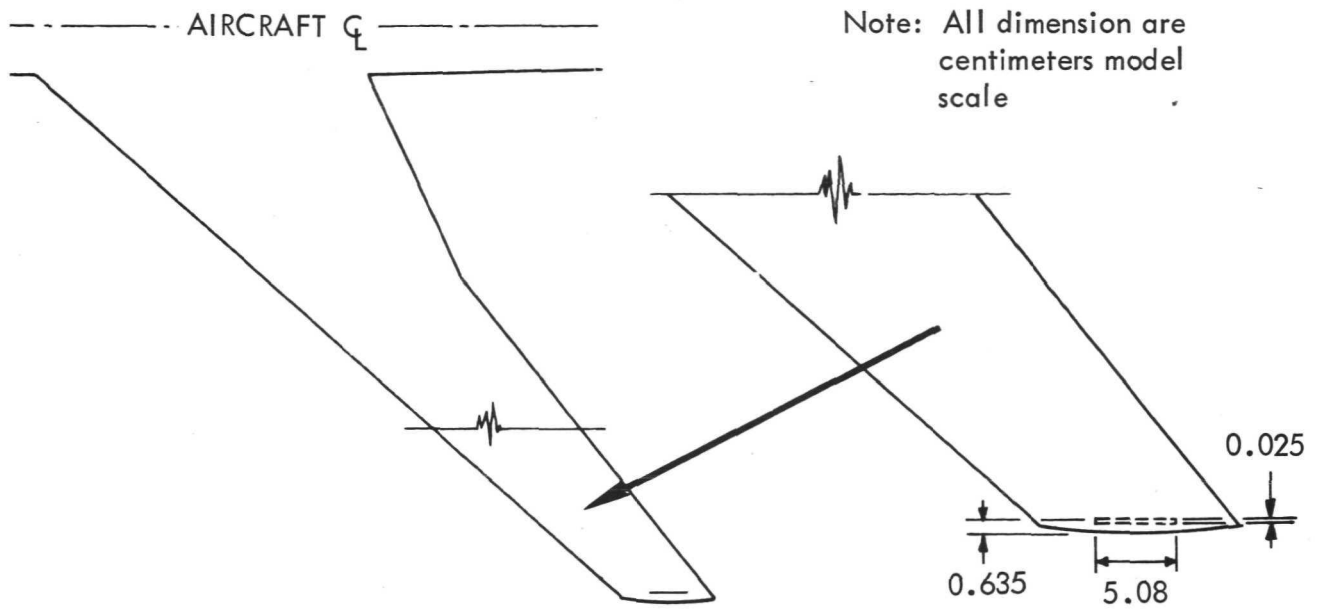


FIGURE 4 - SKETCH AND CLOSE-UP VIEWS SHOWING DEVICE B (DOWNWARD BLOWING JET) ON WING TIP

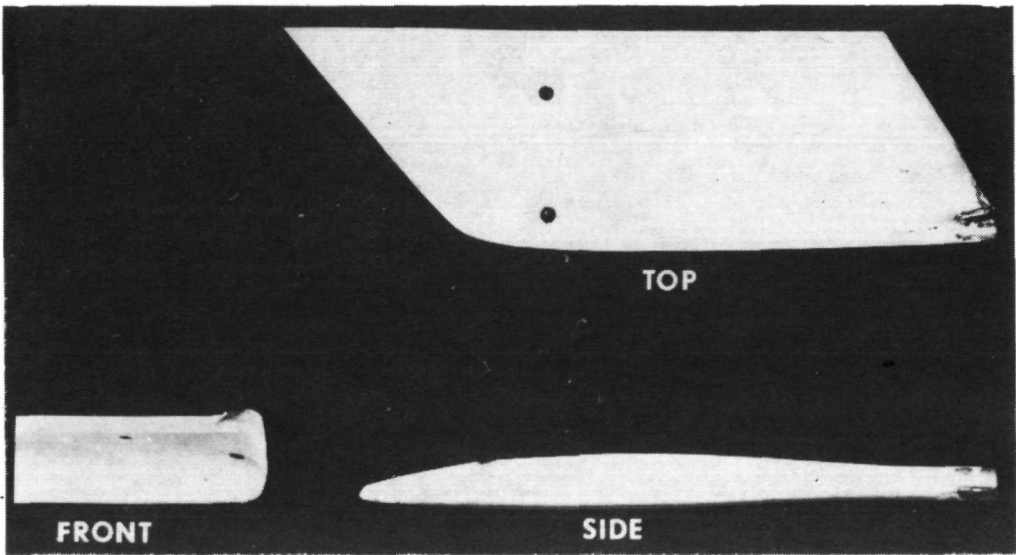
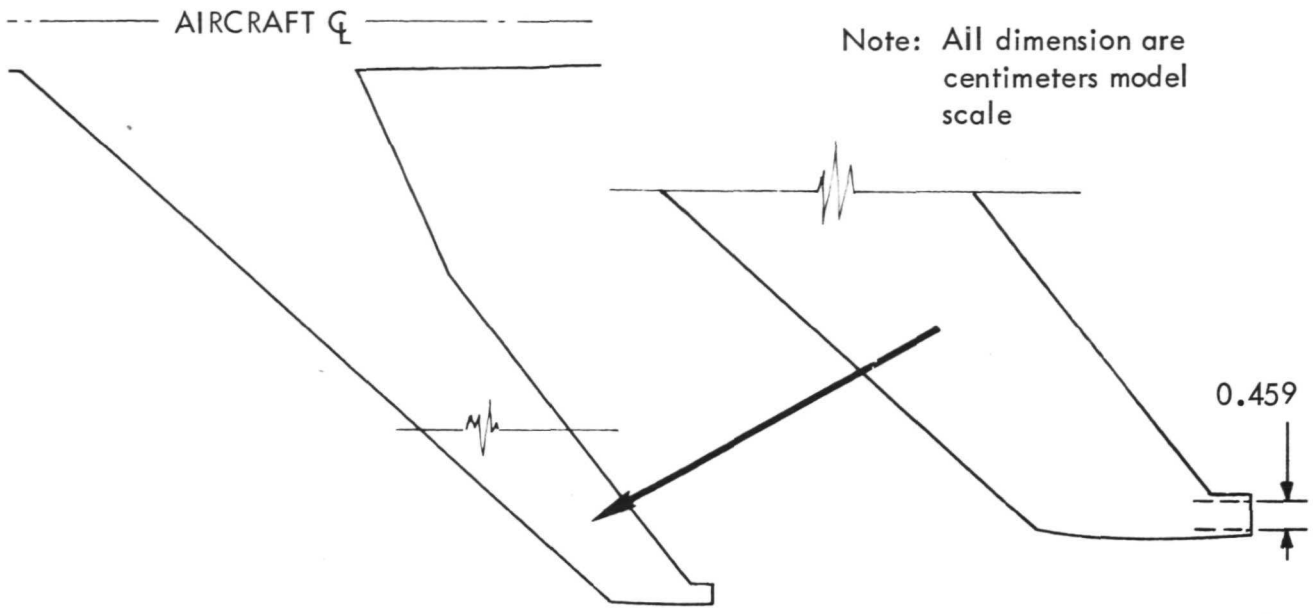


FIGURE 5 - SKETCH AND CLOSE-UP VIEWS SHOWING DEVICE C (REARWARD BLOWING JET) ON WING TIP

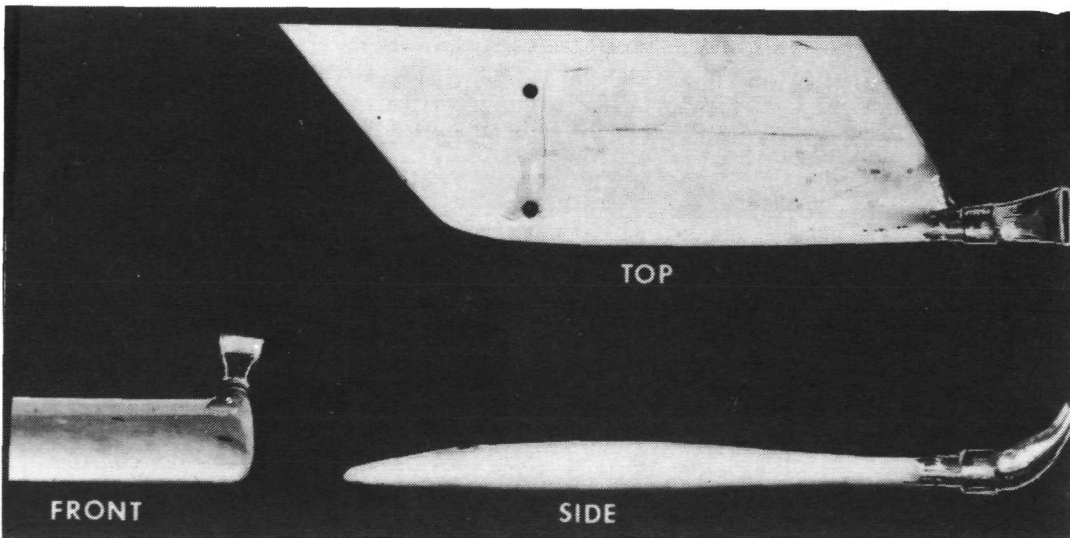
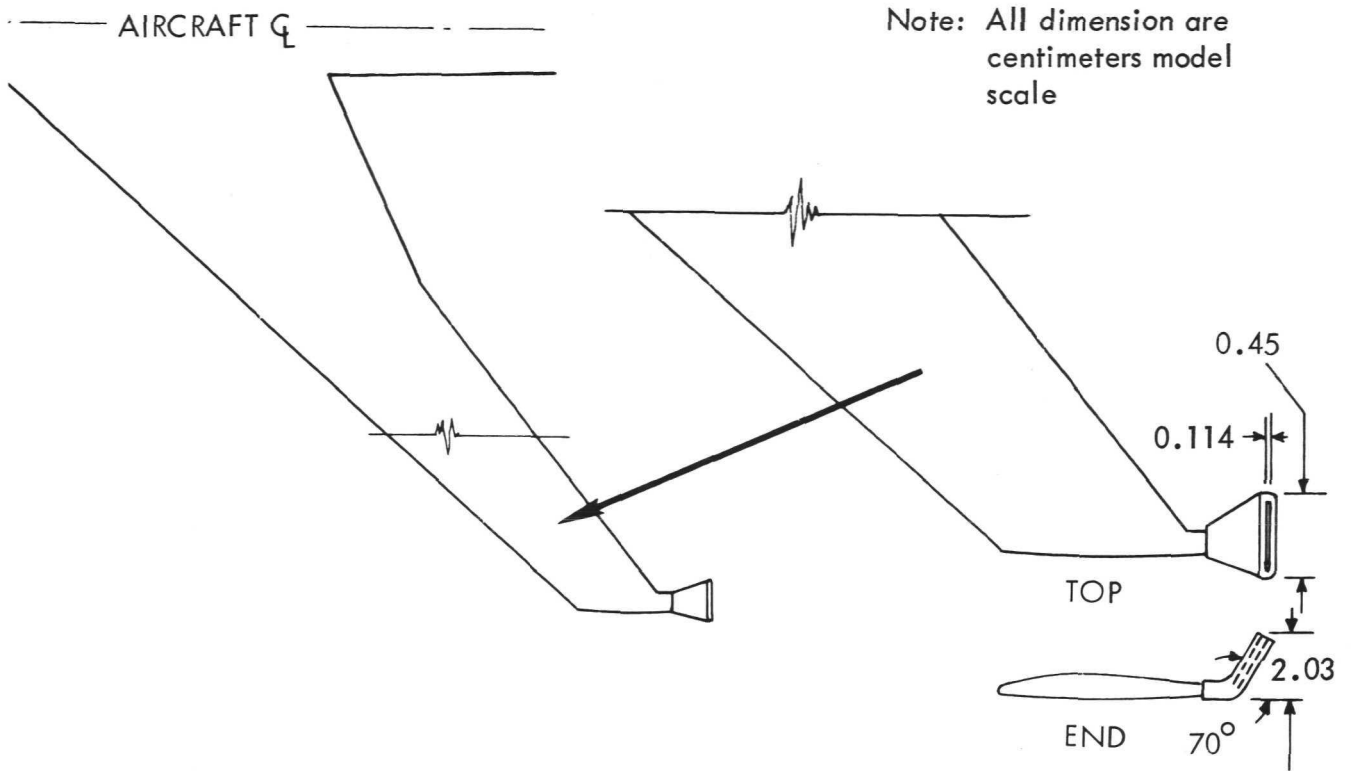
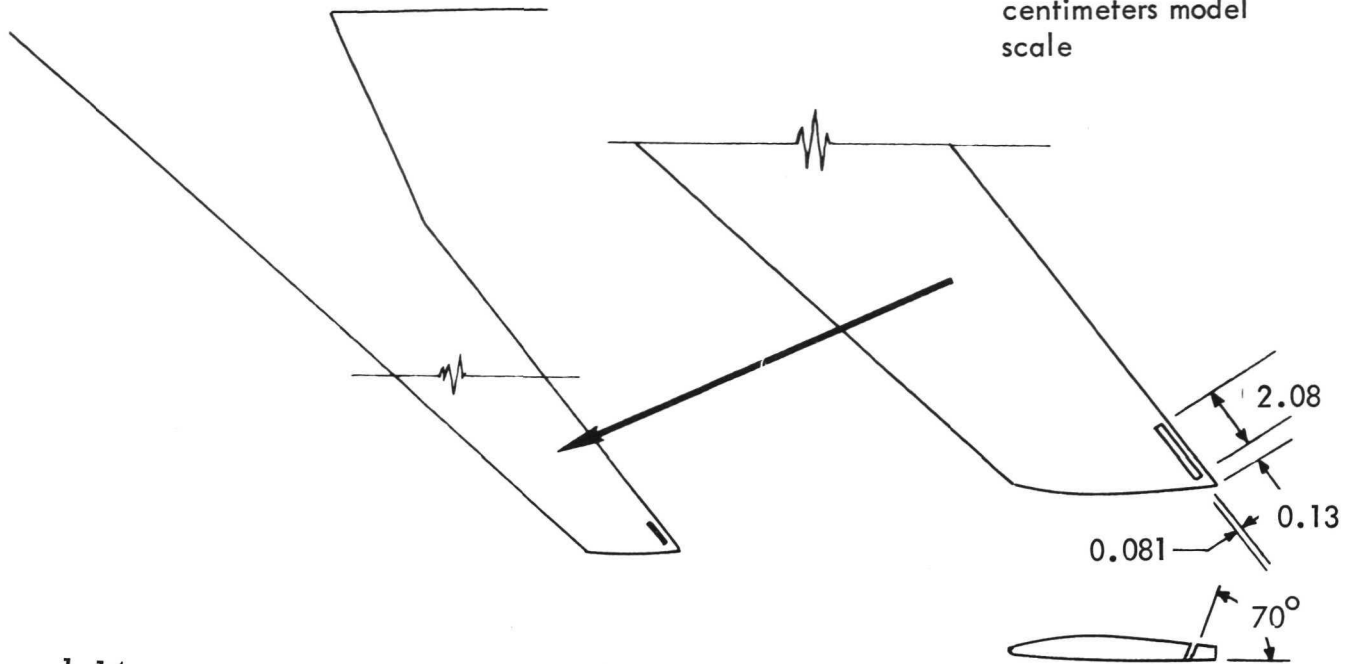


FIGURE 6 - SKETCH AND CLOSE-UP VIEWS SHOWING DEVICE D (DEFLECTED JET) ON WING TIP

AIRCRAFT ζ - - - - -

Note: All dimension are centimeters model scale



1.14

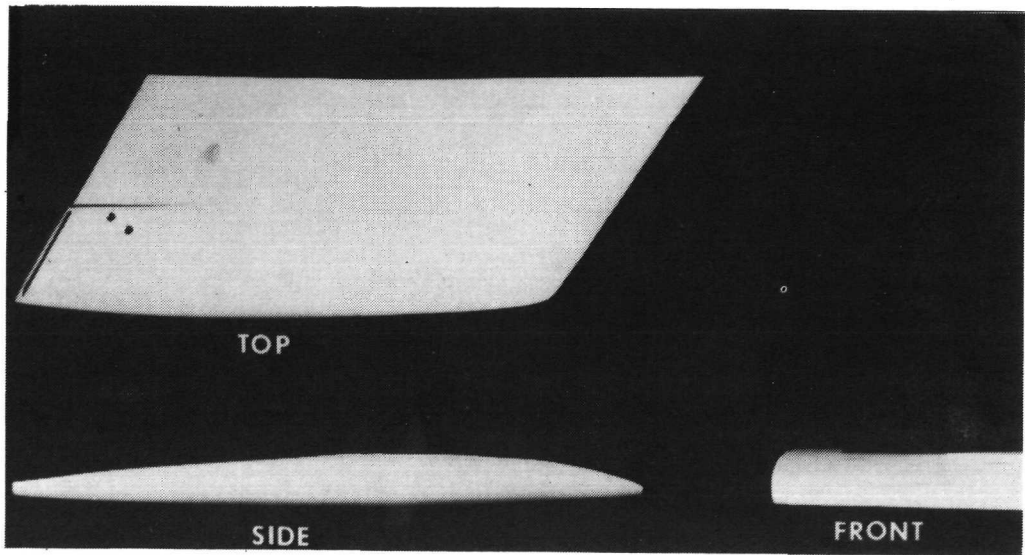


FIGURE 7 - SKETCH CLOSE-UP VIEWS SHOWING DEVICE E (JET FLAP) ON WING TIP

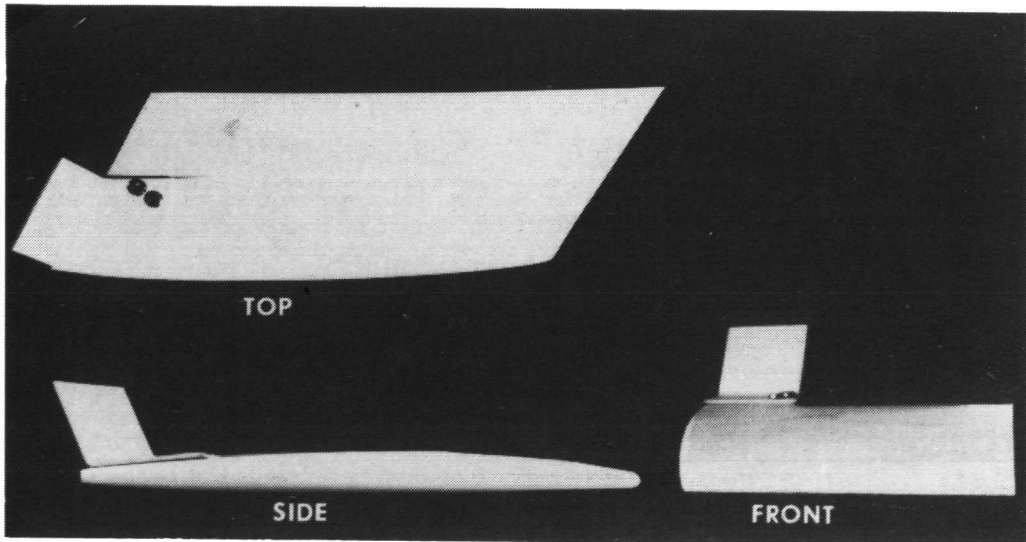
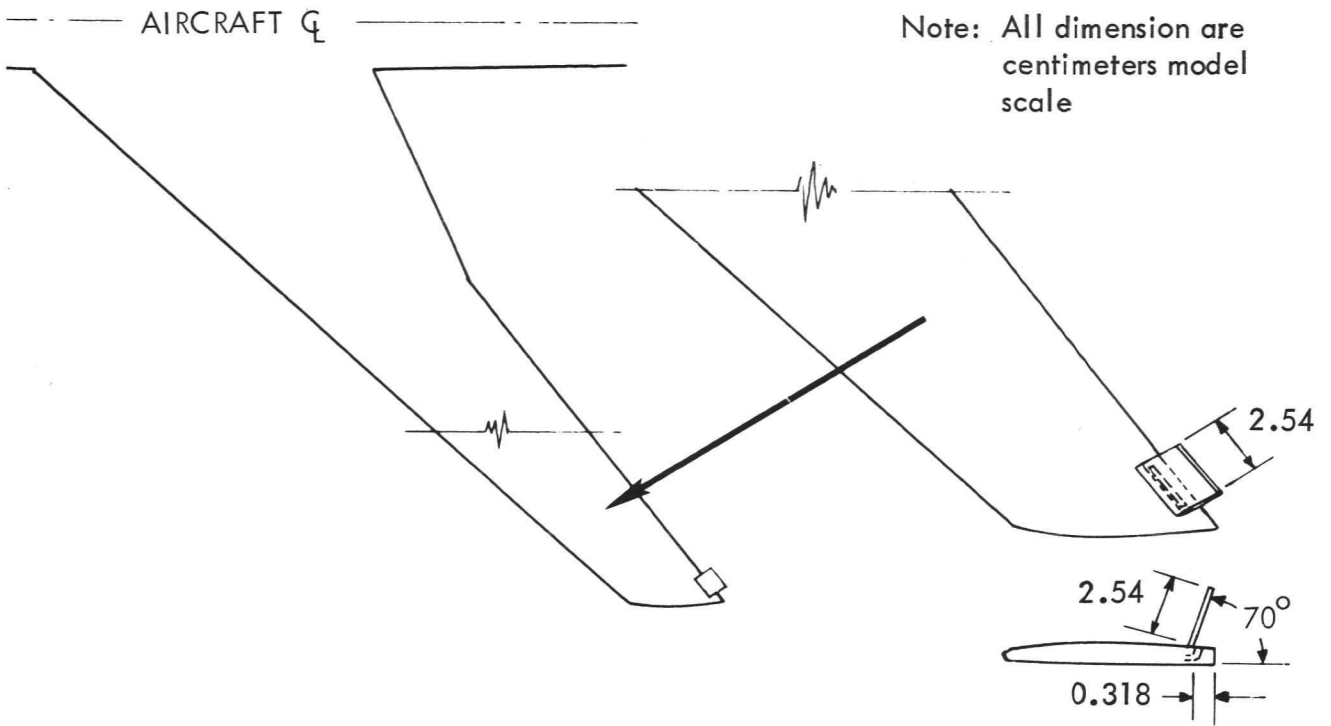


FIGURE 8 - SKETCH AND CLOSE-UP VIEWS SHOWING DEVICE F (BLOWN FLAP) ON WING TIP

Blown flap (Device F). - Figure 8 shows Device F installed near the trailing edge of the wing tip of the basic aircraft model. This device was formed by adding a mechanical flap set at an angle of .70 degrees to the wing tip chordline forward of the slit of Device E so that blowing takes place along the lifting surface of the flap.

Passive Devices

Five different types of passive vortex-attenuation devices were evaluated: two of these were designed to be deployed from and to trail behind the wing of the basic aircraft and the other three were intended for installation upon the wing surface. The models of the passive devices investigated are shown by photographs and sketches in Figures 9 through 13, and are briefly described in the following paragraphs.

Cabled drogue cone (Device G). - Figure 9 shows Device G attached to the trailing edge of the wing of the basic aircraft model. This device was located so that it would float in the trailing vortex core causing the fluid to spill outward. It should be noted that the cable length is not shown to scale in the photograph and sketch. In the model tests, the distance from the trailing edge of the wing to the drogue cone amounted to about 1.5 wingspans.

Spline (Device H). - Figure 10 shows the details of Device H and method of attachment to the wing of the basic aircraft model. Three splines having model diameters of 10.16, 15.24, and 20.32 cm, designated as Devices H-1, H-2, and H-3 respectively, were investigated to determine maximum effectiveness with minimal drag addition to the basic aircraft. The splines were fabricated from aluminum plate.

Vortex generators (Device I). - Figure 11 shows Device I which consists of an array of vortex generators mounted on both the upper and lower surfaces of the basic aircraft. Also shown in the figure is a profile view of an individual vortex generator giving its principal model dimensions.

Spoiler dissipator (Device J). - Figure 12 shows Device J mounted on top and near the tip of the wing of the basic aircraft model. This device is essentially a wing tip spoiler which was previously tested and reported in Reference 7.

Note: All dimensions are in centimeters
Model Scale

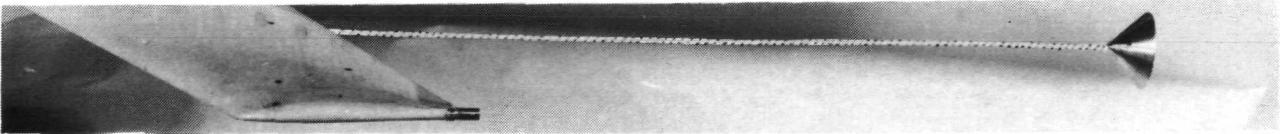
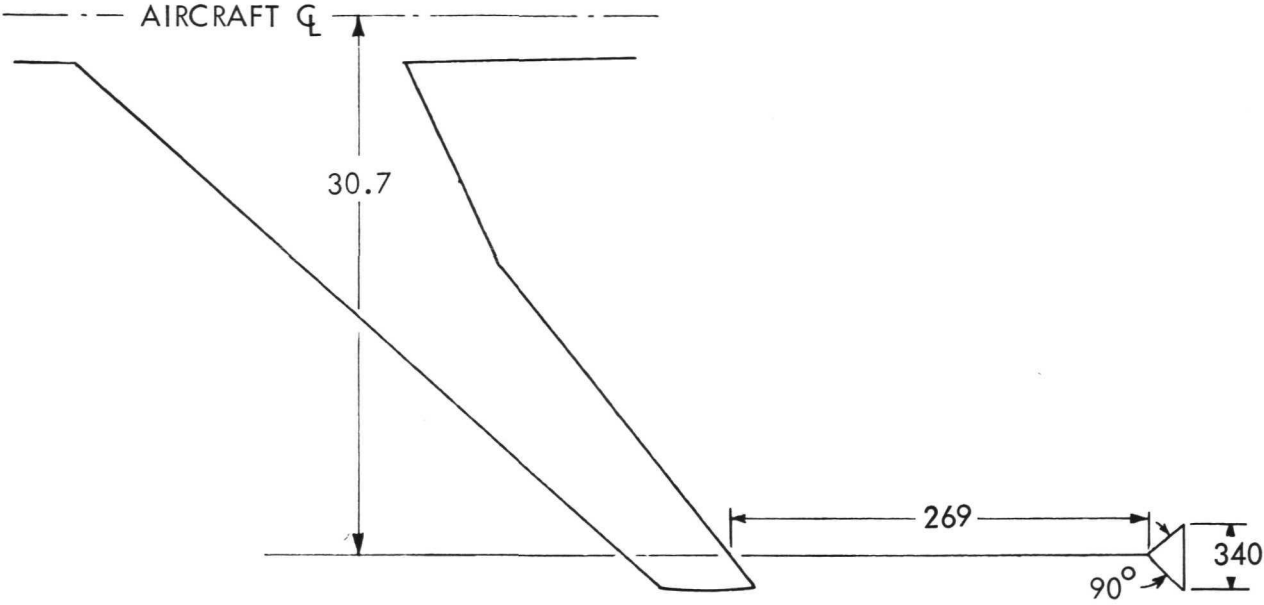
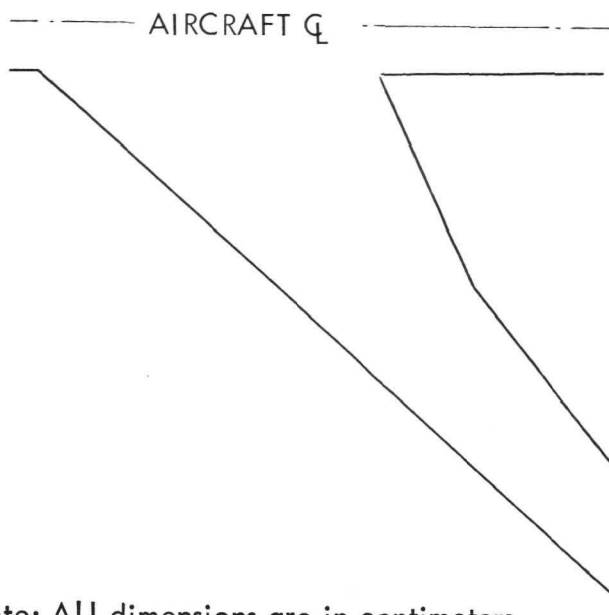


FIGURE 9 - SKETCH AND CLOSE-UP VIEW SHOWING DEVICE G (CABLED DROGUE CONE) AND ITS LOCATION RELATIVE TO WING



A	B
cm	cm
20.32	2.54
15.24	1.91
10.16	1.27

Note: All dimensions are in centimeters
Model Scale

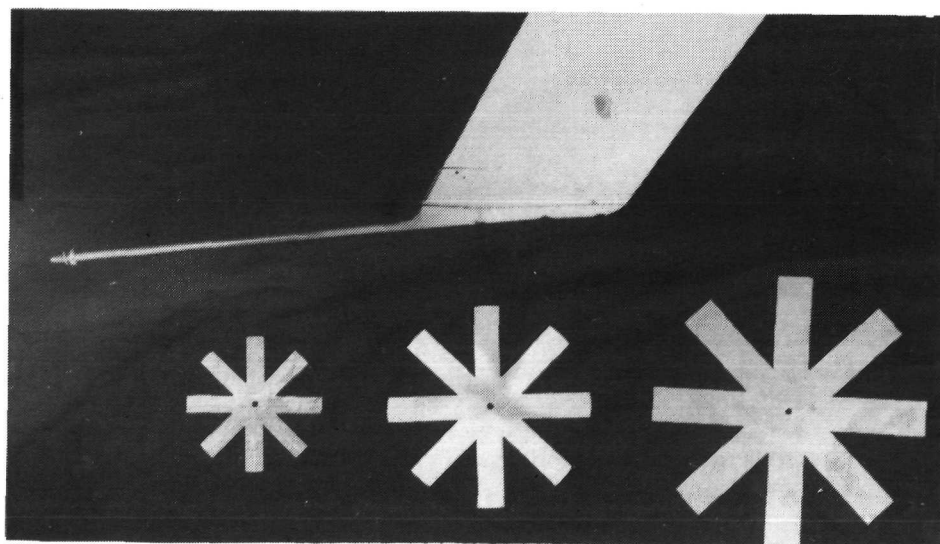
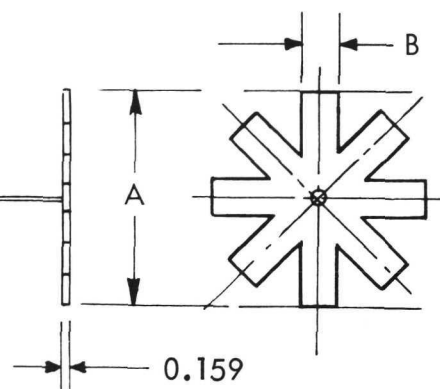


FIGURE 10 - SKETCH AND CLOSE-UP VIEW SHOWING DEVICES H-1, H-2, AND H-3 (SPLINES) WITH WING TIP MOUNTING STING

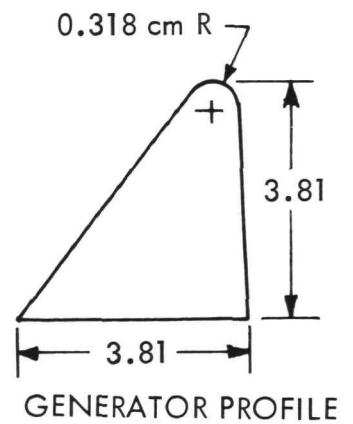
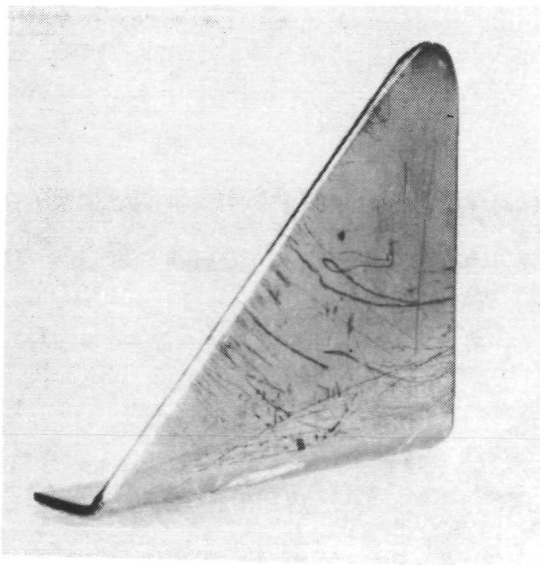
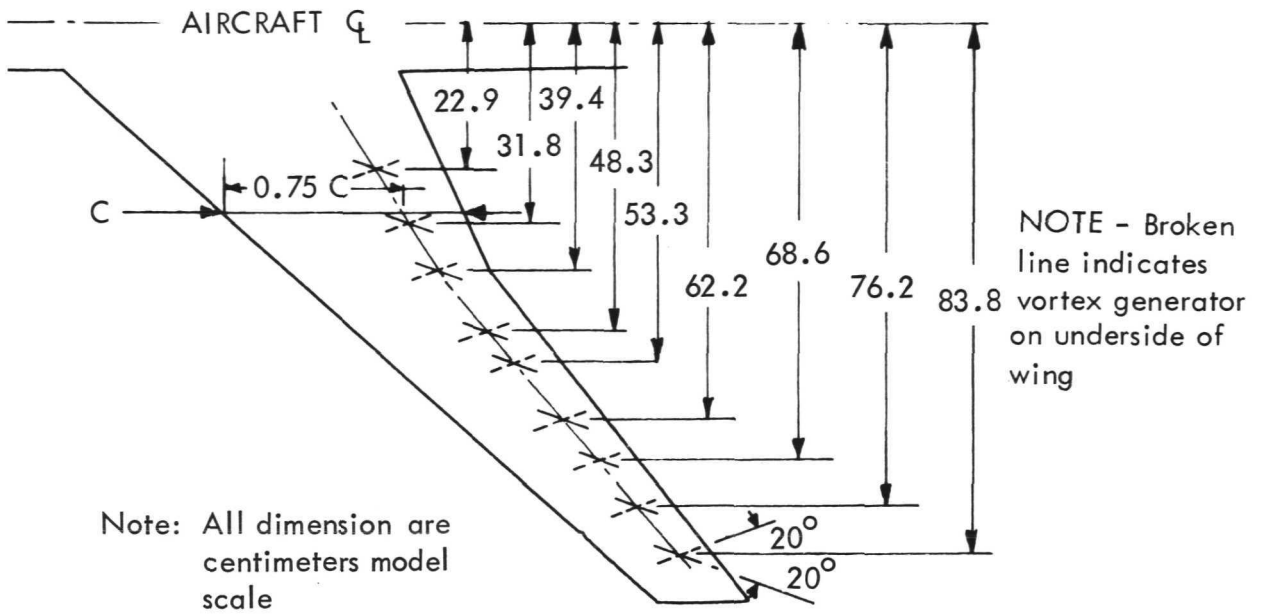


FIGURE 11 - SKETCH AND CLOSE-UP VIEWS SHOWING DEVICE I (VORTEX GENERATOR) ON WING TIP

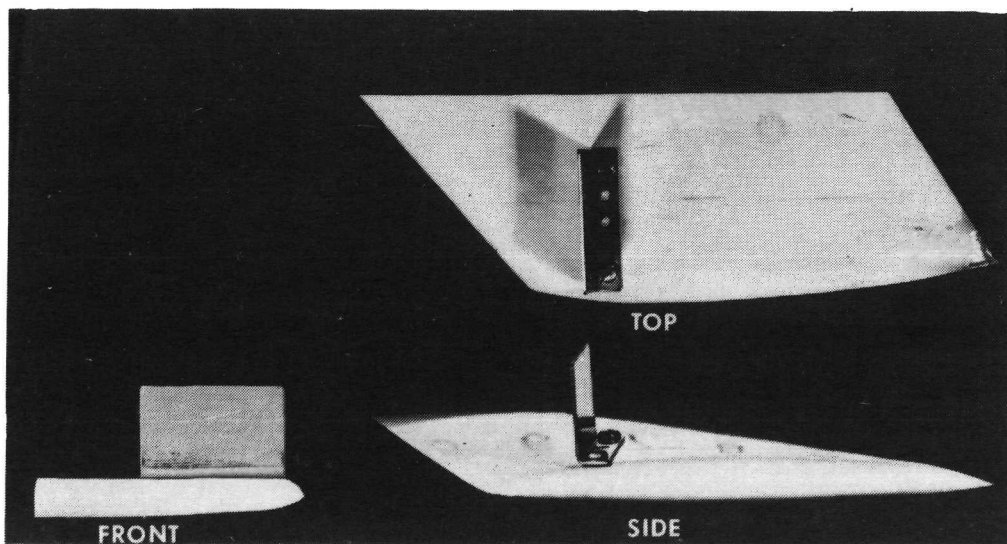
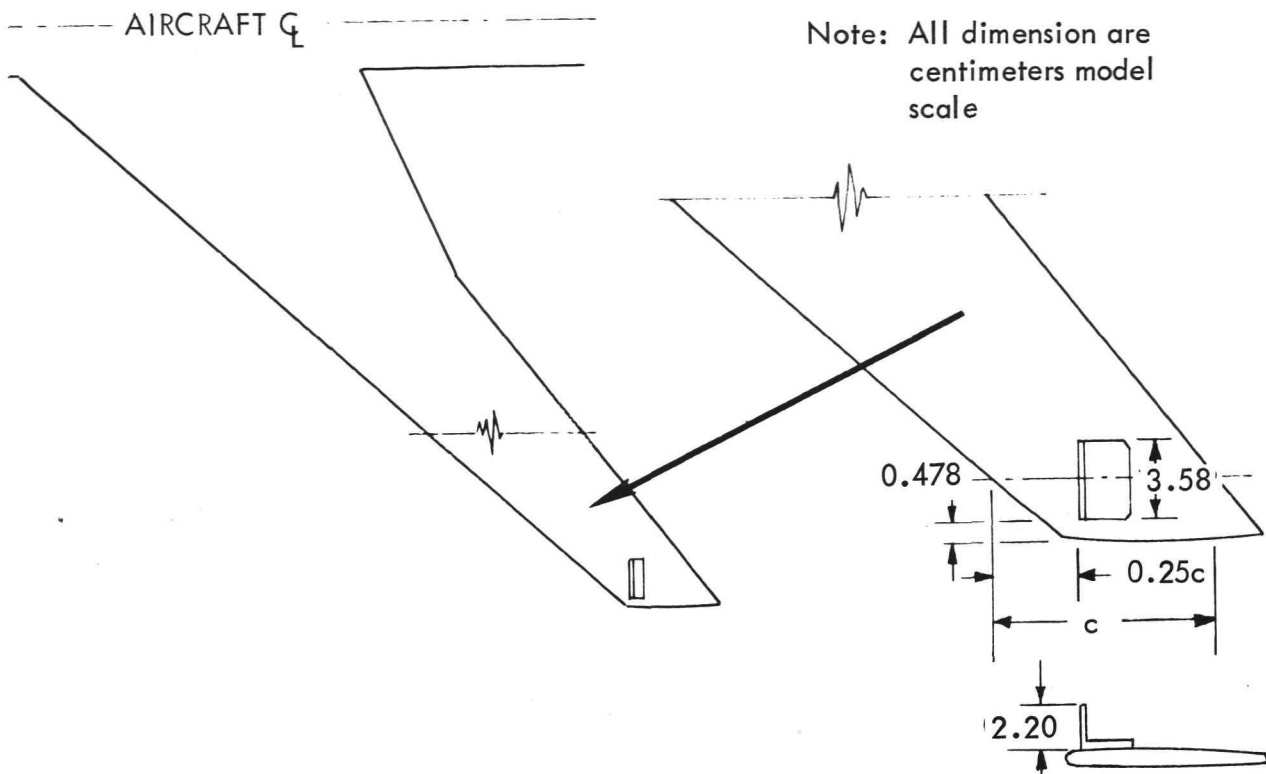


FIGURE 12 - SKETCH AND CLOSE-UP VIEWS SHOWING DEVICE J (SPOILER DISSIPATOR) ON WING TIP

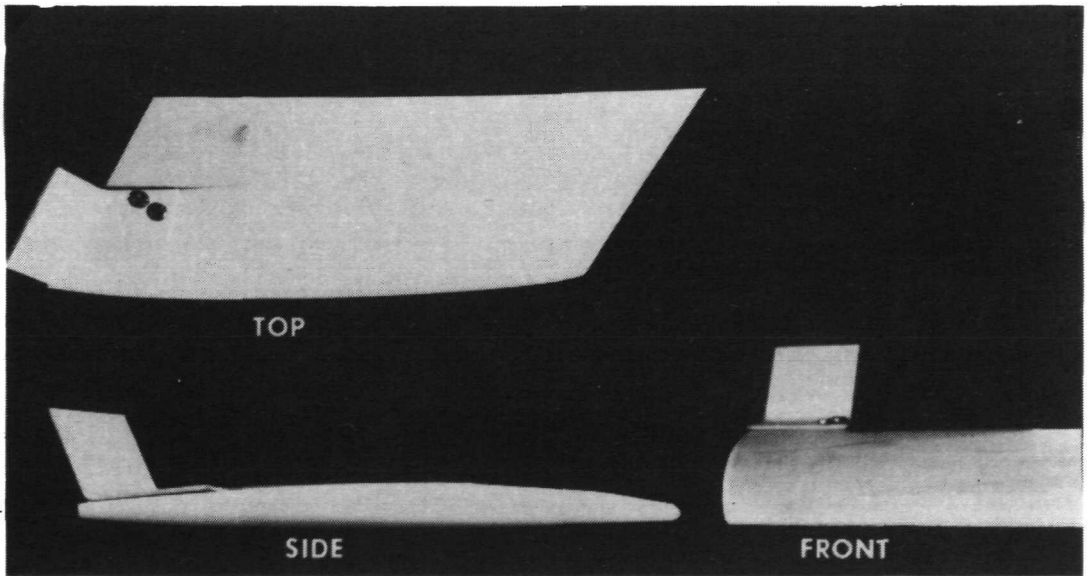
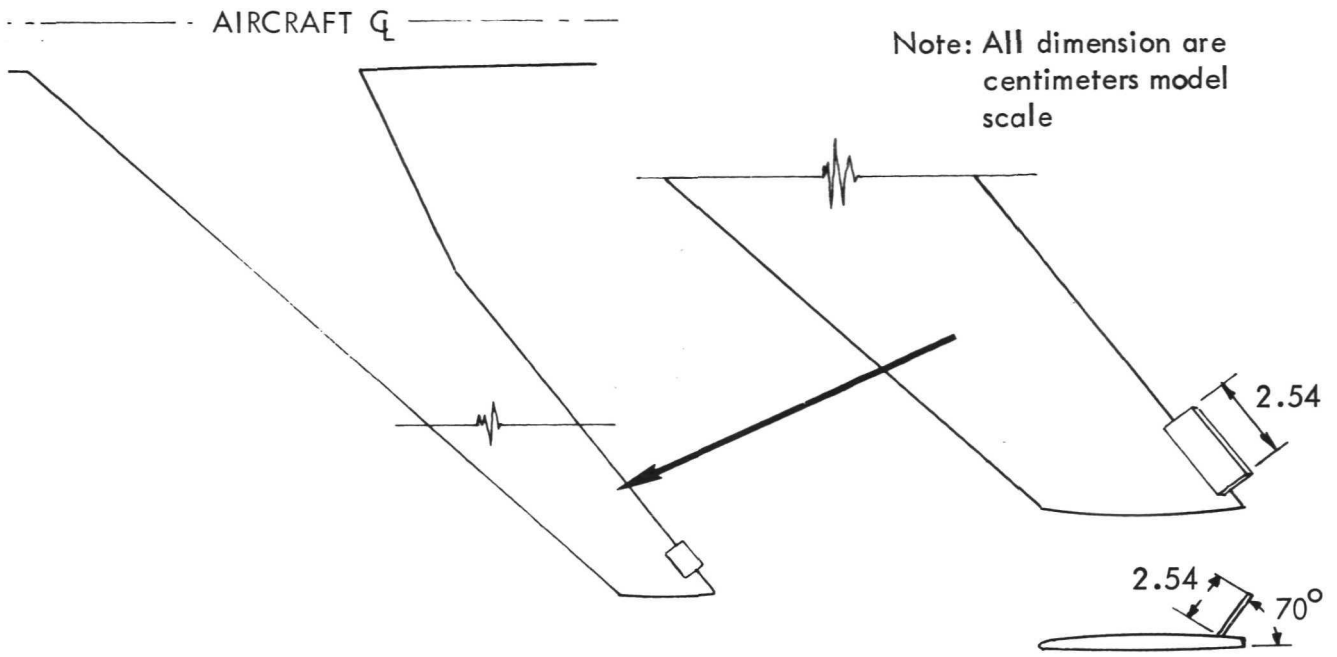


FIGURE 13 - SKETCH AND CLOSE-UP VIEWS DEVICE K (TRAILING EDGE FLAP) ON WING TIP

Trailing edge spoiler (Device K). - Figure 13 shows Device K mounted on the wing tip of the basic aircraft model. This device is identical to the mechanical part of the model blown flap (Device E) except there is no slit and the supply system for discharging fluid along its lifting surface is not operative.

TEST PROGRAM AND PROCEDURES

The test program for the subject investigation is summarized in Table 4 which lists the test number, the number of runs associated with each test, the model speed, the configuration of the basic aircraft, the designation of the device being investigated, and the types of data recorded. It may be noted from Table 4 that runs were made for all devices at the Cruise Condition but not at the Flaps-30 Condition which is considered to be of primary interest. This was because the Cruise Condition was used as a means of screening the most promising devices for subsequent evaluation at the Flaps-30 Condition.

The experiments were all performed in accordance with the scaling laws discussed in Appendix A using the facilities and apparatus described in Appendix B. The test procedures were essentially the same as those developed as the result of the experimental program of Reference 11.

In the present program, however, the major effort was devoted to obtaining quantitative measurements of vortex velocity distribution as affected by the installation of the various vortex-attenuation devices at some reference distance downstream of the generating aircraft. Therefore, time-sequence photographs were used selectively as an aid to the velocity measurements in defining the location and size of the core. Also, since scale effects and other model test procedural problems had been investigated in detail in the earlier program, it was possible to limit the number of test conditions to the minimum required to directly achieve the test objectives. Accordingly, all tests were conducted at model speeds of either 3.05 or 3.81 meters per second corresponding to Reynolds numbers based on mean aerodynamic chord of 0.75×10^6 and 0.93×10^6 , respectively. All velocity measurements were taken at distances downstream of the generating aircraft corresponding to 4.42 and 2.25 kilometers full scale for the Cruise and Flaps-30 Conditions, respectively. The specific procedures followed in preparation for and during the tests are described in more detail in the following paragraphs.

TABLE 4

Program of Test Runs Made with Basic Aircraft Model (Boeing 747)
with and without Vortex-Attenuation Devices Installed

Test	No. of Runs	Speed m per sec	Flight Condition	Device	Measurements*	
1-4	4	3.05	Cruise	None	F	
5-8	7		Cruise	J	F	
9-12	4		Cruise	G	F	
13-16	4		Cruise	I	F	
17-20	4		Flaps-30	I	F	
21-24	4		Flaps-30	None	F	
25-28	4		Flaps-30	G	F	
29-32	4		Flaps-30	J	F	
33	17		Cruise	None	F, V, P	
34	7		Cruise	J	F, V, P	
35	7		Cruise	G	F, V	
36	6		Cruise	I	F, V, P	
37	7		Flaps-30	I	F, V, P	
38	8		Flaps-30	None	F, V, P	
39	6		Flaps-30	J	F, V, P	
40	4		Flaps-30	G	F, V, P	
41	25		Cruise	C	F, V	
42	5		Cruise	C	F, V	
43-44	6		3.05	Cruise	None	F, V
45-49	17		3.81	Cruise	None	F, V
50	7	3.81	Cruise	C	F, V	
51	6		Cruise	None	F, V	
52	6		Flaps-30	C	F, V, P	
53	8		Cruise	D	F, V, P	
54	12		Cruise	B	F, V, P	
55	9		Cruise	A	F, V	
56	10		Cruise	E	F, V	
57	9		Cruise	F	F, V, P	
58	6		Cruise	None	F, V	
59	4		Cruise	K	F, V	
60-65	25		Cruise	None	F, V, P	
66	6		Cruise	H-2	F, V	
67	3		Cruise	None	F, V	
68	5		Flaps-30	None	F, V	
69	2		Flaps-30	H-2	F, V	
70	2		Flaps-30	H-1	F, V	
71	4		Cruise	H-1	F, V	
72	1		Cruise	H-3	F, V	

* Symbols denote data measured and recorded as follows:

F - Force and Moment Data
V - Velocity Surveys
P - Photographic Coverage

Prior to the formal tests, the force measurement system, the flow-velocity measurement system, and the fluid discharge system used for the active devices were calibrated as follows: the force gages were first calibrated individually in accordance with standard procedures using standard weights. The sign conventions were then established and the calibrations checked with gages assembled in the model by applying deadweight loads in the vertical and longitudinal directions. The sensitivities of the force gages permitted steady-state readings on the integrating digital voltmeters to within 0.02 and 0.01 kg for the Z- and X-force gages, respectively. The hot-film probes for the flow-velocity measurements were calibrated in the test area using the motor-driven support arm described in Appendix B. The rate of vertical ascent of the support arm was recorded along with the corresponding probe output voltages over a range of discrete drive-motor speed settings. In addition, precise calibrations were made against towing carriage speed. The data so obtained were used to prepare fair calibration curves of velocity versus output voltage for each probe. Spot checks were made periodically throughout the test program to ensure the continuing validity of these calibration curves. Using these calibration curves, the peak vortex velocity values could be resolved to within 3 cm per sec on the stripchart recorder. The flow discharge rates for each of the active devices were calibrated by metering the mass of liquid discharge rates for various applied system pressures. The resulting data were used to prepare curves of pressure difference versus flow rate for each active device.

The formal tests consisted in runs made either with the model representing the basic aircraft or with the model equipped with one of the vortex-attenuation devices, as shown by the program in Table 4. Prior to each run, the dye-ejection system was loaded with a mixture of 7 grams per liter of red-orange dye (Rhodamine B), and the manifold valves were preset to eject dye from selected ports; the probe rake in the test area was adjusted to the desired vertical and lateral position, and the paper-chart recorder was activated; and the floodlights were turned on and a run number was photographed by the underwater cameras. The procedure for a typical run was as follows:

The model was set at an angle of attack which was preselected to give the desired lift coefficient for the basic aircraft ($C_L = 0.4$ and 1.2 for Cruise and Flaps-30 Conditions, respectively), and all the necessary zero readings were taken. Then the towing carriage was started, brought up to the selected speed, and dye-ejection was begun by an electrically operated solenoid valve. Once the carriage had settled out at steady speed, a 10-second integration was taken of the force gage outputs and printed out by the automatic

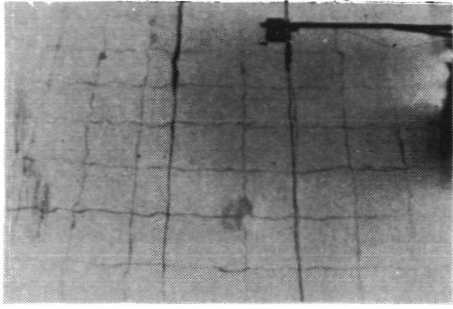
digital data acquisition system. As the model passed through the center of the test area, time-sequence photographs were initiated, and an events marker was made on the velocity-probe recorder to provide a reference for determining vortex age. The carriage was allowed to proceed at constant speed at least 20 to 25 wingspans beyond the test area so that, disturbances due to stopping would not propagate back to the test area during the period of interest (Ref. 11). Immediately upon completing the test (including the acquisition of all the necessary photographic and velocity-probe data), the floodlights were extinguished to minimize the formation of thermal cross currents in the tank, and the carriage was returned to the starting end of the basin for a 30-minute waiting period prior to the next run.

REDUCTION AND PRESENTATION OF DATA

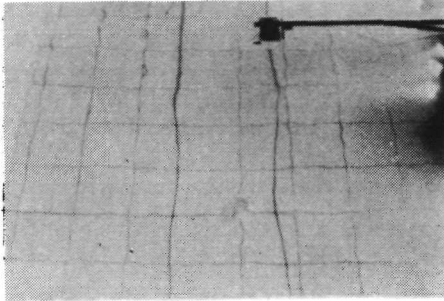
The flow visualization data obtained from the various tests are illustrated by Figure 14 which presents typical time-sequence photographs of the trailing vortices generated by the Basic Aircraft (Boeing 747) operating in the specified Cruise Condition. The corresponding typical trajectory data for the vortex pair which were derived from the complete set of photographic data taken are shown by Figure 15. The dimensions in both figures are given in terms of the full-scale aircraft. As mentioned earlier, flow visualization data such as those of Figure 15 were used in the present investigation mainly as an assist for locating the probes used to obtain quantitative measurements of the desired vortex velocities.

As mentioned previously, the primary data taken in the present investigation were the vortex velocity data measurements using the hot-film probes. The interpretation of these data can be explained with the aid of the sketches given in Figure 16. Time $t_m = 0$ is defined as the point in time at which the wing tip of the generating aircraft is directly over the probe rake as shown in Figure 16a. The tip vortex descends progressively with time from the wing tip elevation at $t_m = 0$ down through the probe rake, as shown in Figure 16b. Although a vertical vortex path is shown for simplicity, in reality the vortex moves in a lateral direction as well. Figure 16c is a sketch which illustrates the time history of vortex velocity obtained from each of the six probes. It should be emphasized that the probes actually sense any component of velocity in the transverse plane (tangential velocity component). For purposes of this study, however, the transverse velocity components

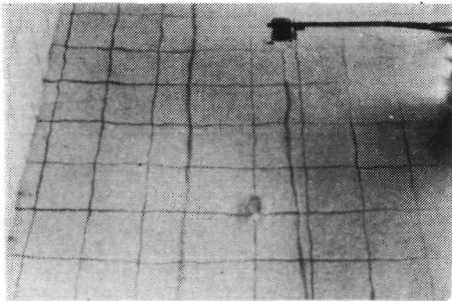
Overhead View
Distance Behind Full-Scale Aircraft
Kilometers



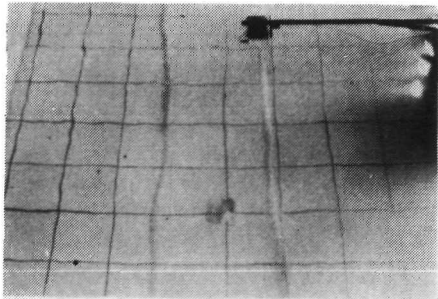
2.01



4.02

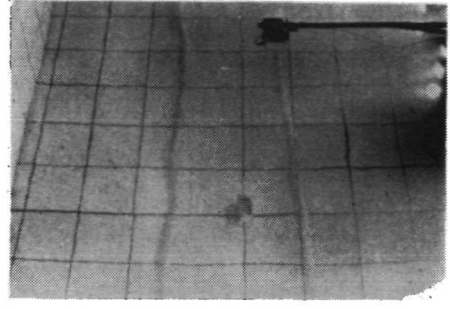


6.03

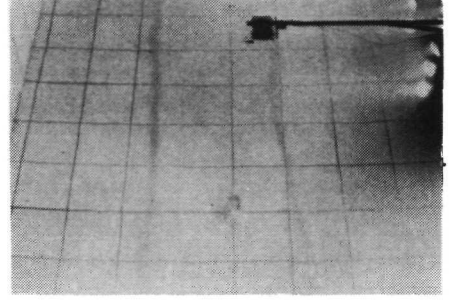


8.04

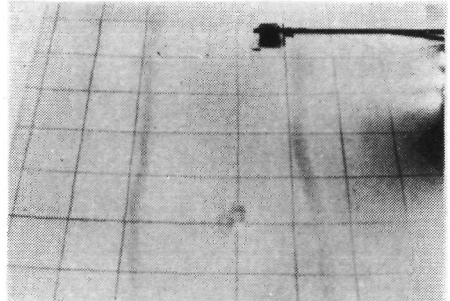
Overhead View
Distance Behind Full-Scale Aircraft
Kilometers



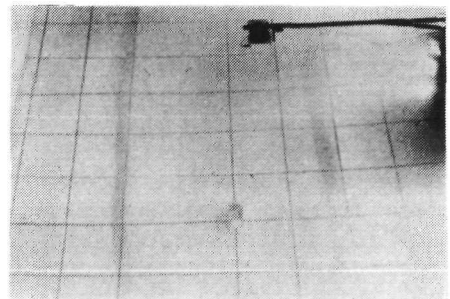
10.05



12.06



14.07



16.08

FIGURE 14 - TYPICAL TIME-SEQUENCE PHOTOGRAPHS OF TRAILING VORTICES FROM BASIC AIRCRAFT AT CRUISE CONDITION

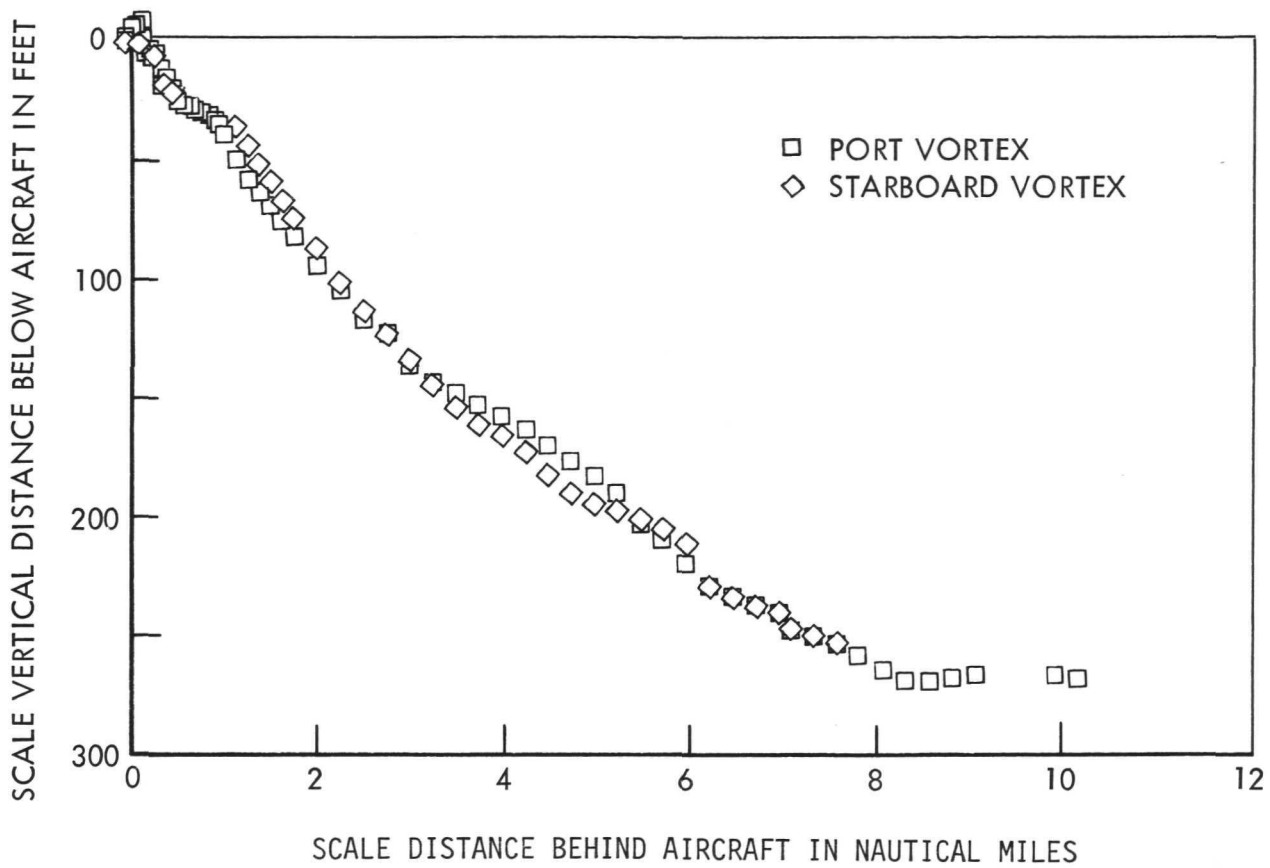
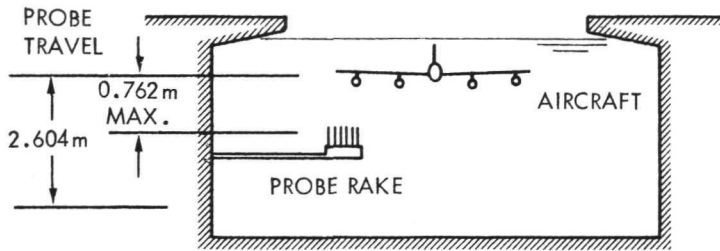
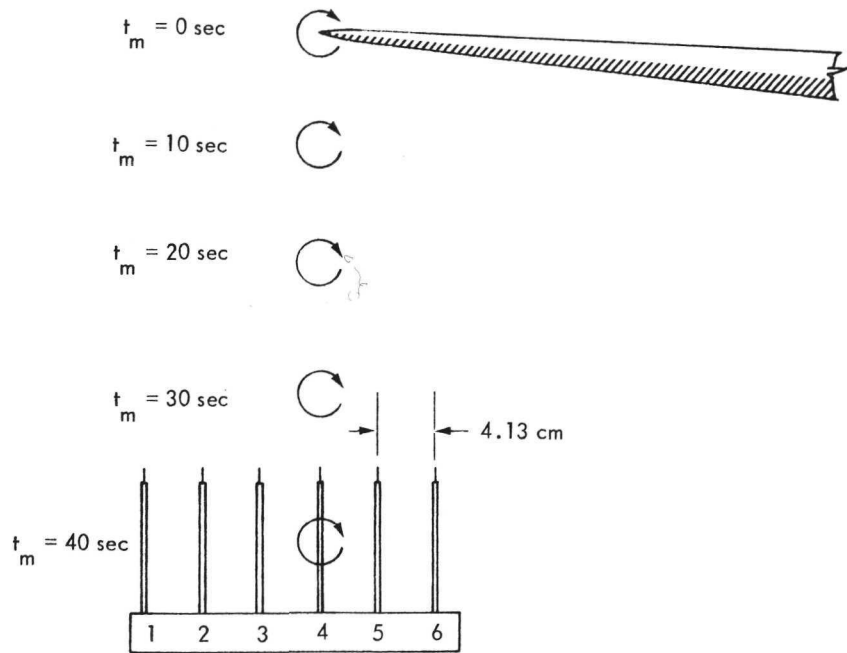


FIGURE 15 - TYPICAL TRAJECTORY OF VORTEX PAIR FOR BASIC AIRCRAFT IN CRUISE MODE DERIVED FROM TIME-SEQUENCE PHOTOGRAPHS

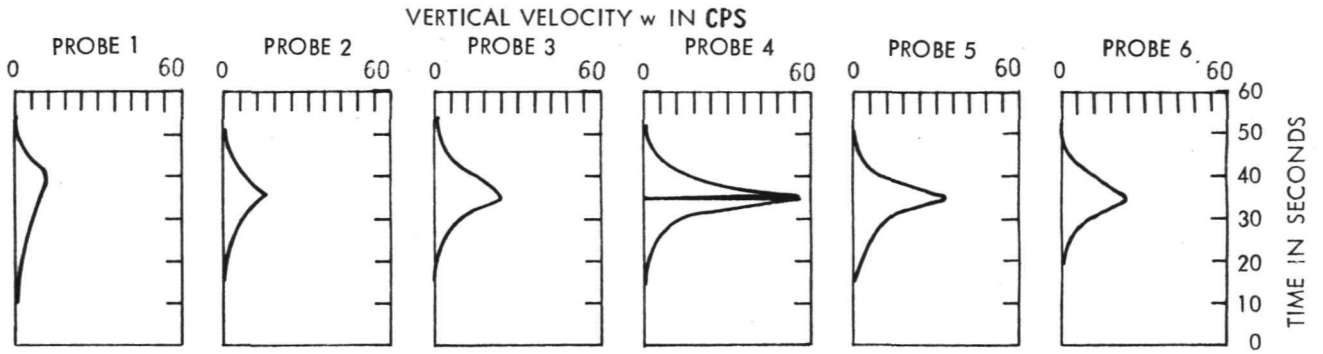


(a) ORIENTATION OF GENERATING AIRCRAFT AND PROBE RAKE

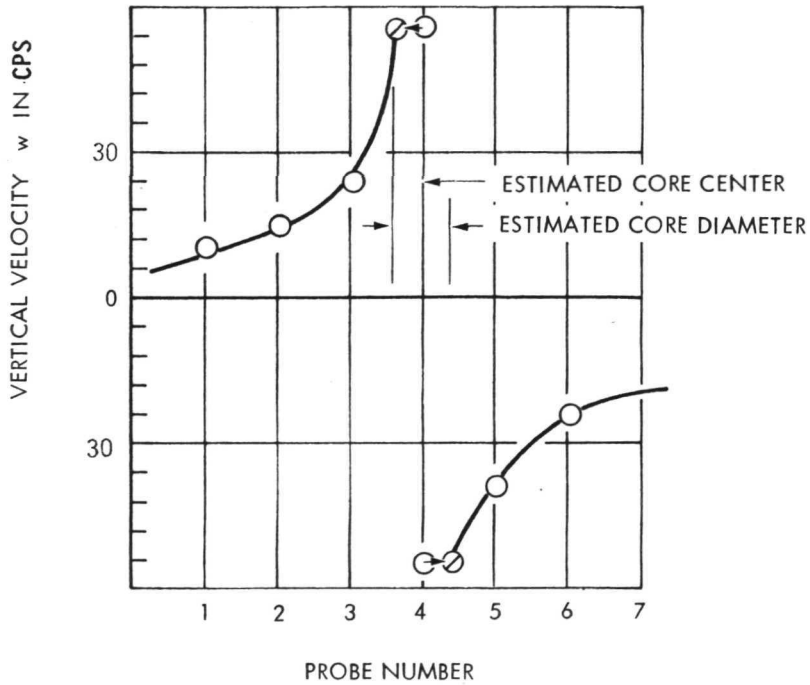


(b) TIME SEQUENCE SKETCH SHOWING VORTEX PATH

FIGURE 16 - SKETCHES SHOWING INTERPRETATION OF VELOCITY DATA



(c) SKETCH OF PROBE VELOCITY TIME HISTORY



(d) SAMPLE DATA PLOT

FIGURE 16 - CONCLUDED

are treated as vertical velocity components or downwash velocities in the remainder of this report. The peak values obtained from the time-history traces are plotted as a function of probe number or lateral distance from core center to obtain the desired downwash velocity distribution, as shown in Figure 16d. Superimposed on Figure 16d is a line which indicates the lateral location of the vortex core center and a pair of lines denoting the vortex core diameter. The vortex core center is estimated in two ways: first by sighting down on the dye trace directly above the rake during a test run and later from considerations of symmetry with respect to the measured peak velocity values such as those shown by 16d. The vortex core diameter is estimated on basis of the dip in the recorded signal trace, which is interpreted as being caused by the passage of the vortex core over the probe, and is shown schematically for Probe Number 4 in Figure 16c. The product of the time duration of the dip and the corresponding vortex sink rate determined from a photographic record, such as is shown in Figure 14, is defined as the estimated vortex core diameter.

Figure 17 presents actual sample time-history records of the velocity-probe output voltages obtained from a test with the model of the Basic Aircraft in the Cruise Condition (note dip in signal trace of Probe Number 4). These output voltages are converted into velocities using calibration curves such as shown in Figure 18. The velocity data so obtained are converted to nondimensional form as values of downwash velocity divided by speed of the generating aircraft, or w/V . To permit independent analysis, the nondimensional data points corresponding to each of the various vortex-attenuation devices investigated are presented for the cases of the Cruise and Flaps-30 Configurations in Appendixes C and D, respectively. Also, to provide a permanent record, typical time-histories of the hot-film velocity probe measurements recorded during the tests are presented in Appendix E. The nondimensional velocity data have been faired and are presented as summary graphs to support the discussion in the body of the report.

The force and moment data were taken to determine whether the vortex-attenuation devices would have any adverse effects on the performance characteristics of the generating aircraft. As mentioned earlier, the forces were measured with respect to a body-axis system, namely as values of X and Z. The digital values of these forces were therefore converted into nondimensional coefficient form in accordance with aerodynamic convention by the following relationships:

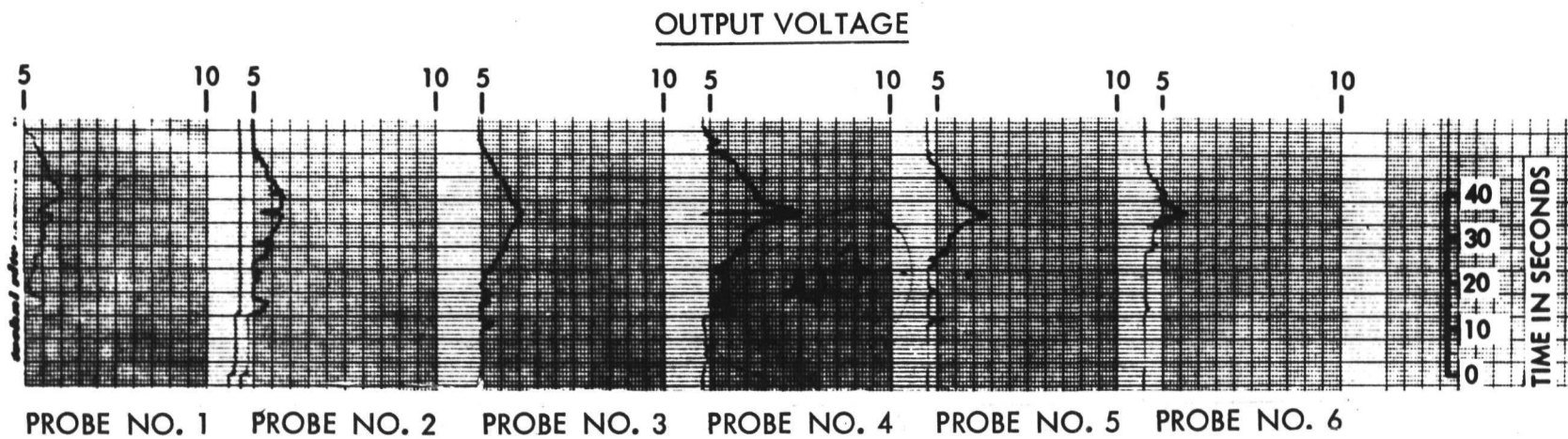


FIGURE 17 - SAMPLE TIME HISTORIES OF PROBE OUTPUT VOLTAGE FOR BASIC AIRCRAFT
IN CRUISE CONFIGURATION

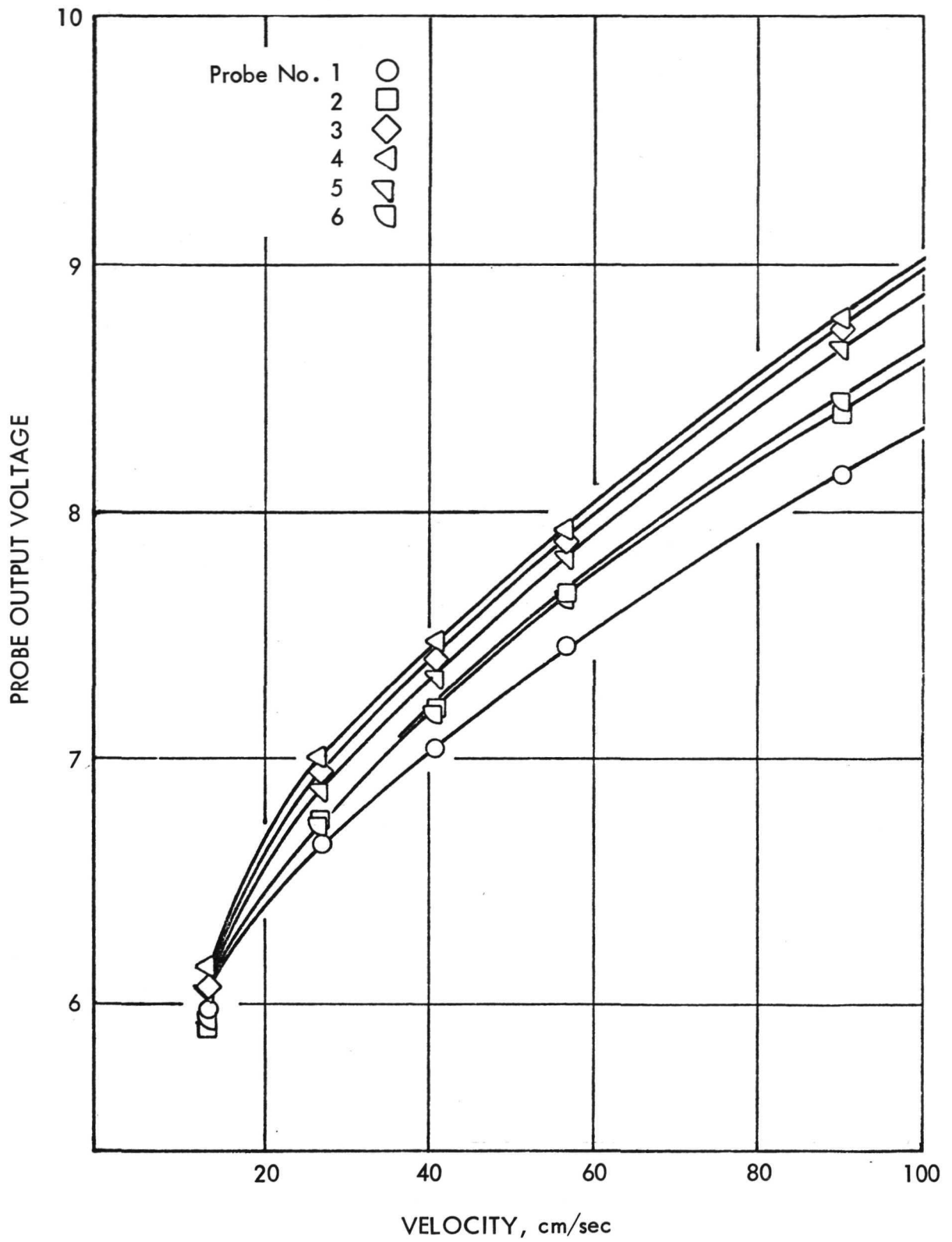


FIGURE 18 - SAMPLE HOT FILM ANEMOMETER VOLTAGE-VELOCITY CALIBRATION CURVES

$$C_L = \frac{L}{\frac{1}{2}\rho SV^2} = \frac{Z \cos \alpha - X \sin \alpha}{\frac{1}{2}\rho SV^2}$$

$$C_D = \frac{D}{\frac{1}{2}\rho SV^2} = \frac{Z \sin \alpha + X \cos \alpha}{\frac{1}{2}\rho SV^2}$$

$$(C_m)_{\bar{c}/4} = \frac{M_{\bar{c}/4}}{\frac{1}{2}\rho SV^2 \bar{c}} = \frac{(Z_1 - Z_2)(0.622)}{\frac{1}{2}\rho SV^2 \bar{c}}$$

The values of the nondimensional lift, drag, and pitching moment coefficients so obtained for each of the cases investigated are presented in a summary table in the next section of this report.

DISCUSSION OF RESULTS

The various vortex-attenuation devices are evaluated herein on basis of the results of the subject model experiments. The discussion of the experimental results is divided into two sections: one dealing with the relative effectiveness of the devices from the standpoint of their ability to attenuate the vortex wake velocity at specified distances downstream of the generating aircraft, and the other dealing with the effect of each device on the performance characteristics of the generating aircraft itself. The effects of the altered vortices on the rolling characteristics of a typical small following aircraft, based on calculations using the experimental data in conjunction with existing theory, are evaluated and discussed in Appendix F.

It should be reemphasized at this point that the tests at the Cruise Condition were conducted mainly for screening purposes to facilitate selection of the more promising devices for later evaluation in the Flaps-30 Condition. It should not be implied, therefore, that the clean wing (or cruise) tests represented a full-scale situation in which a desirable vortex-attenuation device was needed.

Effect on Vortex Velocity

The experimentally determined vortex wake velocities generated by the Basic Aircraft (Boeing 747 without devices) at distances downstream of 4.42 and 2.25 kilometers for the Cruise and Flaps-30 Conditions, respectively, are used herein to provide common bases for evaluating the effectiveness of the various devices. Before proceeding with the evaluation, however, it is of interest to note how the measured values for the basic aircraft compare with those calculated using existing aerodynamic theory. The best available theory for this purpose is that due to Betz in Reference 12 as modified by Reference 2, which gives the total theoretical downwash as:

$$w/V = \frac{C_L}{\pi^2 A} \left[\frac{(y-y_c)}{|y-y_c|} \left(\frac{6b}{|y-y_c|} - 9 \right)^{\frac{1}{2}} + \frac{b}{(y+y_c)} \right] \quad [1]$$

The relationship of Equation [1] has been used to compute the vortex velocity distributions for the Basic Aircraft. The results are shown by the line superimposed on the data points on each of the figures in Appendixes C and D for the reference Cruise and Flaps-30 Conditions, respectively. For the calculations, the Betz elliptical span load distribution was used in lieu of that for the Boeing 747 which was not known. Also, the experimentally determined value for the separation distance between the two cores was used. This distance is somewhat smaller than the free-flight value due to the presence of free surface effects in the basin tests. It may be noted from Figures 33 and 45 that the theoretically based values for the Basic Aircraft (without devices) are in good agreement with the measured values. This provides added confirmation as to the validity of using the large towing basin technique for making quantitative studies of trailing vortices in the far field.

The effects of the active vortex-attenuation devices on the downwash velocity distribution for the Cruise Condition are summarized by the faired curves in Figure 19. The curves for Devices A, B, C, and E are not shown since they produced no significant change in the vortex-velocity profile (see Appendix C, Figures 34, 35, 36, and 38). It may be seen that Device F (Blown Flap) is the most effective active-type device among those tested from the standpoint of reducing downwash velocities at the reference distance (4.42 kilometers) downstream of the generating aircraft in the Cruise Condition. It should be emphasized in connection with the evaluation of the active devices that the momentum coefficients

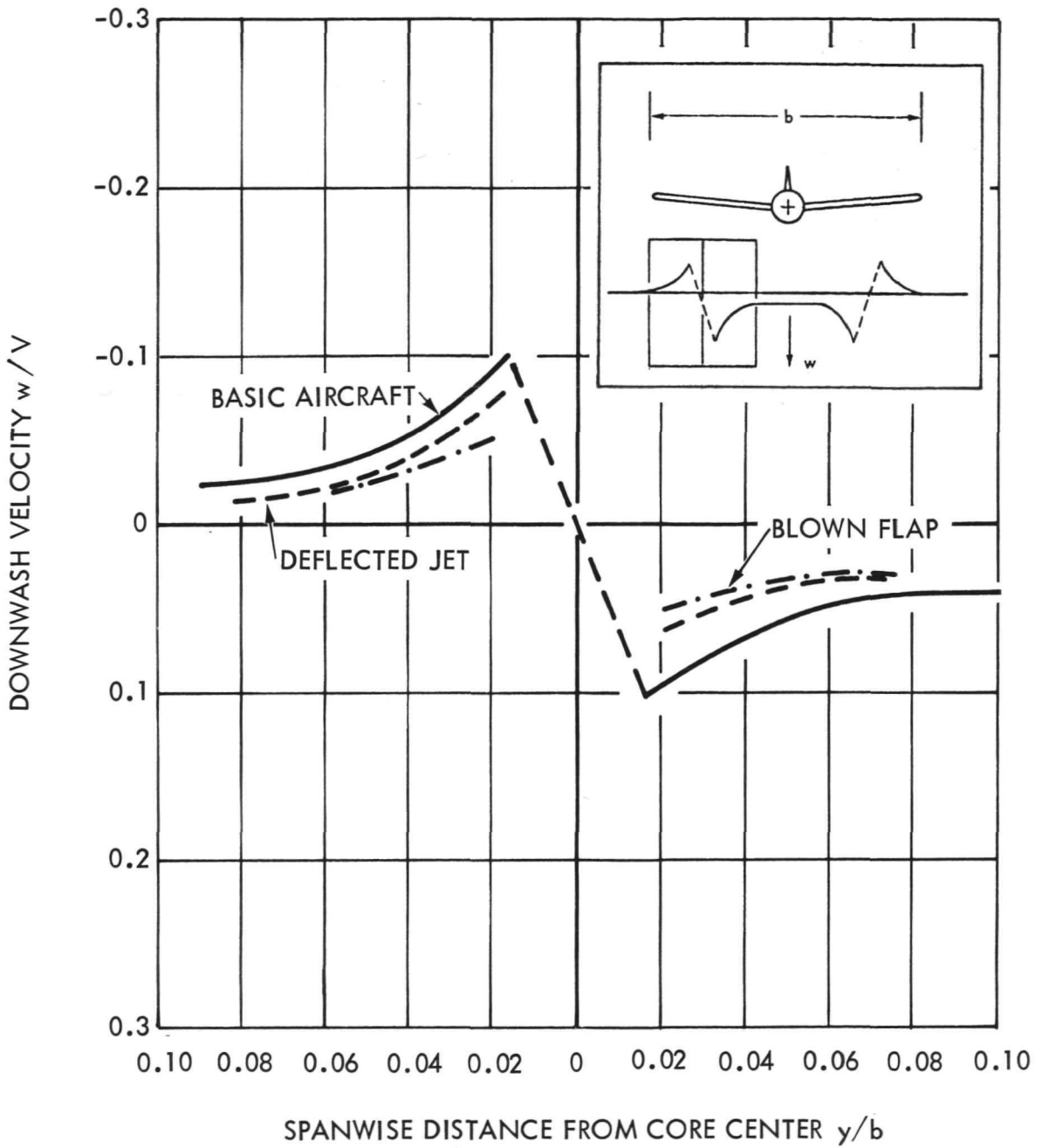


FIGURE 19 - COMPARISON OF EFFECTS OF ACTIVE VORTEX ATTENUATION DEVICES ON DOWNWASH VELOCITY DISTRIBUTIONS FOR CRUISE CONDITION

used in the present series of experiments are substantially lower than those that can be achieved in practice with the full-scale aircraft (see Table 3). It may be reasonably expected, therefore, that greater degrees of effectiveness can be obtained with the active devices than are shown.

The effects of the passive vortex-attenuation devices on the downwash velocity distribution for the Cruise Condition are summarized by the faired curves in Figure 20. The curves for Devices G and K are not shown since they produced no significant change in vortex-velocity profile (see Appendix C, Figures 40 and 44). Devices H-2 and H-3 (15.24- and 20.32- cm Splines) produced substantial reductions in the downwash velocities (see Appendix C, Figure 41) but their curves are not shown since these devices were considered to be impractical for reasons discussed in the next section. It may be seen that Device I (Vortex Generators) is the most effective of the practical passive devices investigated from the standpoint of its ability to reduce the downwash velocities at the reference distance (4.42 kilometers) downstream of the generating aircraft in the Cruise Condition.

Summary curves are not given for the case of the Flaps-30 Condition since none of the devices investigated produced a significant reduction in downwash velocities. This can be readily seen from the data shown in Appendix D.

Effect on Performance of Generating Aircraft

The lift, drag, and pitching moment coefficients derived from HSMB tests for the Basic Aircraft (Boeing 747 without devices) are presented in Figure 21 as functions of angle of attack for both the Cruise and Flaps-30 Conditions. No corrections have been made to the data to account for possible blockage or strut interference effects which are estimated to be small. Furthermore, the incremental changes in the coefficients due to the addition of the vortex-attenuation devices are determined from uncorrected measurements of total values obtained on the model both with and without devices. Therefore, the resulting values should be about equal to those that would be obtained if the small corrections had been applied to both sets of data. However, it is of interest to note that the lift-curve slope $C_{L\alpha}$ derived for the Basic Aircraft is equal to 0.08 per degree which is in close agreement with the value of 0.079 per degree computed from theory and given in Reference 13.

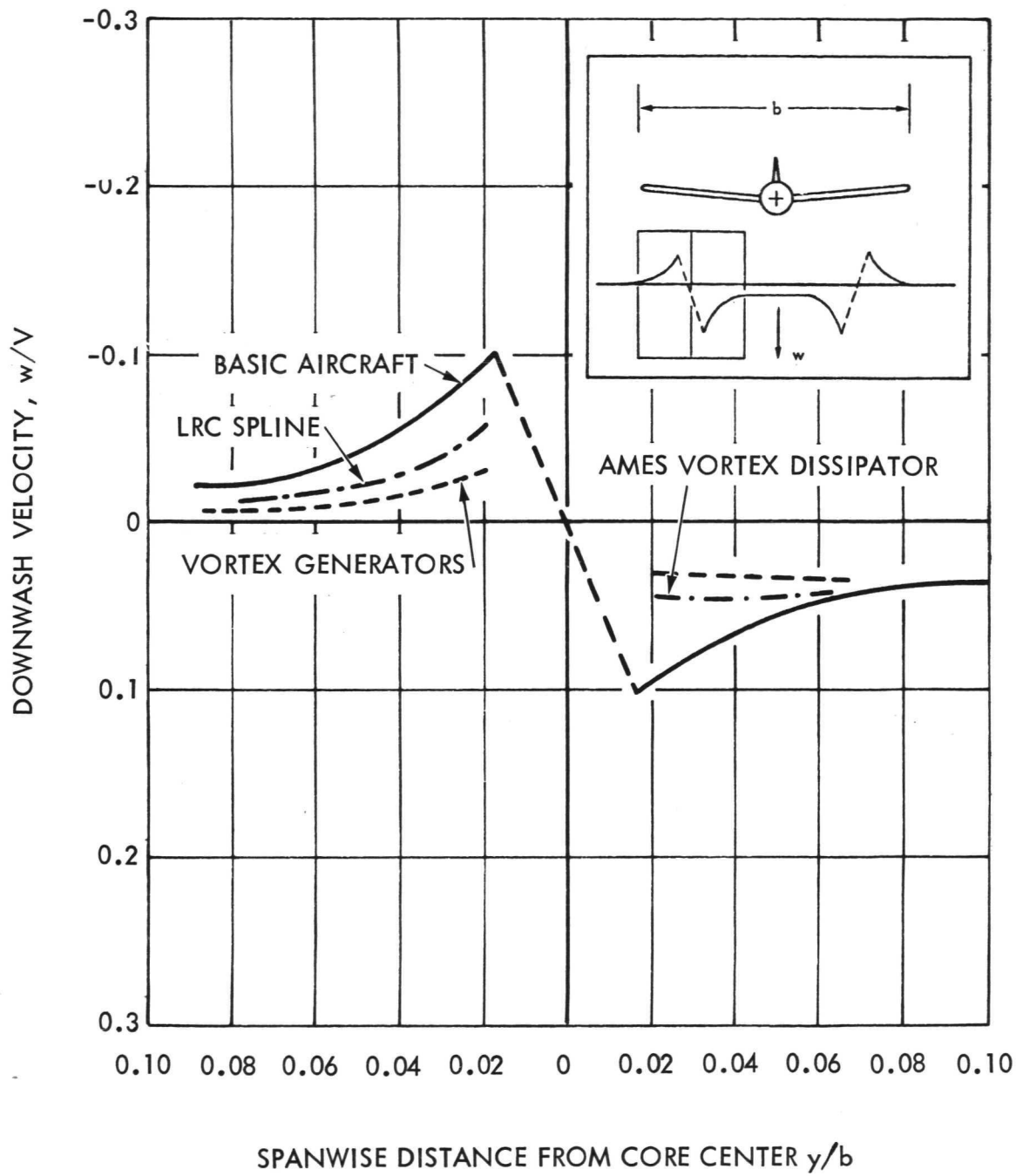
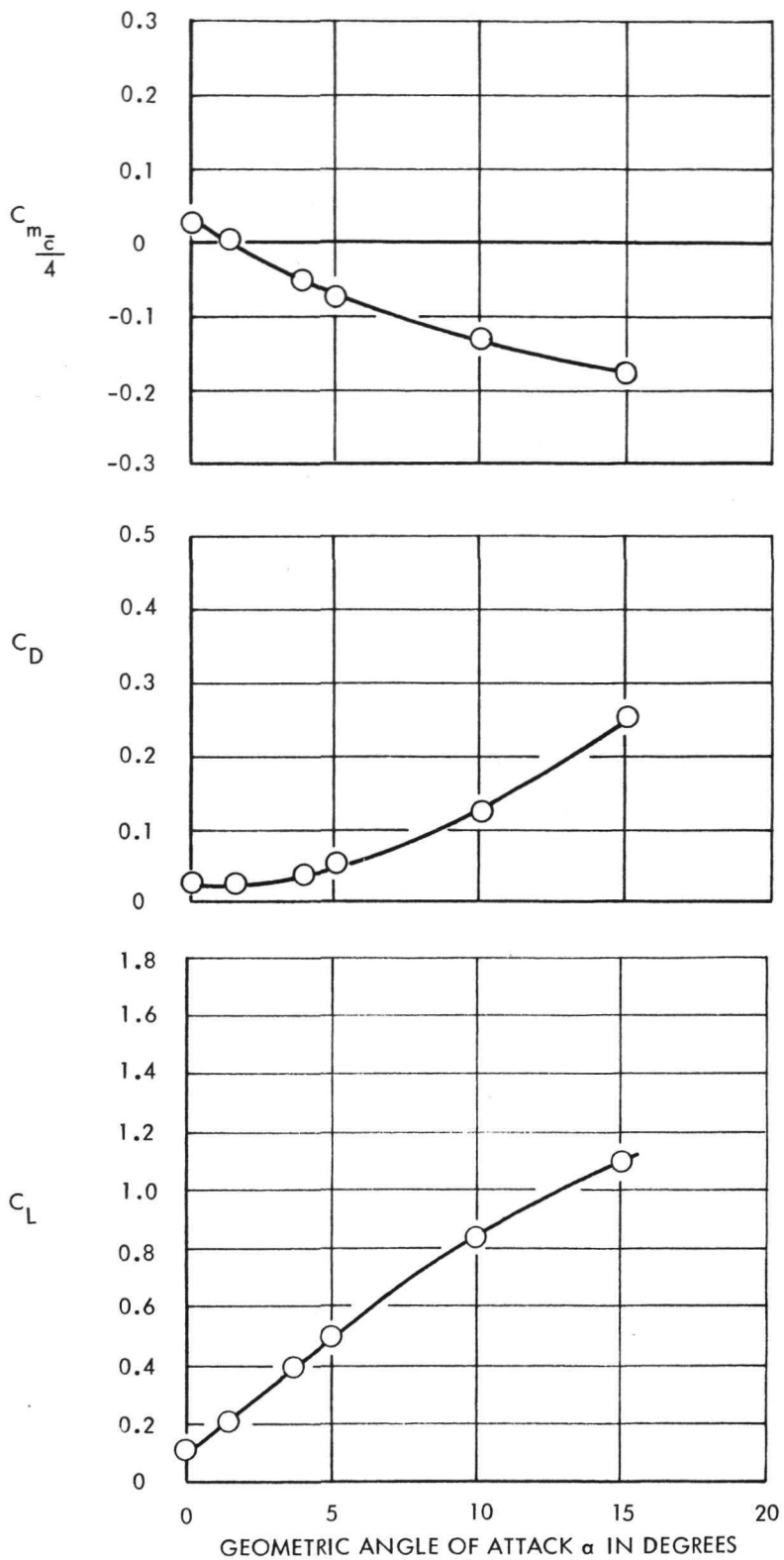
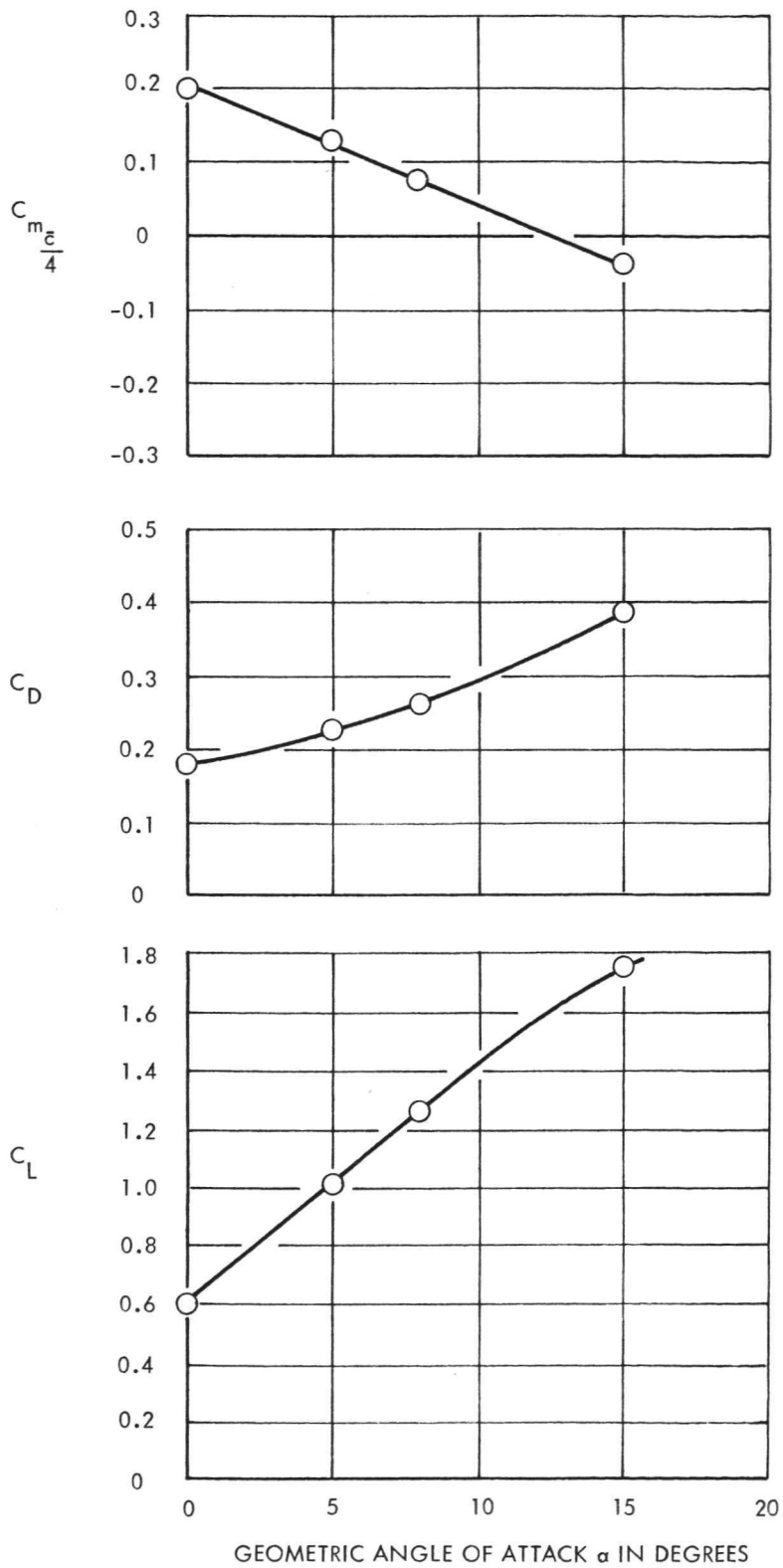


FIGURE 20 - COMPARISON OF EFFECTS OF PASSIVE VORTEX - ATTENUATION DEVICES ON DOWNWASH VELOCITY DISTRIBUTIONS FOR CRUISE CONDITION



(a) CRUISE CONDITION

FIGURE 21 - LIFT, DRAG, AND PITCHING MOMENT COEFFICIENTS FOR BASIC AIRCRAFT



(b) FLAPS - 30 CONDITIONS

FIGURE 21 - CONCLUDED

The incremental changes in lift, drag, and pitching moment coefficients due to addition of the vortex-attenuation devices to the Basic Aircraft are summarized in Tables 5 and 6 for the Cruise and Flaps-30 Conditions, respectively. In addition, the increase in drag is shown as a percentage of the appropriate total drag of the basic aircraft at the Cruise and Flaps-30 Conditions which correspond to lift coefficients of 0.4 and 1.2, respectively.

TABLE 5

Changes in Lift, Drag, and Pitching Moment Coefficients
Due to Addition of Vortex-Attenuation Devices to
Basic Aircraft in Cruise Condition

Device	Incremental Change			Percentage Increase in drag
	ΔC_L	ΔC_D	$\Delta(C_m)_{\bar{c}/4}$	
A Forward Blowing Jet	0	0.002	0.013	5
B Downward Blowing Jet	0	0	0.007	0
C Rearward Blowing Jet	0	0	0.020	0
D Deflected Jet	0	0.007	0.037	16
E Jet Flap	0	0	0.017	0
F Blown Flap	0	0.003	0.025	7
G Cabled Drogue	0	0.010	0.003	23
H-1 10.16- cm Spline	0	0.030	0.021	70
H-2 15.24- cm Spline	0	0.060	0.021	140
H-3 20.32- cm Spline	0	0.120	0.024	280
I Vortex Generators	-0.02	0.020	0.028	47
J Spoiler Dissipator	-0.01	0.010	0.016	23
K Trailing Edge Flap	0	0.004	0.018	9

Note: Positive value denotes that the incremental coefficient change is an increase with respect to the Basic Aircraft.

TABLE 6

Changes in Lift, Drag, and Pitching Moment Coefficients
Due to Addition of Vortex-Attenuation Devices to
Basic Aircraft in Flaps-30 Condition

Device	Incremental Change			Percentage Increase in drag
	ΔC_L	ΔC_D	$\Delta(C_m)_{\bar{c}}/4$	
I Vortex Generators	-0.10	0.030	0.031	12
J Spoiler Dissipator	0	0.010	0.031	4
K 15.24-cm Spline	0	0.060	0.009	25

Note: Positive value denotes that the incremental coefficient change is an increase with respect to the Basic Aircraft.

For the Cruise Condition, it may be noted from Table 5 that none of the active devices cause any noticeable change in lift of the Basic Aircraft. The only two passive devices that cause lift-changes are Device I (Vortex Generators) and Device J (Spoiler Dissipator); the largest change amounts to a loss in lift of only about 5 percent for the Cruise Condition. The percentage increases in drag are small for most of the active devices investigated. It is of interest to note that Device F (Blown Flap) which is the most effective active device from the standpoint of vortex-velocity attenuation, adds only about 7 percent to the aircraft drag. As expected, the passive devices H-2 and H-3 (15.24-cm and 20.32-cm Splines) cause an excessively large drag addition. Device I (Vortex Generators), which is the most effective of the passive devices investigated, causes an increase in drag of about 47 percent in the Cruise mode.

For the Flaps-30 Condition, Table 6 lists the incremental changes only for the three devices which showed the most promise from the standpoint of vortex-velocity attenuation in the Cruise Condition. As mentioned earlier, none of the devices investigated were effective from this standpoint in the Flaps-30 Condition.

CONCLUSIONS

Based on a comprehensive program of 0.03-scale model experiments conducted in a large towing basin, supplemented by theoretically based calculations, the following conclusions are drawn concerning the effectiveness of various vortex-attenuation devices proposed for installation on the wings of a large aircraft (Boeing 747):

1. In the Cruise Condition, Device I (Vortex Generators) will be the most effective among the devices investigated from the standpoint of reducing the downwash velocities of the trailing vortices at a distance of 4.42 kilometers downstream of the generating aircraft.

2. In the Flaps-30 Condition, none of the devices investigated will produce a significant reduction in the downwash velocities at a distance of 2.25 kilometers downstream of the generating aircraft.

3. Device I will add about 50 percent to the drag (with a loss of lift of about 5 percent) of the Boeing 747 in the Cruise Condition. Device F (Blown Flaps) will add less than 10 percent to the drag with no measurable loss in lift, but is somewhat less effective in reducing vortex velocities.

4. Based on calculation, a small following aircraft (Gates Learjet) will be unable to cope with the induced rolling moment using maximum aileron control when flying through the core center of a trailing vortex generated by the Boeing 747 in the Cruise Condition at a distance of 4.42 kilometers downstream. This will be true even if the generating aircraft is equipped with the best of the devices among those investigated.

5. The measured values of the downwash velocities for both the Cruise and Flaps-30 Conditions of the Basic Aircraft (without devices) are in close agreement with those calculated using a modified Betz theory.

APPENDIX A

DISCUSSION OF SCALING LAWS
PERTINENT TO EXPERIMENTS

Page intentionally left blank

In general, the scaling laws for modeling various fluid phenomena including those involved in the study of vortex wakes are essentially the same for tests conducted in water as those followed for standard aerodynamic tests. There are, however, certain differences which must be taken into account to assure complete interchangeability between results of tests conducted in air and water. Among these are: (1) that air is more compressible than water (Mach Number effects), (2) the possible occurrence of cavitation in water (Cavitation Number), and (3) the possible existence of free-surface effects in water (Froude Number). Therefore, in planning the subject model test program, it was necessary beforehand to examine the effects on vortex wakes of these and other dimensionless parameters such as Reynolds number, Weber number, Richardson number, Strouhal number, Knudsen number, Prandtl number, and a Schmidt number. These parameters as well as the time scaling that relates model to full-scale measurements are discussed herein in terms of how they affect the test conditions established for the HSMB program.

Mach Number - is the ratio of aircraft velocity to the velocity of sound. Under usual test conditions, the matching of Mach number in water and air is not possible. Fortunately, for tests involving subsonic aircraft, the effects of Mach number on vortex wakes can be shown to be negligible. The speed of sound in water is very high, about 1524 m/sec, and therefore the Mach number associated with model tests in water is always very low. On the other hand, aircraft Mach numbers of interest may vary from very low values to 0.7 or 0.8. The effect of Mach number at sub-critical flight is mainly confined to a change in lift-curve slope with a second order change in span load distribution. The induced drag and hence the energy shed into the wake vortex system is known to be essentially independent of Mach number at a given lift coefficient. It can be concluded, therefore, that at a given lift coefficient for the generating aircraft, the trailing vortex system should closely approximate that at low Mach number. Furthermore, rolled up vortex system measurements from several sources (Refs. 7, 11, 14, 15) show maximum tangential and axial disturbance velocities which are less than one-half the flight speed. Thus, for a flight Mach number of 0.7 which corresponds to the Cruise Condition in the present study, the peak rotary and axial Mach numbers would be only 0.35 or less relative to the undisturbed fluid. The Mach number would be smaller yet for the Flaps-30 Condition. Under these conditions, it is clear that air compressibility effects are negligible and the flow pattern and behavior should be closely that obtained at Mach number near zero. It can be concluded, therefore, that towing tests involving behavior of vortex systems will not be

invalidated because of air compressibility effects so long as the full-scale aircraft Mach numbers are below typical critical values of 0.7 or 0.8.

Cavitation Number - is the ratio of cavity suppressing pressure to the dynamic pressure used as a basis for scaling in hydrodynamic model tests where cavitation or boiling is of interest; cavitation will occur when the cavitation number is exceeded. To properly model aerodynamic phenomena in water, cavitation must be completely avoided and, therefore, the test conditions in the HSMB were established so that cavitation could not occur. Calculations show that at a depth of submergence of the wing of 2.5 feet, a water temperature of 70°F, and a model velocity of 20 feet per second, a pressure coefficient of -5.5 would be required for cavitation inception. This corresponds to a vortex wake velocity of about 2.4 times the model velocity. As mentioned earlier, measurements have shown that the maximum vortex wake velocity is about half the forward velocity (Ref. 15). Therefore, cavitation phenomena will not occur in model tests which are performed under the foregoing conditions. This is further confirmed by the fact that no visible cavitation was observed during the towing basin tests even at the highest speed investigated.

Froude Number - is the ratio of inertial to gravitational forces used as a basis for scaling in hydrodynamic model tests where free-surface effects are of interest. For the present program, the Froude number (based on depth of submergence of the wing) determines the extent to which the aircraft performance characteristics are affected by the free surface. Reference 16 presents test data which clearly show that the lift and drag characteristics of hydrofoils operated at depths greater than 2 chord lengths are essentially unaffected by the free surface and are equal to those obtained on a wing operating in an infinite medium. This is further confirmed by the HSMB tests of Reference 11 conducted with the 0.03-scale model of the Boeing 747 Aircraft at a depth of about 3 wing-chord lengths. The lift-curve-slope values measured by these tests agree within 1 percent of those predicted for the full-scale aircraft on basis of both aerodynamic theory and wind tunnel data.

There can be a small incremental wavemaking drag produced mainly by the proximity of the model fuselage to the free surface. However, at the depths of submergence used in the HSMB tests of Reference 11, the wavemaking drag amounted to less than 2 percent of the total drag at zero lift coefficient. In view of the foregoing, it can be concluded that the Froude number plays no significant role in towing basin tests with aircraft models provided the

model is run at a sufficient depth below the free-surface; submergences of 3 to 4 times wing chord are certainly adequate.

Irrespective of the question of Froude number scaling, the free-surface in towing basin tests must be considered from the standpoint of the necessity for making boundary corrections. The free-surface acts as a reflection plane or another wall or ceiling and blockage corrections to force data, vortex trajectories, and other flow phenomena can be made, if required, using techniques similar to those used in wind tunnels.

Reynolds Number - is the ratio of inertial to viscous forces and can rarely be matched in small-scale model tests either in an aerodynamic or hydrodynamic facility. Nevertheless, a great body of experience exists for correcting and interpreting model data obtained at Reynolds numbers well below those of full-scale flight. Wind tunnel experience has shown that when test Reynolds numbers are high enough to ensure turbulent flow over most of the model, lift characteristics become independent of Reynolds number and drag values may be corrected using well established data. It has long been known that flows involving jets and wakes are independent of Reynolds number once turbulent flow conditions are established (Ref. 17). It may be concluded, therefore, that studies of vortex wakes and turbulence may be studied at reasonably small scale in towing basins or wind tunnels provided the Reynolds number based on wing mean chord is in excess of about 10^6 , a value found from experience to be adequately high. Also, that the towing basin tests should produce flow patterns which are geometrically similar to those of the corresponding full-scale phenomena.

Other Scaling Parameters - The other scaling parameters listed at the outset are of no direct concern to the subject investigation and therefore, are grouped together and briefly discussed in this section. The Strouhal number which is a ratio defining period of flow oscillations is not a basic parameter but is a generated number similar to pressure or force coefficients. It will always be preserved if the basic similarity numbers are matched between model and full-scale. The Richardson number is important only where flows in a density stratified fluid are to be modeled which is not the case in the present investigation. The Weber number or ratio of surface tension to inertial forces is of no concern here since the flow field energy at typical towing speeds is very large compared with that associated with surface tension. The Knudsen, Prandtl, and Schmidt numbers deal with free molecule phenomena, heat transfer, and mass transfer, respectively and therefore can be safely disregarded within the scope of the subject model tests.

Time Scaling - the time scale of the model flow will of course be altered and will be simply related to full-scale time as follows:

$$\frac{\text{time (model scale)}}{\text{time (full scale)}} = \frac{b_m \times V_{fs}}{b_{fs} \times V_m}$$

where b_m and b_{fs} are the wing spans and V_m and V_{fs} are the flight speeds of the model and prototype, respectively. All nondimensional velocities in the flow fields (wake velocity divided by the aircraft speed) should be similar. All force and pressure coefficients should be identical for model and prototype as well as the Strouhal numbers for oscillatory motions (again providing model Reynolds numbers are sufficiently high). The above expression can be rewritten so that the equivalent full-scale distance in kilometers of the wake behind the generating aircraft can be expressed in terms of the model velocity V_m , linear ratio (b_{fs}/b_m) and time for the model wake to reach the velocity probes t_m

$$\text{Distance (d)} = \frac{t_{fs} V_{fs}}{1942} = \frac{t_m V_m}{1000} (b_{fs}/b_m) \text{ kilometers}$$

where V_{fs} is in knots and V_m is in meters per second.

APPENDIX B

DESCRIPTION OF FACILITIES AND TEST APPARATUS

(Figures 22 through 32)

Page intentionally left blank

The subject experimental investigation was conducted in the HYDRONAUTICS Ship Model Basin located in Laurel, Maryland. An outside view of the building which houses HSMB and adjoining shop is given in Figure 22. The towing basin has the following dimensions:

Length	95 meters
Width	8 meters
Water depth	4 meters

The HSMB is completely equipped with the apparatus and instrumentation necessary to conduct precision model tests to evaluate the hydrodynamic (or aerodynamic) characteristics and to study associated phenomena for a wide variety of vehicles or systems. The specific equipment used for the subject program is described in detail in the following sections.

Towing Carriage

The towing carriage of HSMB, shown by Figure 23, is powered by an electric-hydraulic drive system. The maximum speed of the carriage for conducting constant speed runs is 6 meters per second. The carriage has an open bay and associated handling equipment designed to accommodate a variety of different model support systems and test arrangements. An air-conditioned room located at one end of the carriage serves as the control center and houses a general purpose data acquisition and recording system.

Model Support System

The model support system used for the subject tests is shown in Figure 24. The assembly consists of a pair of faired tow struts which are rigidly attached with a predetermined spacing to a tilt table. A pad on the opposite end of each strut is used for attachment of the model. The tilt table is equipped with a pair of trunnion bearings which fit into the standard support bracket that is installed on vertical rails at one end of the carriage bay. The support bracket is equipped with a motorized screw-jack which is attached at one end of the table and is used to set pitch angles (angles of attack) on the model. In addition to the model, the table is used to support other apparatus such as the tanks used for the dye ejection system; the dye tubes and electrical lead wires for the force gages pass from the table to the model through the hollow support struts.

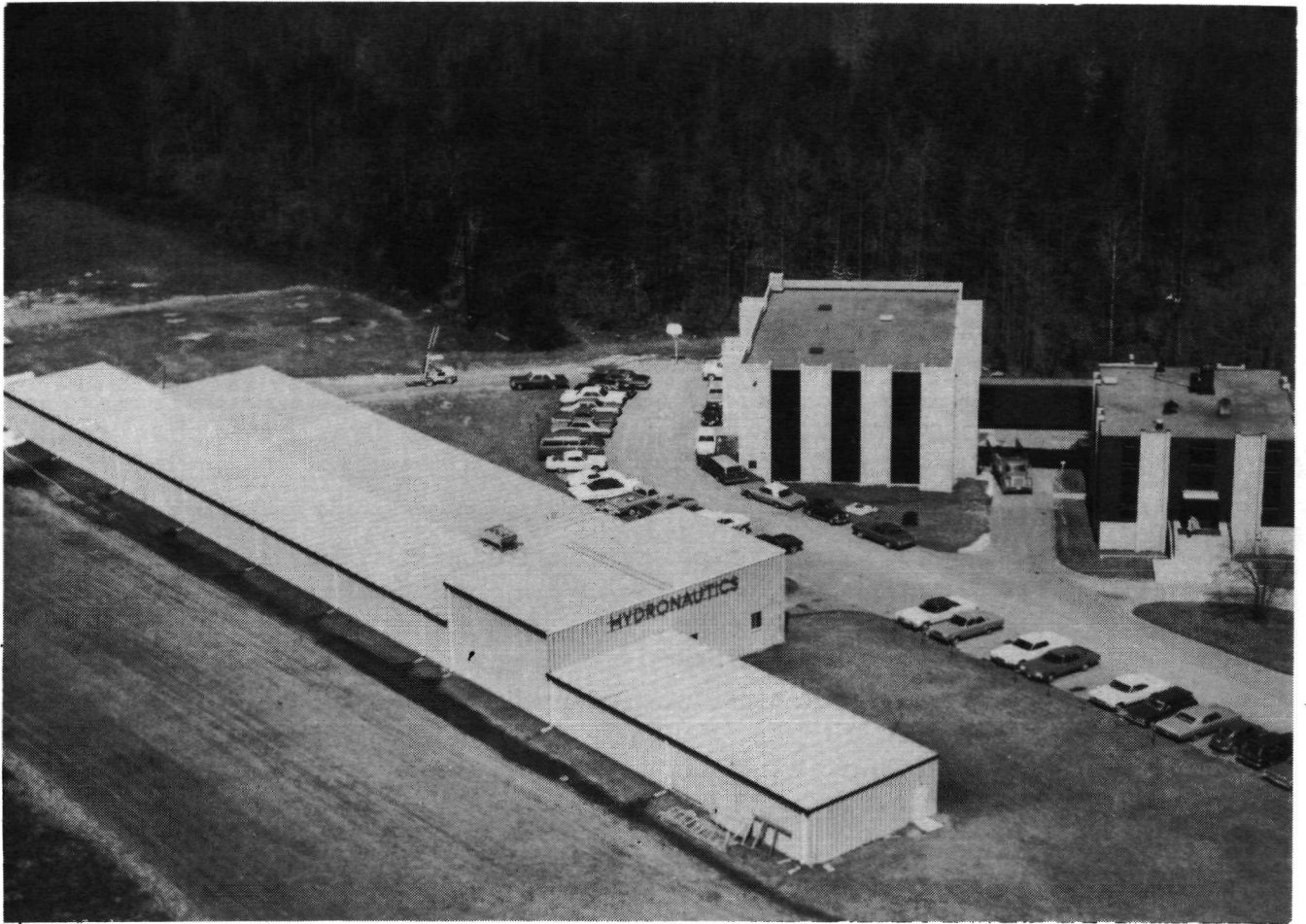


FIGURE 22 - VIEW OF HYDRONAUTICS SHIP MODEL BASIN



FIGURE 23 - HSMB® TOWING CARRIAGE WITH 747 AIRCRAFT MODEL INSTALLED FOR TESTING

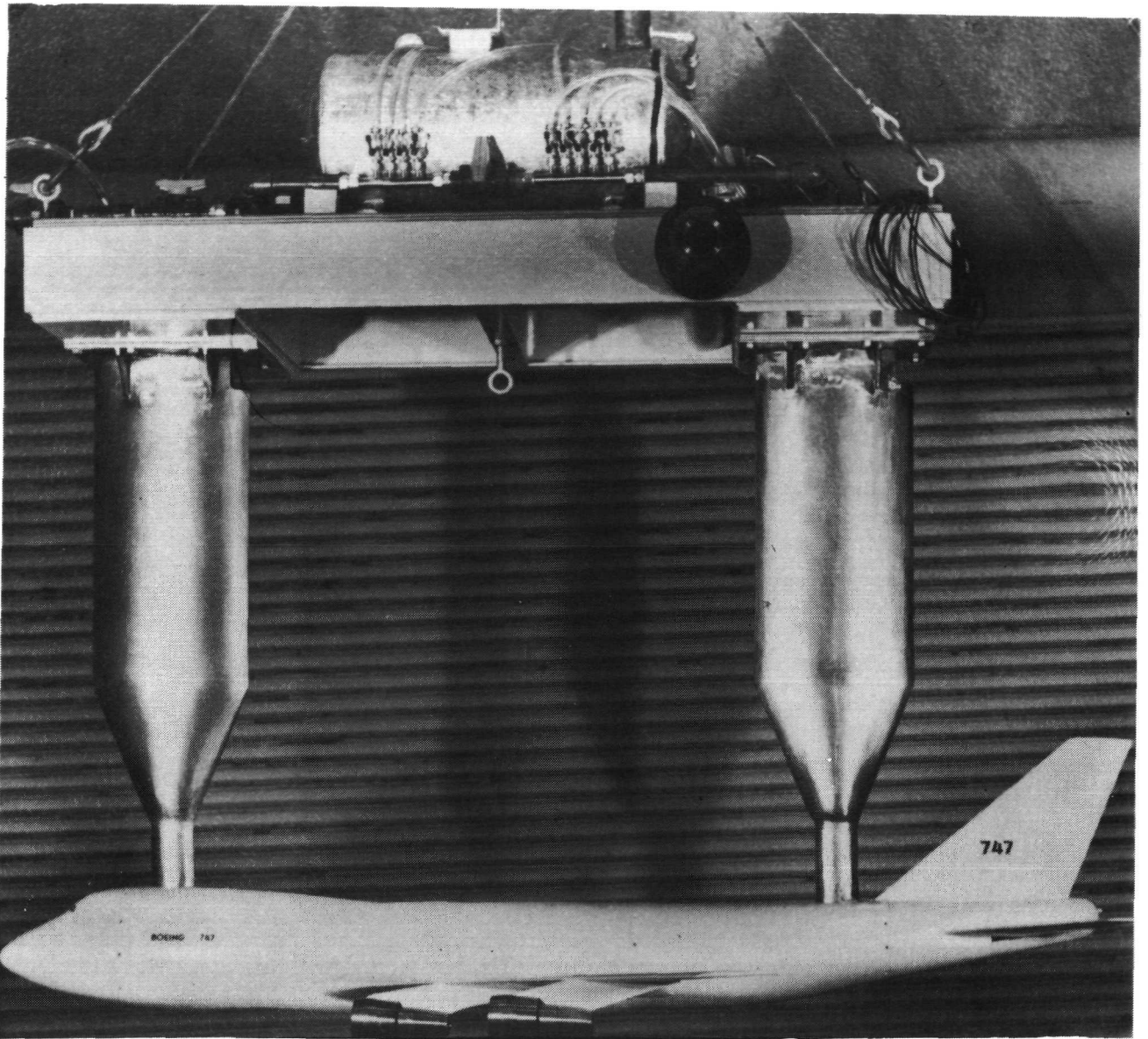


FIGURE 24 - AIRCRAFT MODEL SUPPORT SYSTEM

Force Measurement System

The system used to obtain force measurements on the aircraft model is shown schematically by Figure 25. The system consists of two modular or "block" gage assemblies attached as shown to a strong-back in the model fuselage and, in turn, to each of the two tow struts. The details of the block gage assemblies can be clearly seen in Figure 26. From the point of attachment in the model, each assembly includes block gages oriented to measure Z-force and X-force components with respect to the model body axes, and a precision ball bearing oriented in the pitch direction which connects the gages to the tow strut. With this arrangement, by analogy to a simply supported beam, each gage senses a component of the pure (momentless) reaction force exerted at the appropriate pitch bearing center. The reference point (origin of body axes) is taken as the quarter chord projected in the longitudinal centerplane of the fuselage. The total spacing between bearing centers (which are equidistant with respect to the reference point) was made equal to 1.245 meters on the subject model. Thus the total Z-force measured by the system is equal to the vector sum of the reaction forces sensed by the two Z-gages. The pitching moment M is equal to the vector difference of the two reaction Z-forces times half the spacing between bearing centers (or in this case 0.622 meters). The total X-force is equal to the vector sum of the two reaction X-forces, but since the reaction X-forces are aligned with the axis they do not contribute to the pitching moment. The totals of the Z- and X-force components can be resolved into lift C_L and drag C_D force components to follow the usual aerodynamic convention.

The HSMB standard 10.16-cm variable reluctance block gage used to make up the force measurement system is described in detail in Reference 18 and is shown in Figure 27. The individual block gage is a cube-shaped flexure box machined from a solid block of ARMCO Steel Corporation 17-4 PH stainless steel, a material selected for its practically zero mechanical hysteresis as well as its corrosion resistant properties. Each gage is sensitive to only a single component of force exerted in a direction normal to the flexural face of the cube; interaction effects from other force components or moments are practically nil. The relative movement of the flexures between the two struts and model is sensed electrically by a specially designed variable reluctance transducer which permits reliable and efficient operation when the gage is completely immersed in water. The measurement range of the individual block gages is governed by its spring constant or thickness of its flexures. In the present case, each Z-gage was designed for measurement range of 900 kg and each X-gage was designed for a measurement range of 225 kg.

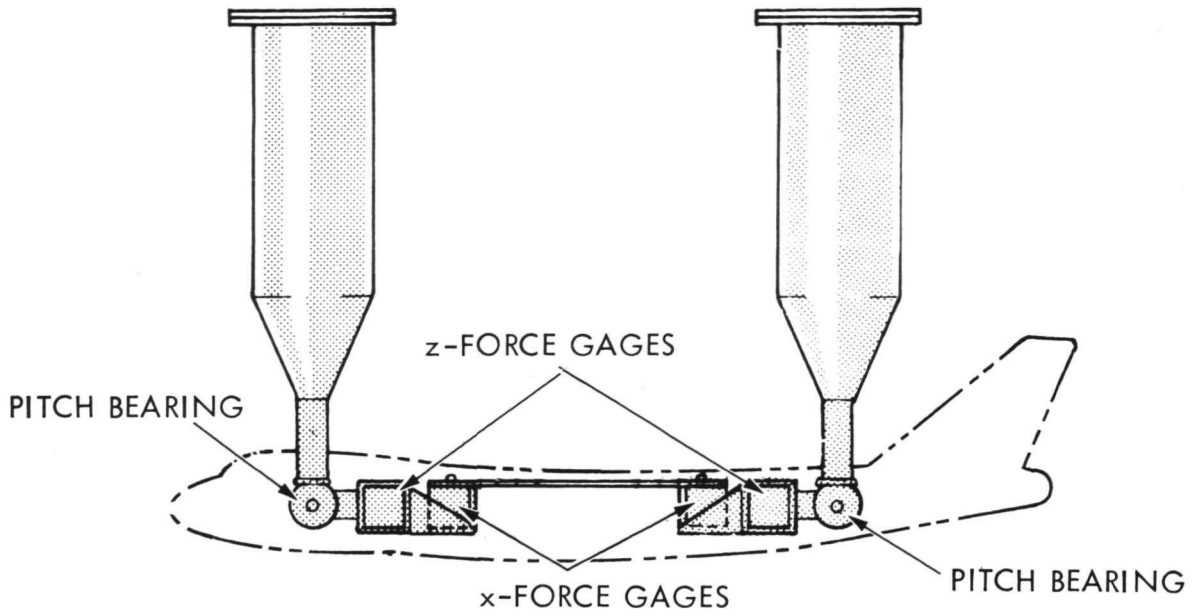
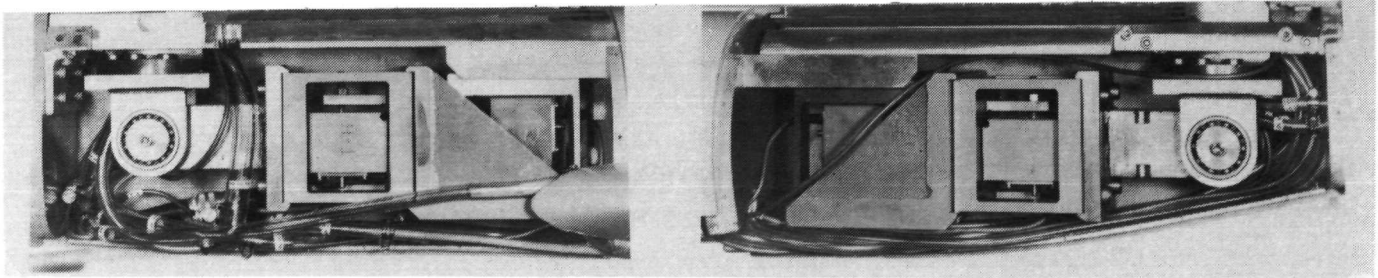


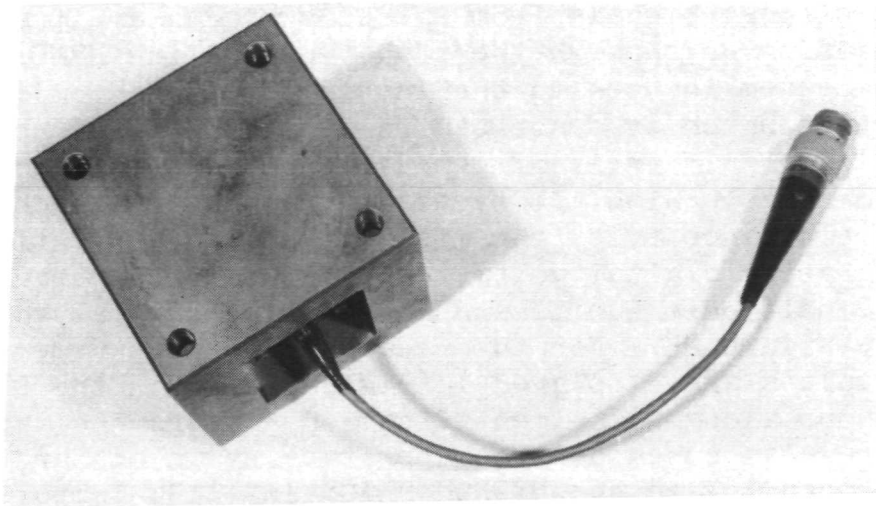
FIGURE 25 - SCHEMATIC SKETCH OF FORCE MEASUREMENT SYSTEM



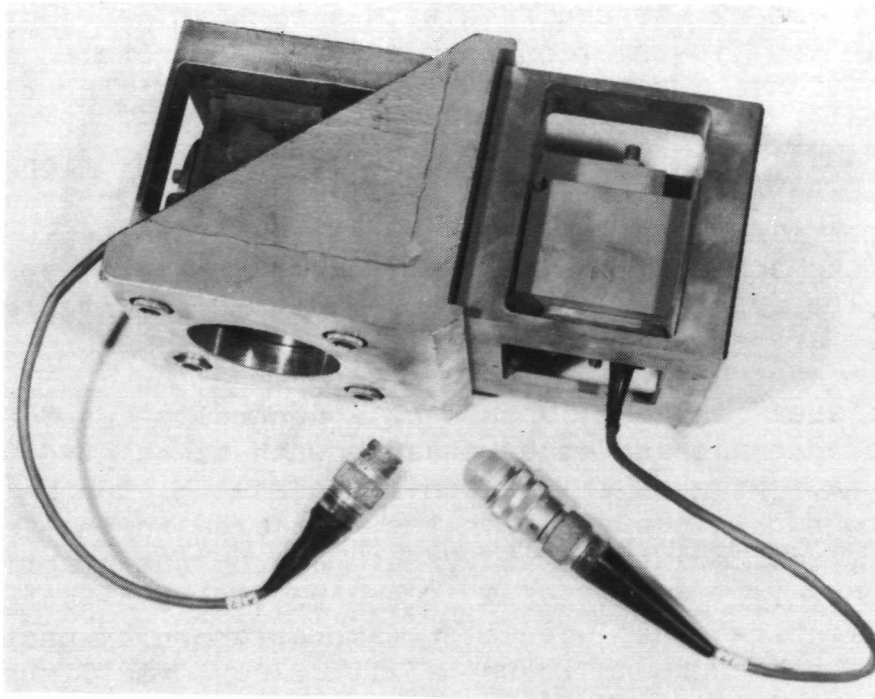
FORWARD BLOCK GAGE
COMPARTMENT

AFT BLOCK GAGE
COMPARTMENT

FIGURE 26 - BLOCK GAGE ASSEMBLIES IN MODEL



BASIC BLOCK GAGE MODULE



BLOCK GAGE ASSEMBLY

FIGURE 27 - CLOSE-UP OF BLOCK GAGES

The electrical signals from the block gages are transmitted by cables passing up through the tow struts to the HSMB Data Acquisition System located in the Instrumentation Room of the towing carriage, which is described in detail in Reference 19. The system consists of an array of general purpose signal conditioning equipment compatible with all types of transducers (such as strain gage type, reluctance type, thermistor type, and potentiometric type); integrating digital voltmeters; and recording equipment. The signal conditioning units and integrating digital voltmeters are shown in Figure 28. For the steady force measurements, the integrated values are displayed in digital form on the DVM's and are printed out along with identification numbers and carriage speed and are also punched into paper tape by an onboard Teletype for later processing in the HYDRONAUTICS IBM 1130 Computer Facility.

Flow Visualization System

To provide the necessary means for flow visualization, the Basic Aircraft model was equipped with a sophisticated dye-ejection system. Thirteen dye-ejection nozzles were distributed on the model as follows: six on the wing trailing edge, two at the tips of the horizontal tail, one in each engine nacelle and one at the after end of the body. Figure 29 shows some of these ejection nozzles. The nozzles were connected via internal ducts to a pressurized supply tank. Control manifolds and solenoid activated valves were used to release various combinations of continuous or pulsed dye traces from the model. The dye tanks and control manifolds mounted on the model support table are shown in Figure 30.

A "test area" in HSMB is used as a general means for obtaining photographic coverage and other measurements associated with various flow phenomena. Figure 31 is a schematic sketch showing the arrangement of photographic equipment in the test area which, for the subject program, was located about 37 meters from the starting end of the towing basin. The test area is equipped with a background grid, underwater lighting, and underwater cameras shown by photographs in Figure 32. The background is white with black grid lines forming 61-cm squares. Thirty-six underwater lights installed along one side of the test area provide the light necessary for time-sequence color underwater pictures. Two cameras (35 mm Nikon Model F with Nikkor UD Auto 1:3.5 F20 mm lens) are used, one mounted below the free surface looking down and the other at about mid-depth on one side. A motor drive permits simultaneous exposures to be made up to a maximum rate of four frames per second. The film magazines used have a capacity of 250 exposures of Ektachrome ER film 5250.

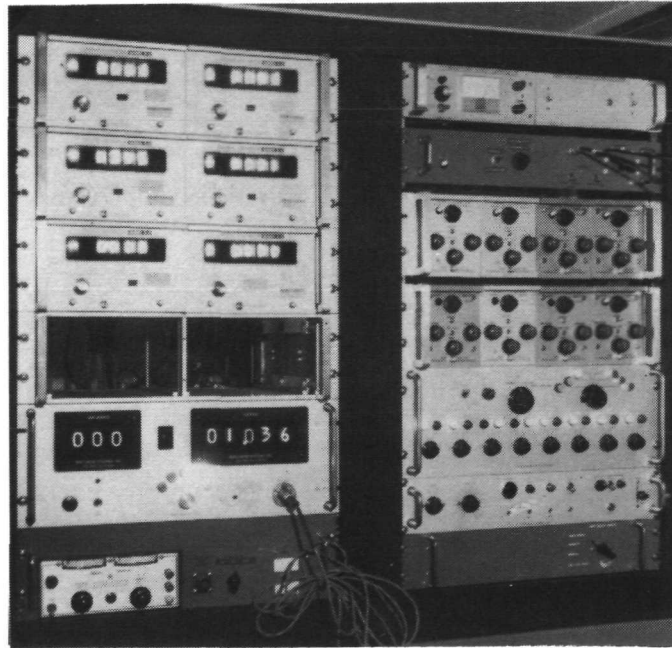
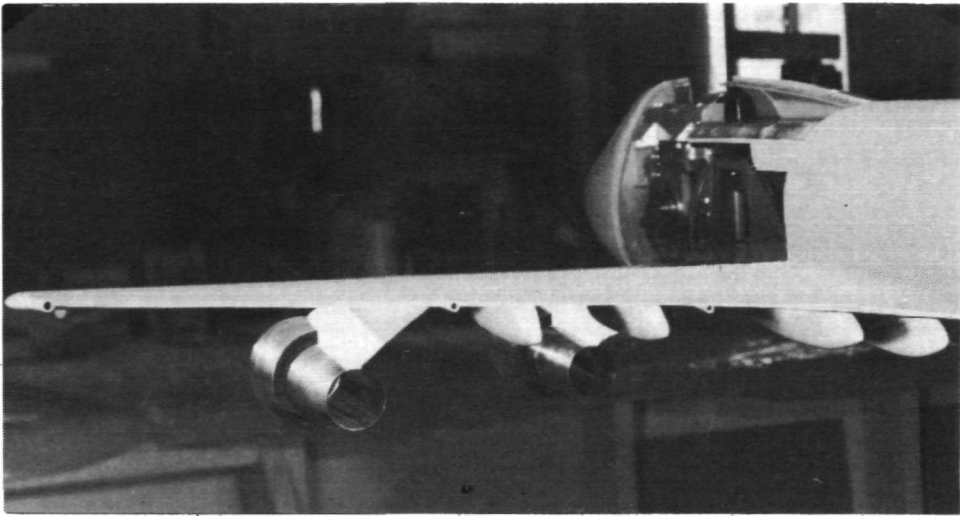
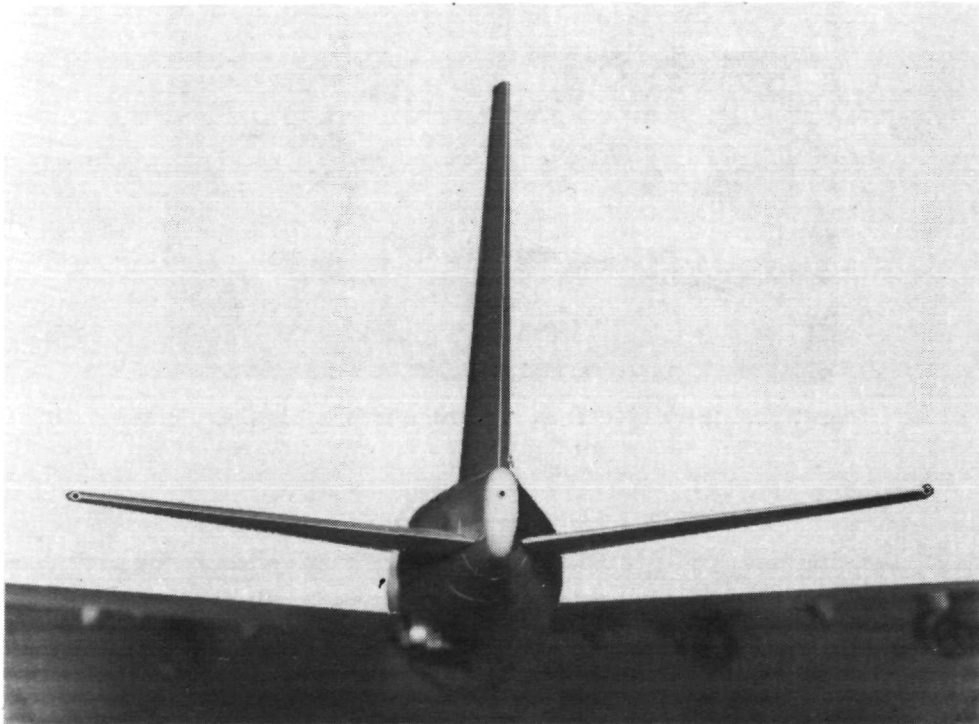


FIGURE 28 - SIGNAL CONDITIONING AND DVM UNITS



NOZZLES ON WING TRAILING EDGE



NOZZLES ON HORIZONTAL TAIL AND BODY CENTERLINE

FIGURE 29 - DYE-EJECTION NOZZLES INSTALLED ON
747 MODEL

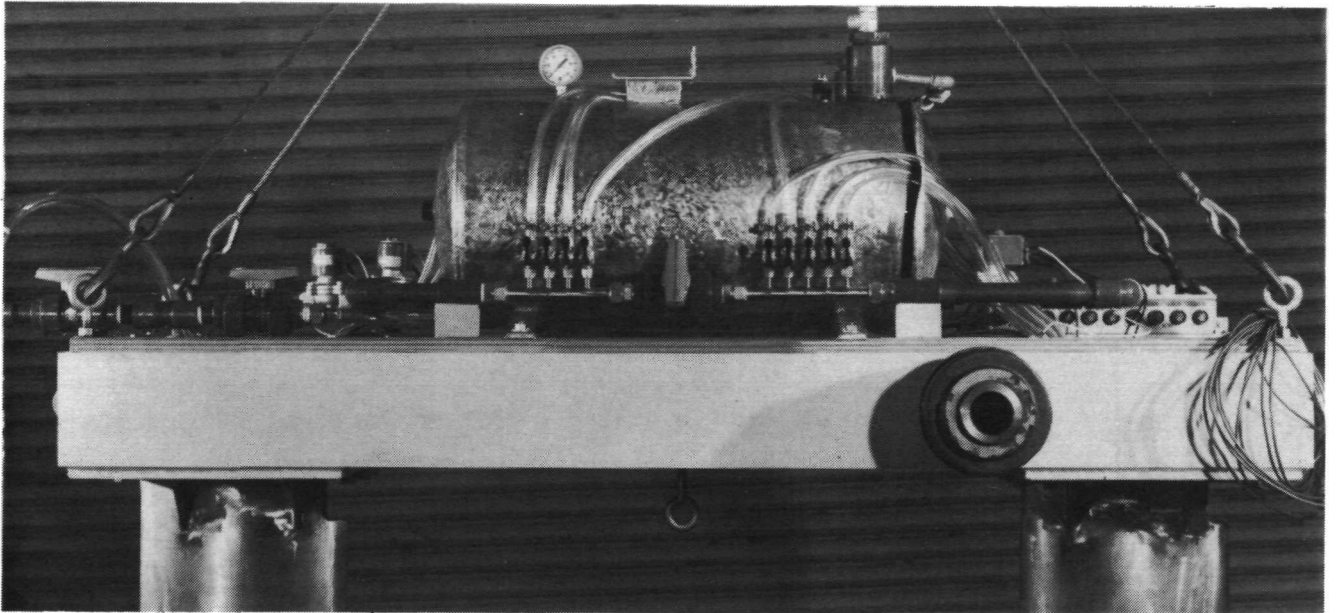


FIGURE 30 - DYE TANKS AND CONTROL MANIFOLDS

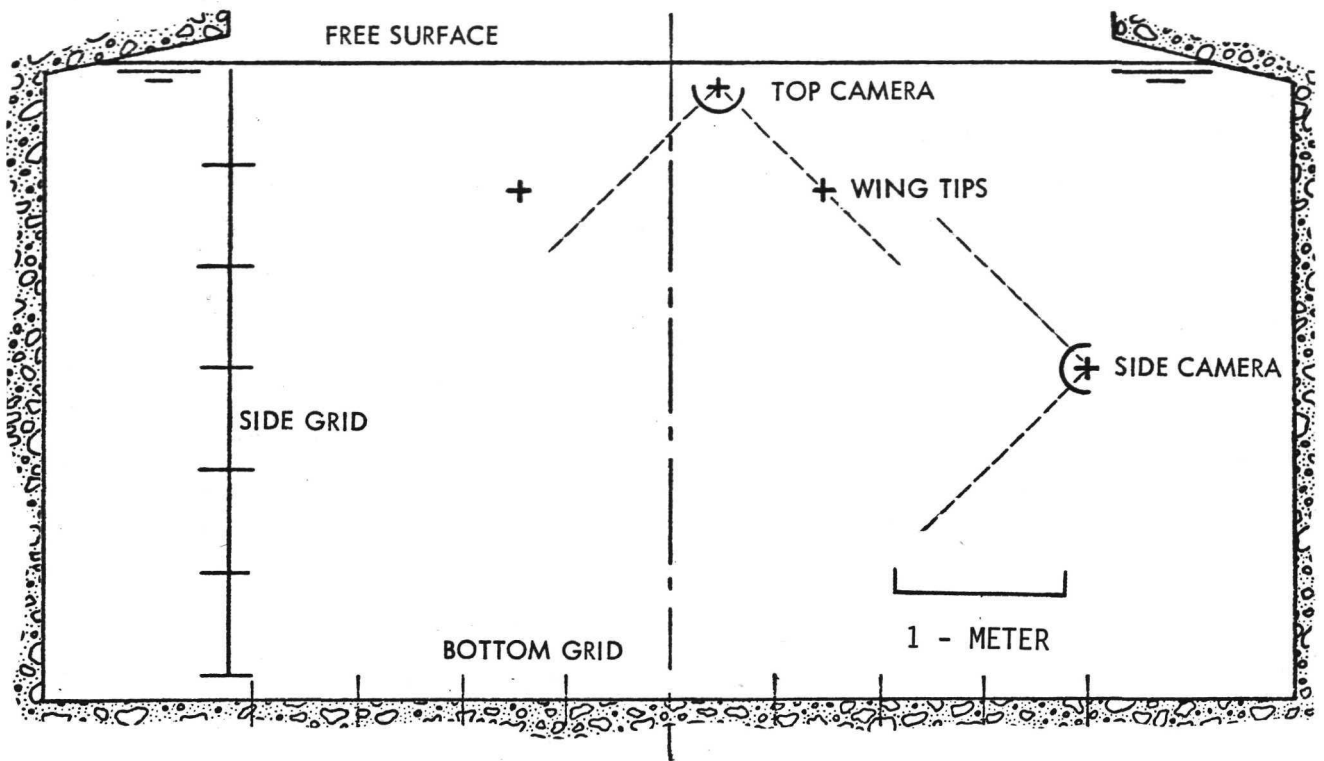


FIGURE 31 - CROSS SECTION OF TEST AREA SHOWING ARRANGEMENT OF PHOTOGRAPHIC EQUIPMENT

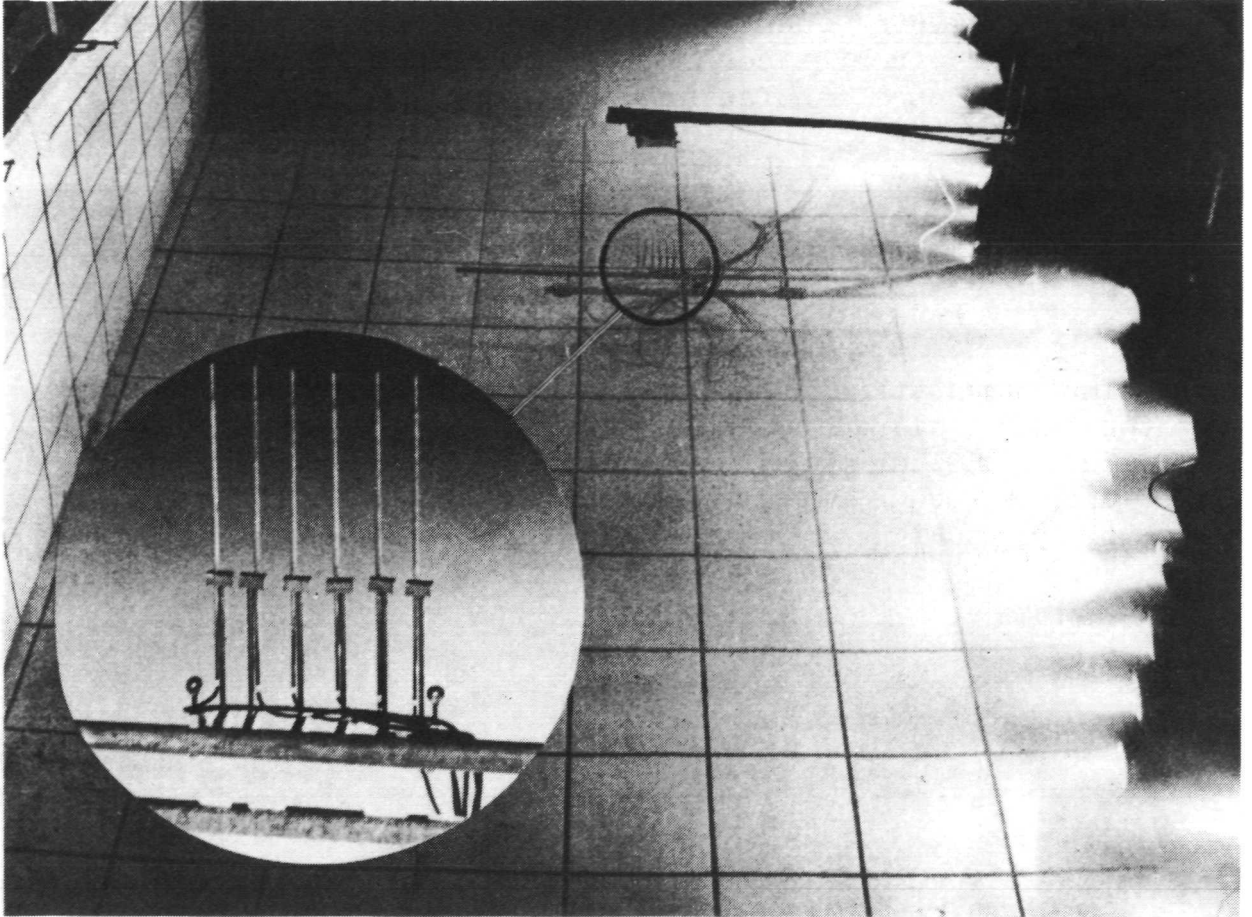


FIGURE 32 - TEST AREA WITH INSERT SHOWING CLOSE-UP VIEW OF HOT FILM ANEMOMETER PROBES

The cameras are encased in watertight boxes fitted with spherical lenses to correct for the difference in index of refraction between air and water.

Flow-Velocity Measuring Apparatus

A rake made up of six hot-film anemometer probes was used as the means for obtaining quantitative measurements of the tangential velocity around the vortex core. The individual probes are quartz-coated cylinder probes manufactured by Thermo Systems Inc. (TSI Model Number 1210-20W). The probes are spaced 4.13 cm center-to-center resulting in the rake of 20.65 cm length shown in the insert to Figure 32. The rake is mounted on a motor-driven positioning device which allows vertical adjustment for the test traverse, and also provides a means for insitu calibration and checking of probes.

The instrumentation used for controlling the probes and providing the output signals consists of TSI Model 1051-2 power supplies and TSI Model 1050A anemometers. Output signals are displayed and recorded upon a Techni Rite, Model TR 888, direct-writing paper-chart recorder located on shore adjacent to the test area.

APPENDIX C

TEST DATA SHOWING EFFECTIVENESS OF VORTEX-ATTENUATION DEVICES ON BOEING 747 AIRCRAFT IN CRUISE CONDITION

(Figures 33 through 44)

The data points are plotted nondimensionally as downwash velocity w/V versus spanwise distance from vortex-core center. They correspond to a nominal downstream distance of 4.42 kilometers for the full-scale generating aircraft operating at a lift coefficient $C_L = 0.4$ and a forward speed of 528 knots. The line superimposed in each figure is the vortex velocity distribution for the Basic Aircraft (without vortex-attenuation device) that is obtained for the same Cruise Condition using a modification of the Betz Theory (Ref. 12).

Page intentionally left blank

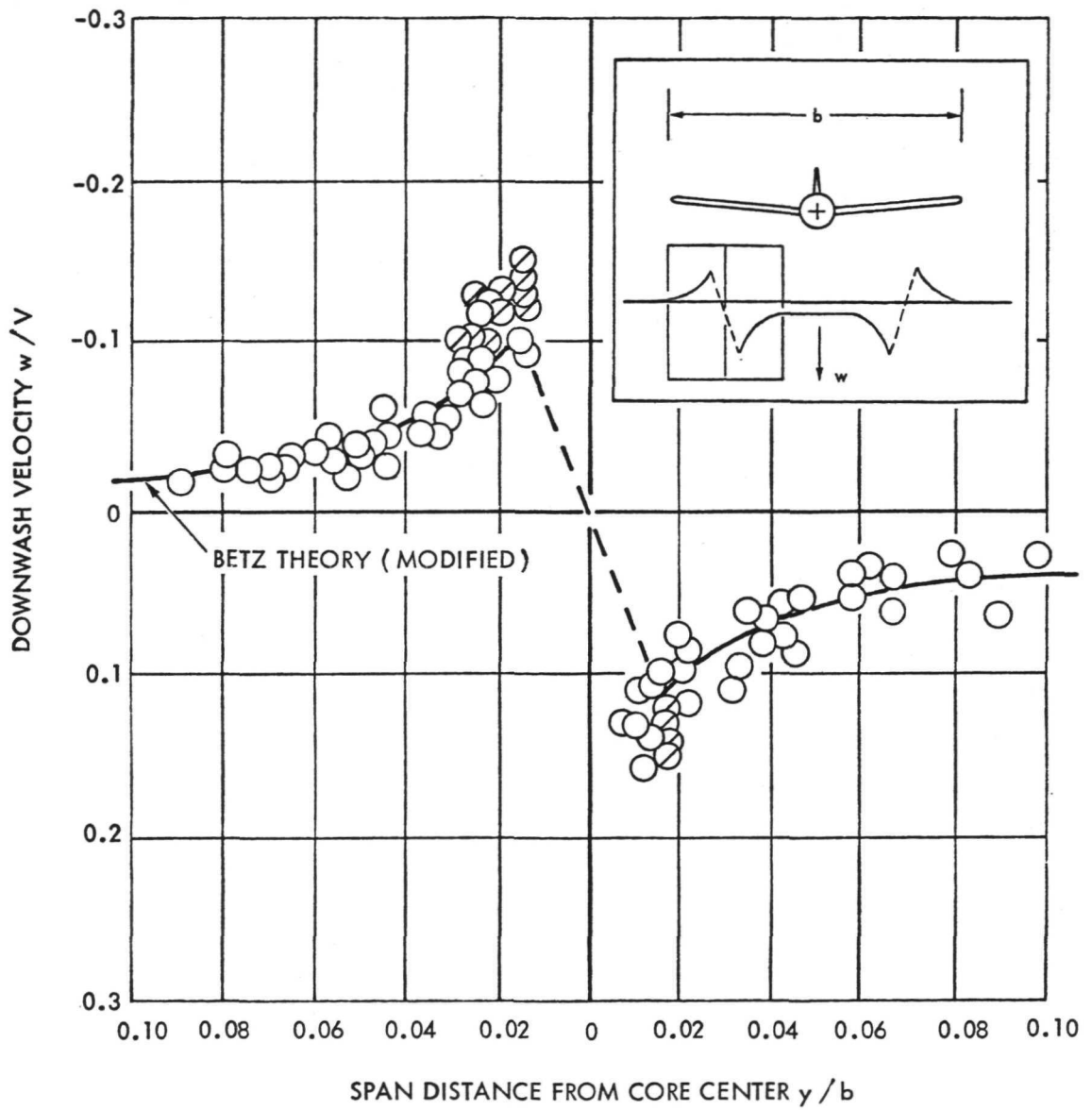


FIGURE 33 - VORTEX VELOCITY DISTRIBUTION FOR BASIC AIRCRAFT

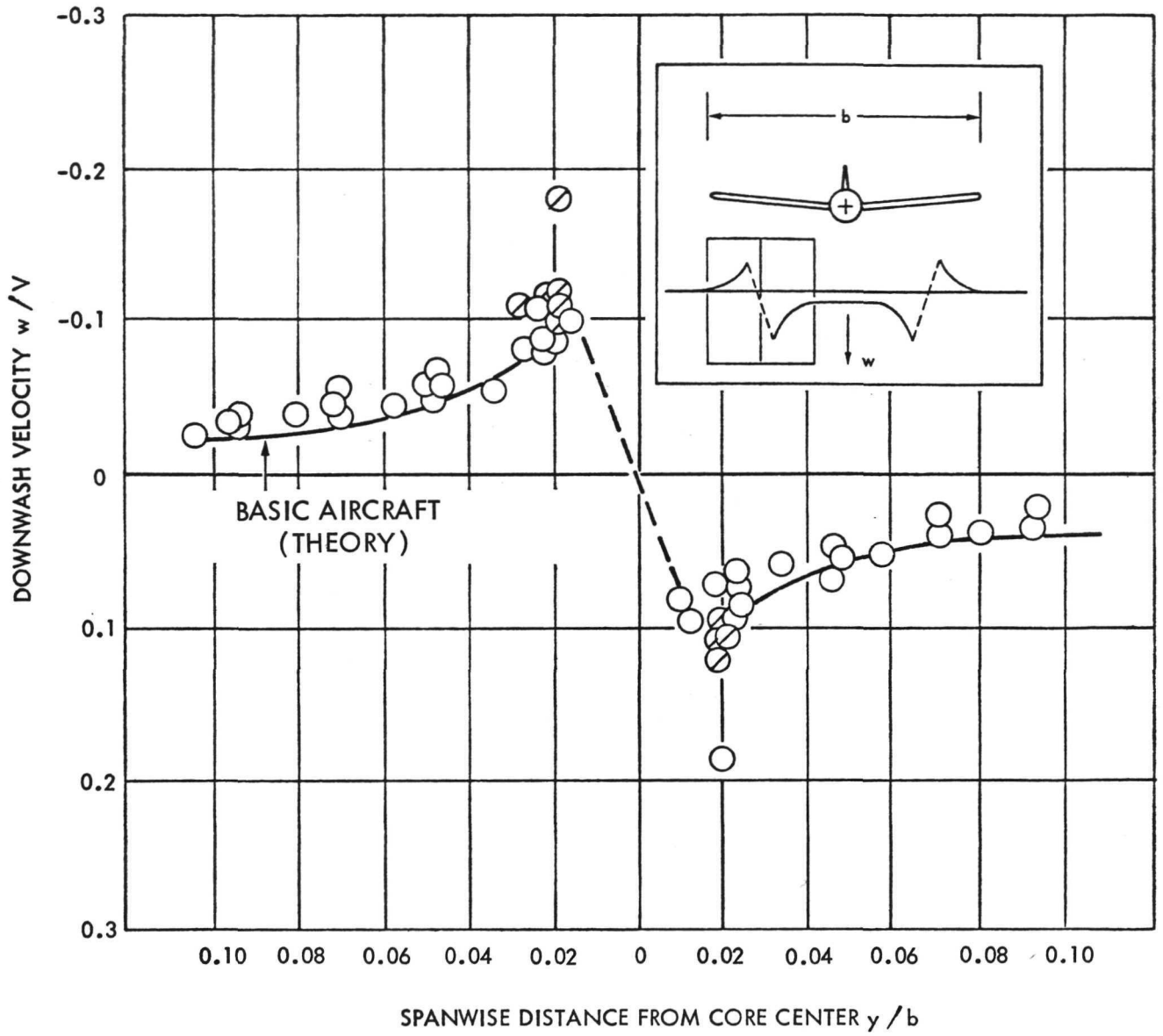


FIGURE 34 - EFFECT OF DEVICE A (FORWARD BLOWING JET) ON VORTEX VELOCITY DISTRIBUTION

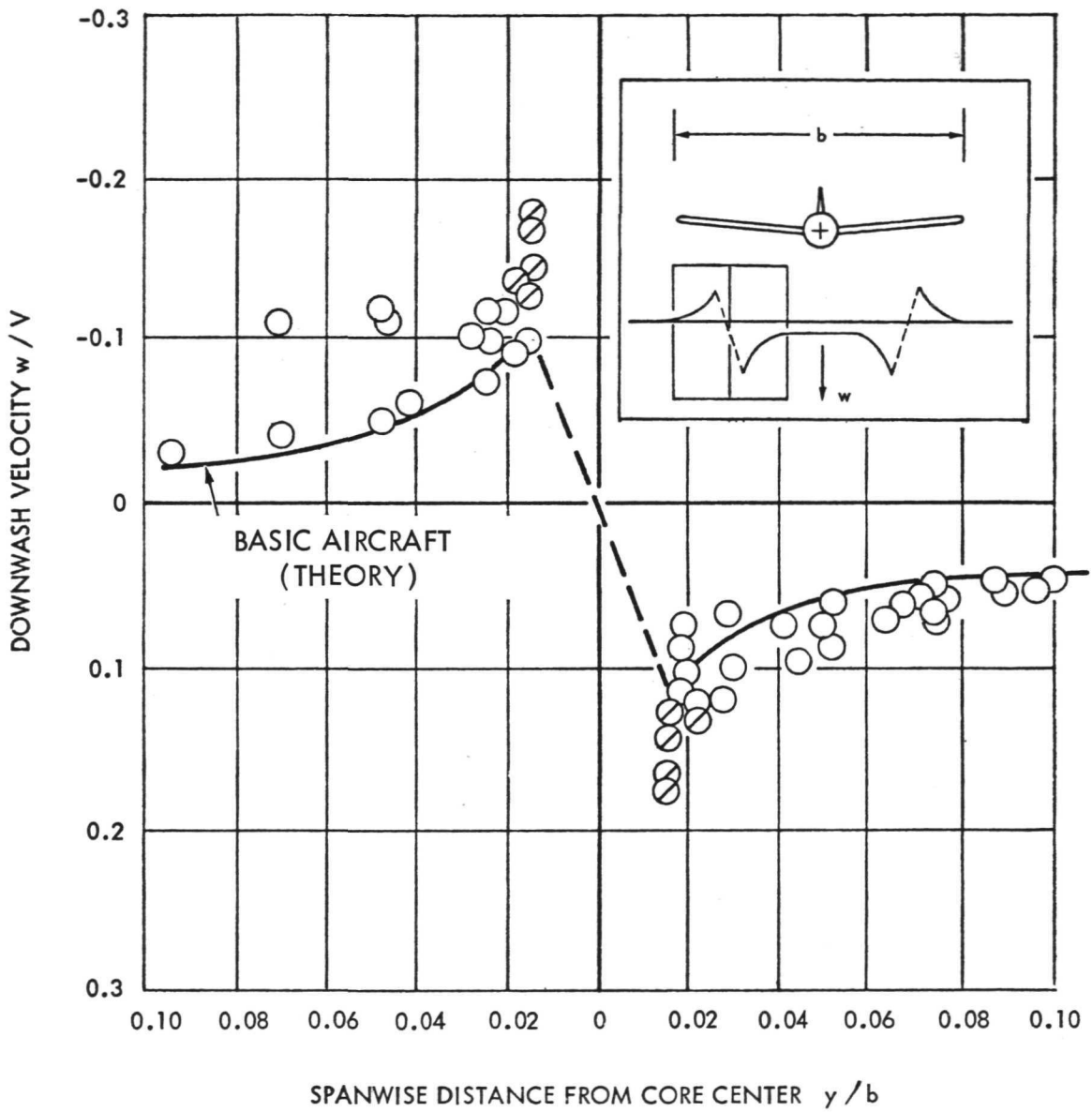


FIGURE 35 - EFFECT OF DEVICE B (DOWNWARD BLOWING JET) ON VORTEX VELOCITY DISTRIBUTION

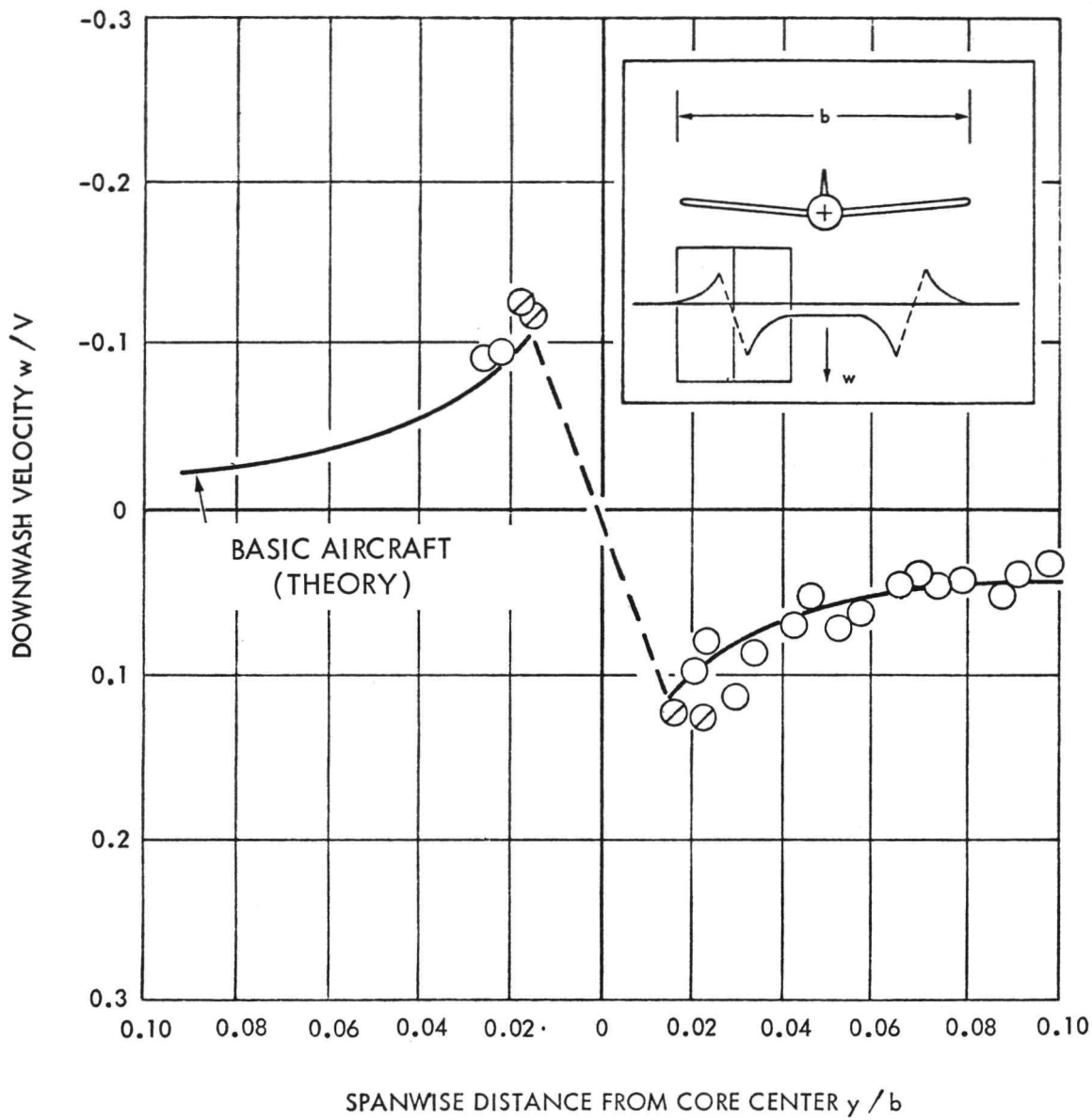


FIGURE 36 - EFFECT OF DEVICE C (REARWARD BLOWING JET) ON VORTEX VELOCITY DISTRIBUTION

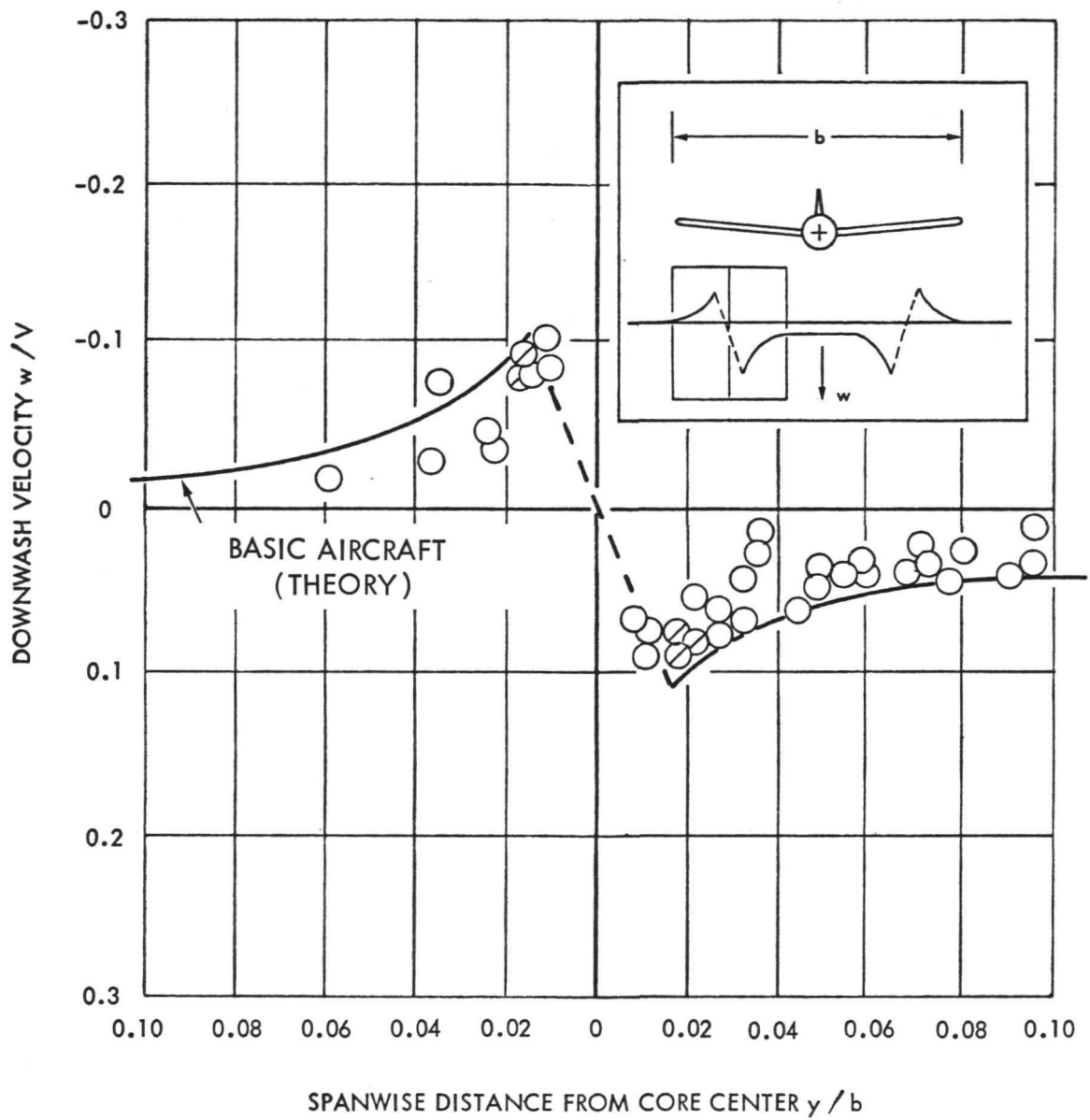


FIGURE 37 - EFFECT OF DEVICE D (DEFLECTED JET) ON VORTEX VELOCITY DISTRIBUTION

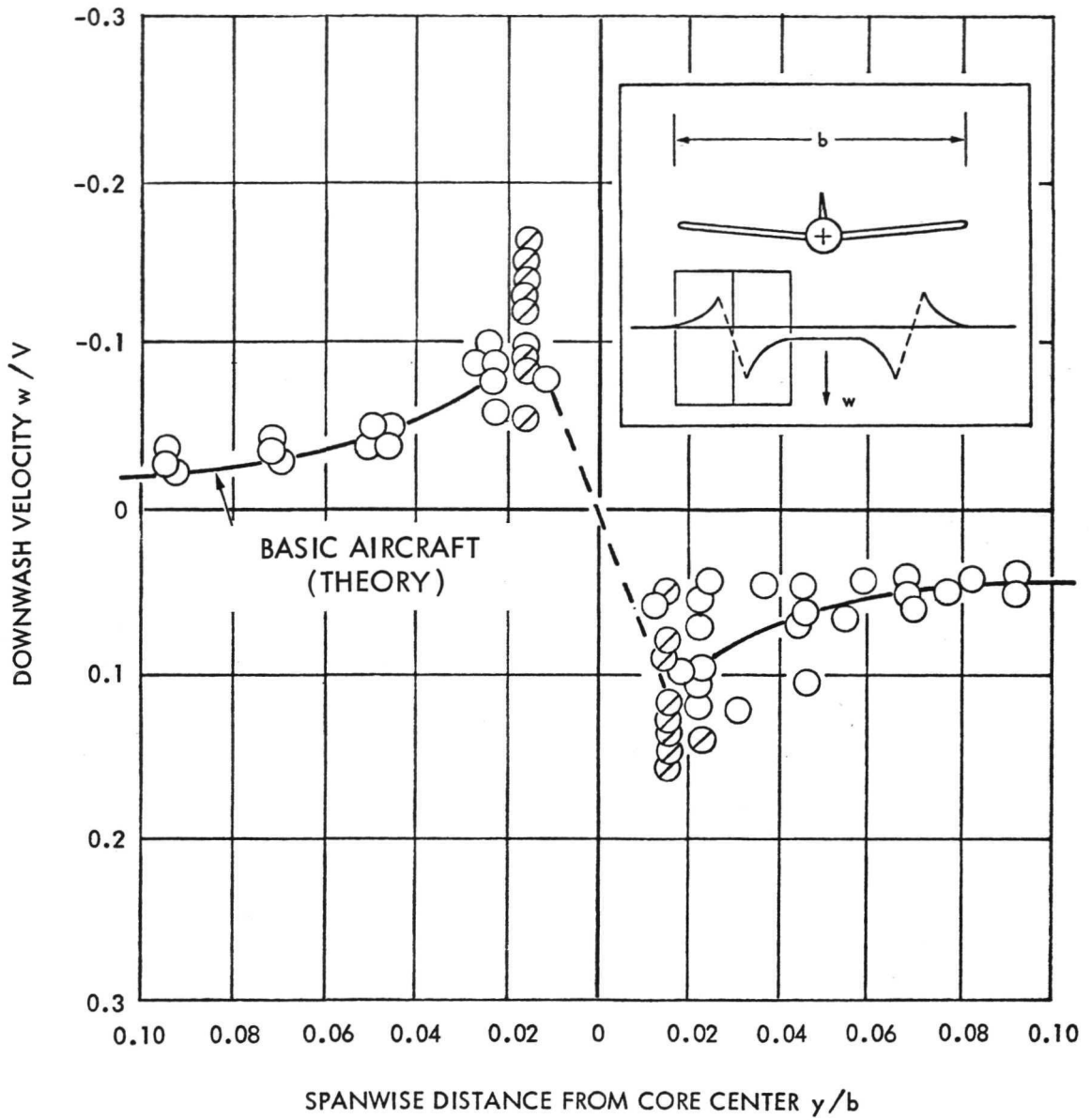


FIGURE 38 - EFFECT OF DEVICE E (JET FLAP) ON VORTEX VELOCITY DISTRIBUTION

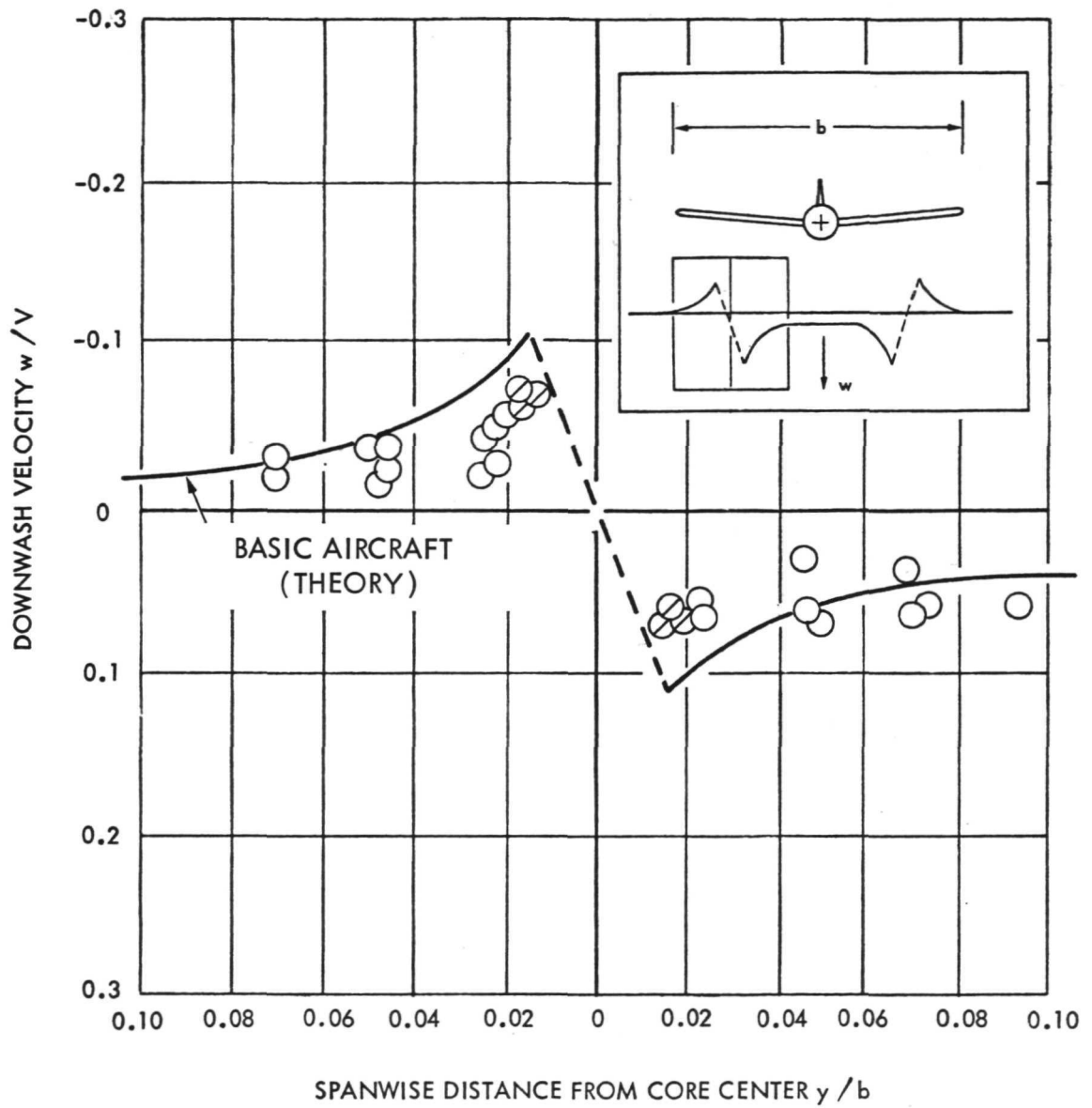


FIGURE 39 - EFFECT OF DEVICE F (BLOWN FLAP) ON VORTEX VELOCITY DISTRIBUTION

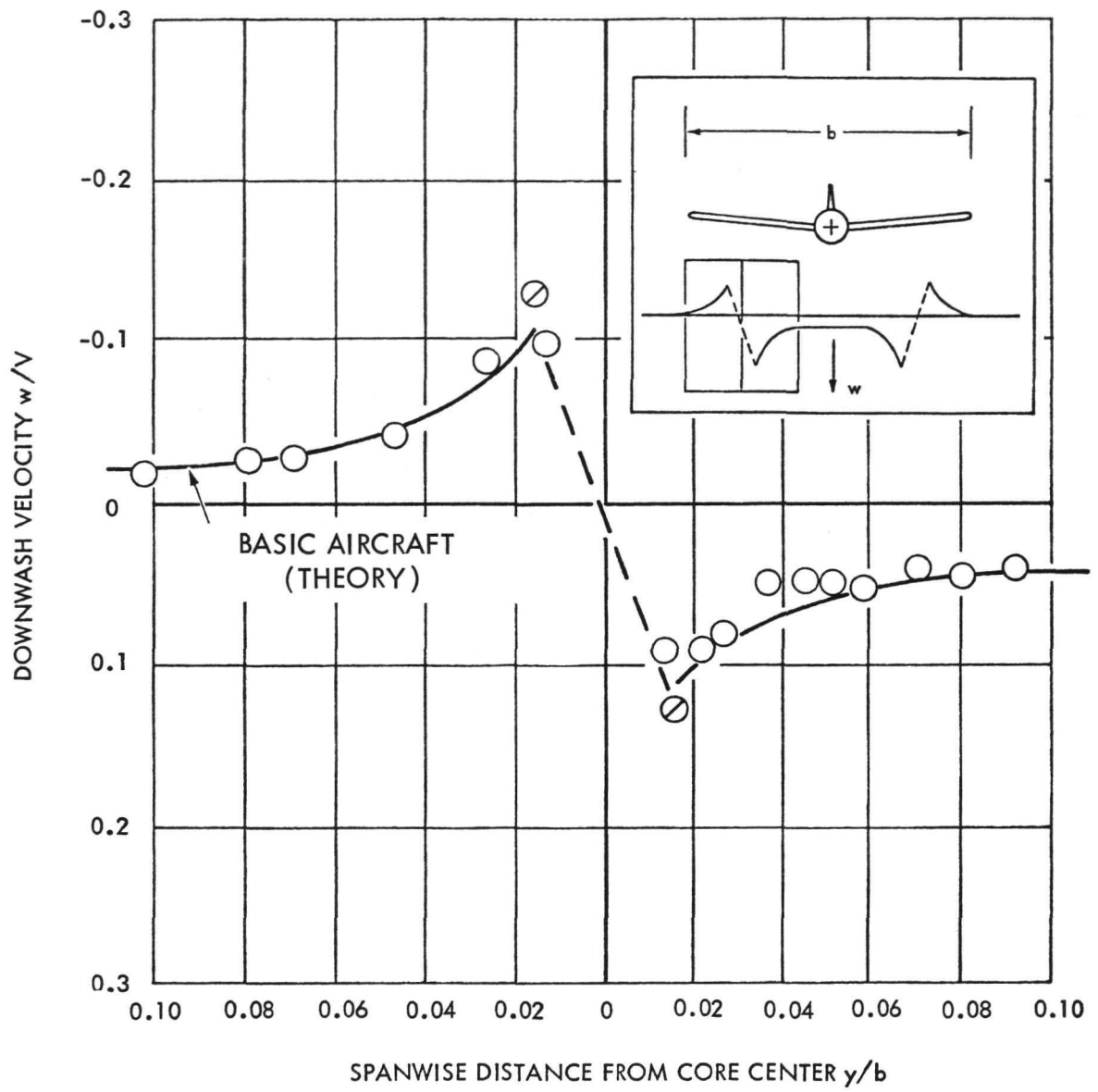


FIGURE 40 - EFFECT OF DEVICE G (CABLED DROGUE CONE) ON VORTEX VELOCITY DISTRIBUTION

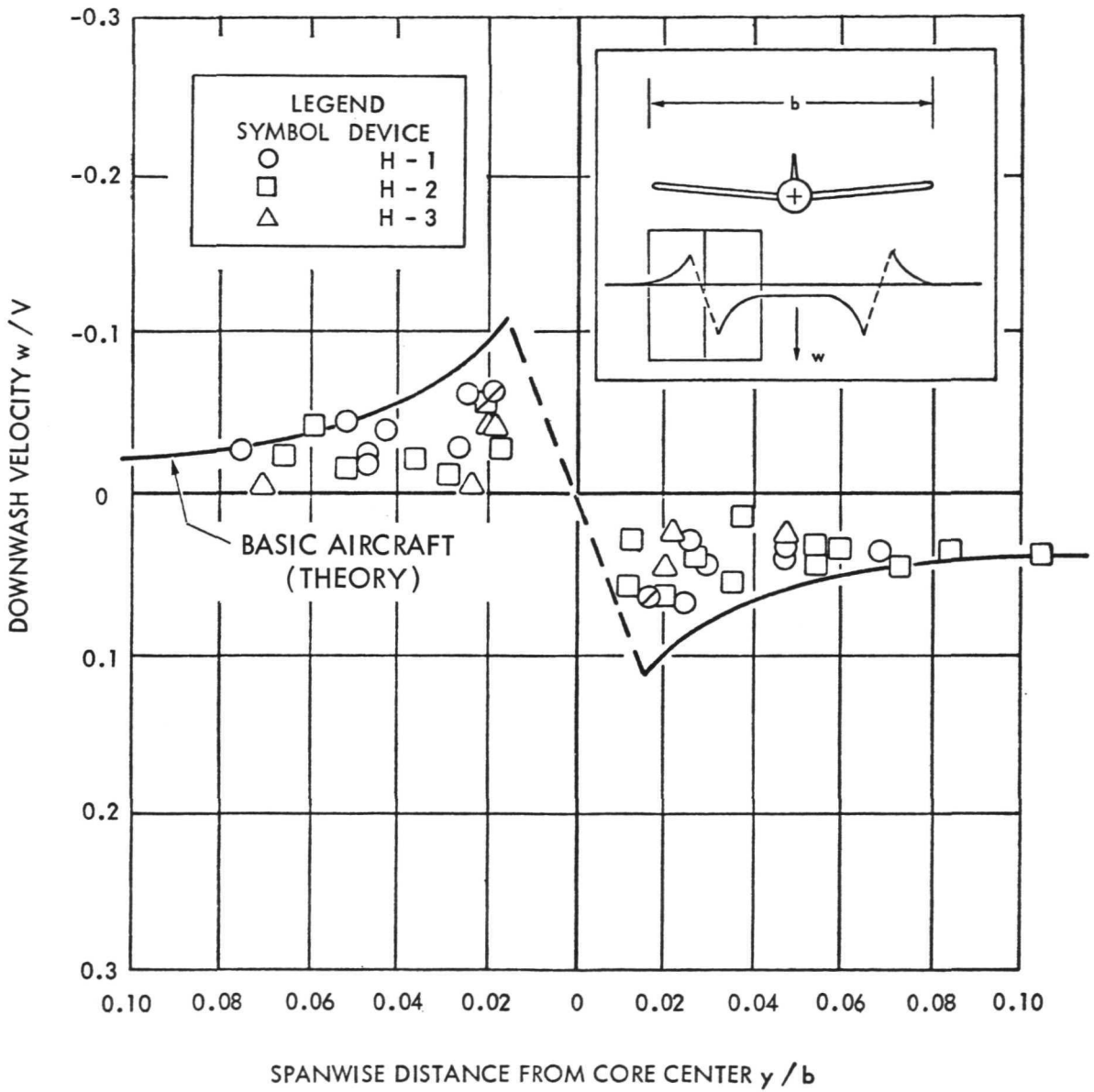


FIGURE 41 - EFFECT OF DEVICE H (SPLINES) ON VORTEX VELOCITY DISTRIBUTION

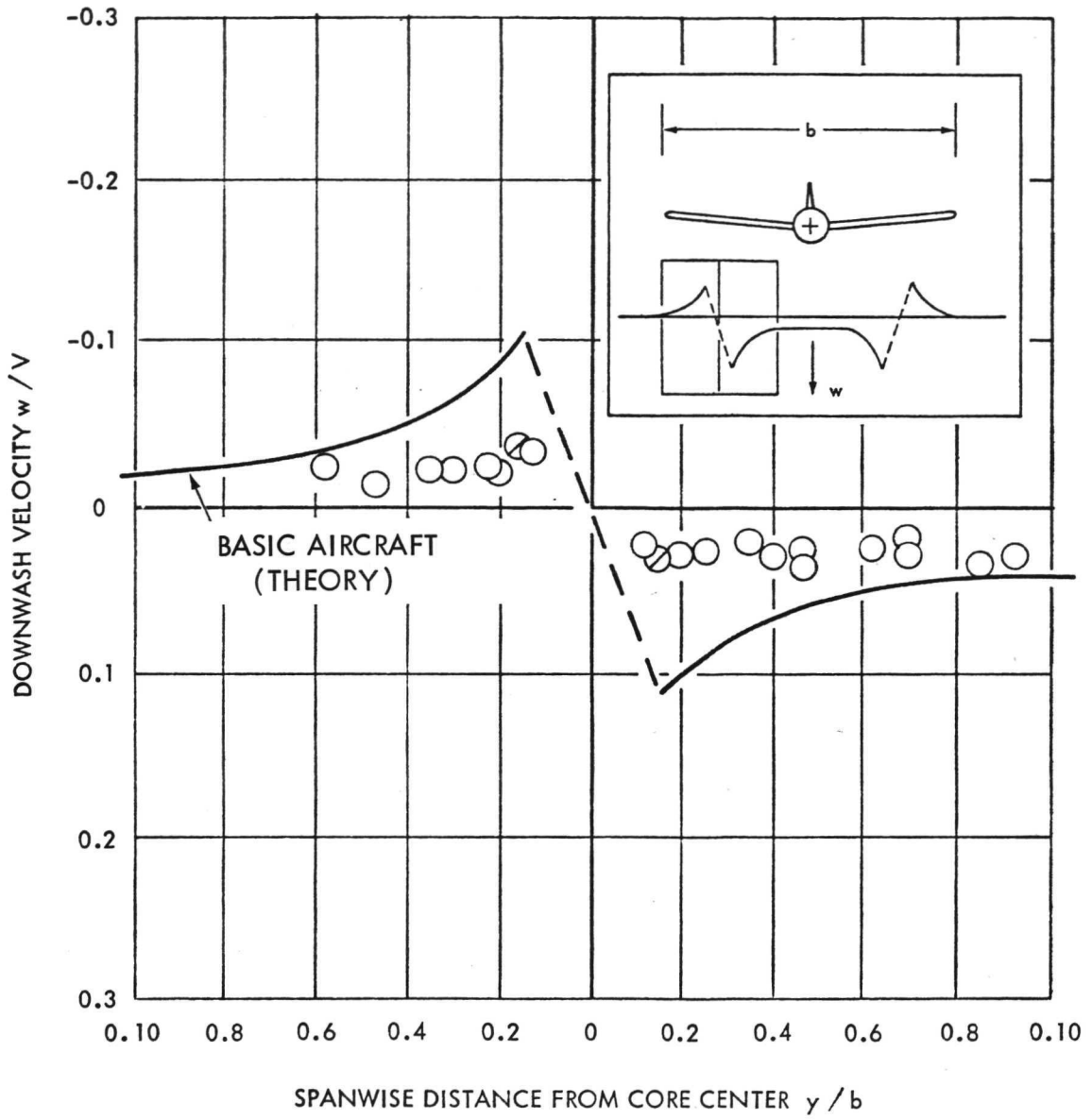


FIGURE 42 - EFFECT OF DEVICE I (VORTEX GENERATOR) ON VORTEX VELOCITY DISTRIBUTION

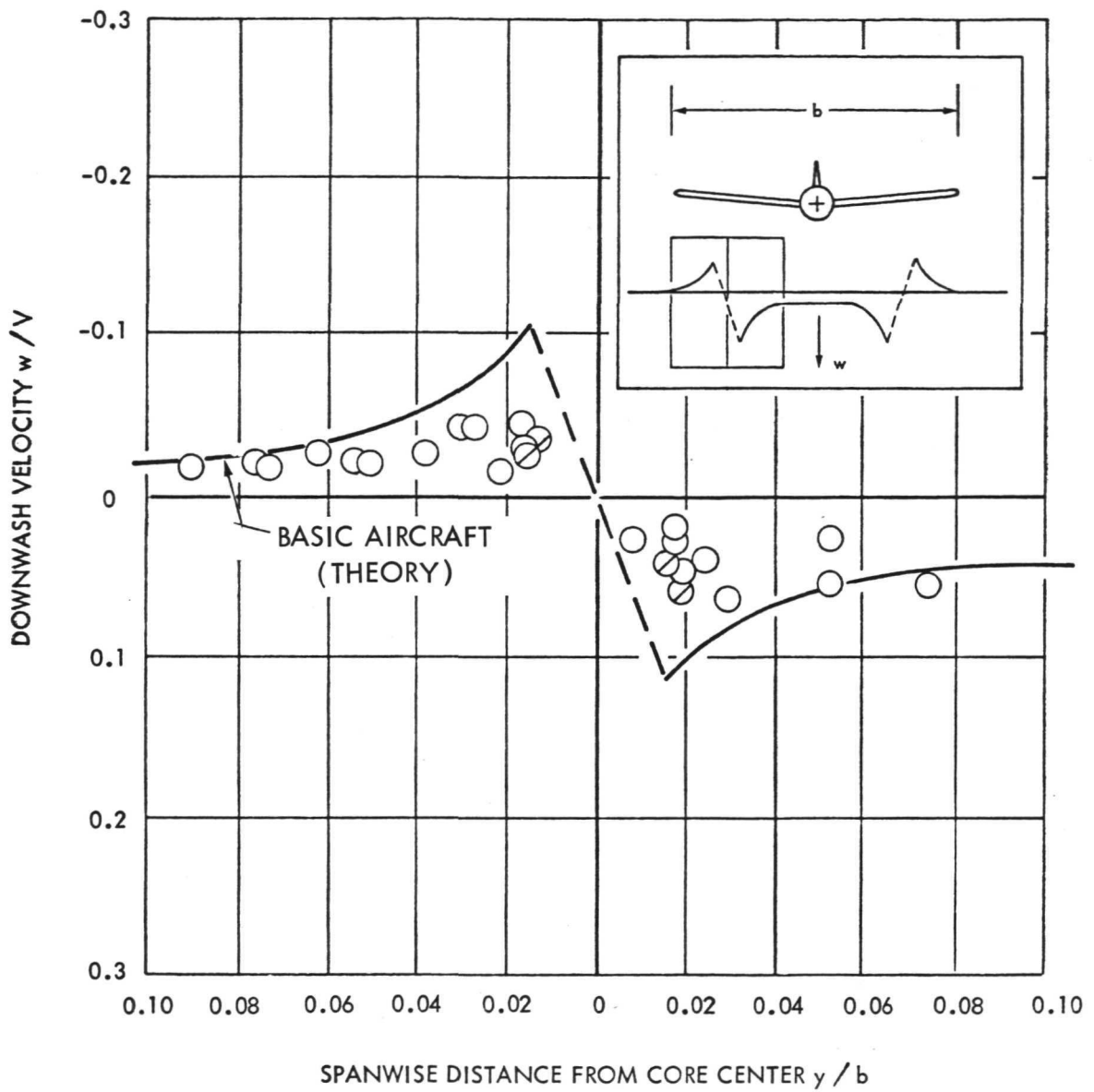


FIGURE 43 - EFFECT OF DEVICE J (SPOILER DISSIPATOR) ON VORTEX VELOCITY DISTRIBUTION

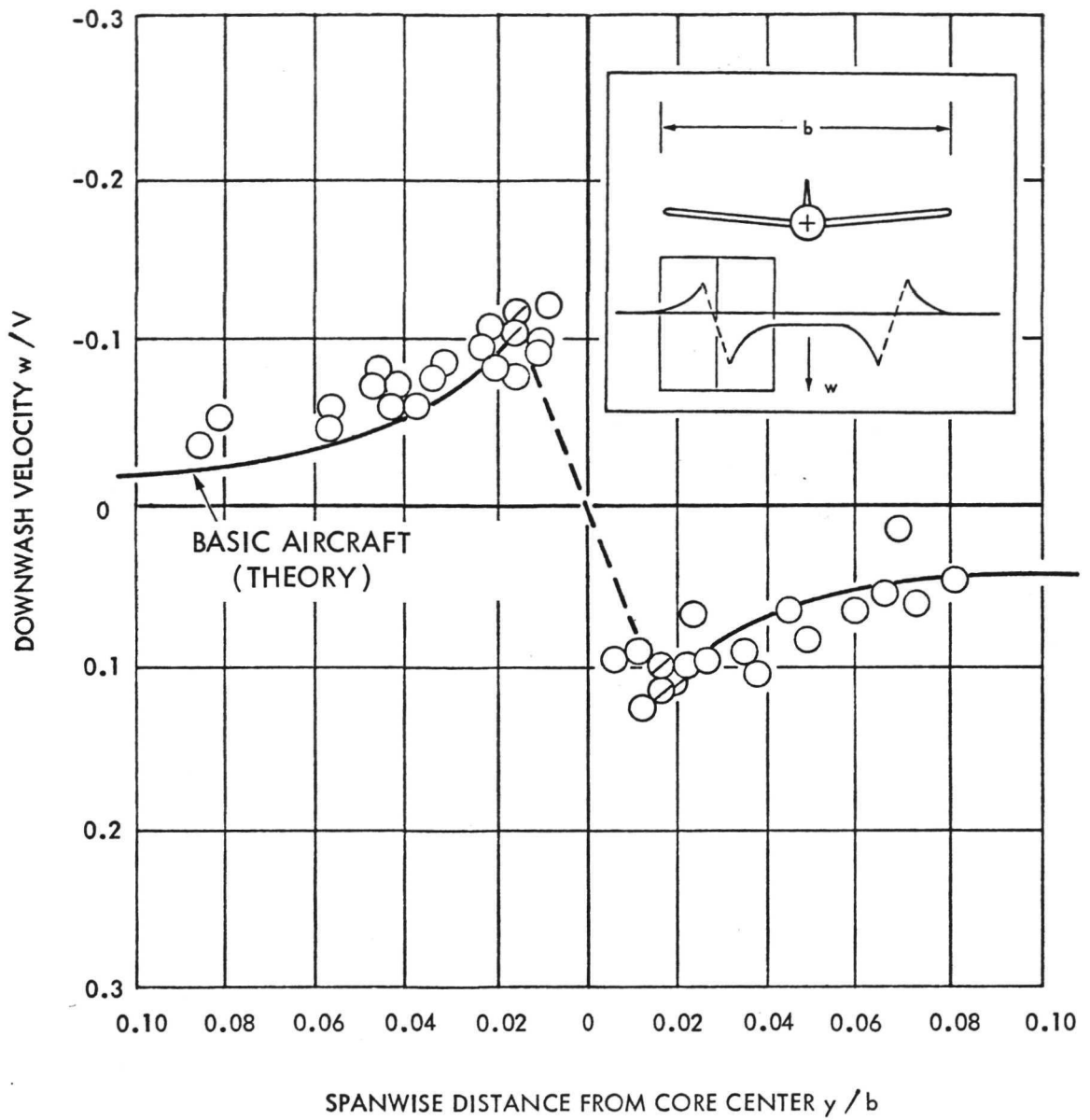


FIGURE 44 - EFFECT OF DEVICE K (TRAILING EDGE FLAP) ON VORTEX VELOCITY DISTRIBUTION

APPENDIX D

TEST DATA SHOWING EFFECTIVENESS OF VORTEX- ATTENUATION DEVICES ON BOEING 747 AIRCRAFT IN FLAPS-30 CONDITION

(Figures 45 through 48)

The data points are plotted nondimensionally as downwash velocity w/V versus spanwise distance from vortex-core center. They correspond to a nominal downstream distance of 2.25 kilometers for the full-scale generating aircraft operating at a lift coefficient $C_L = 1.2$ and a forward speed of 105 knots. The line superimposed in each figures is the vortex velocity distribution for the Basic Aircraft (without vortex-attenuation device) that is obtained for the same Flaps-30 Condition using a modification to the Betz Theory (Ref. 12).

Page intentionally left blank

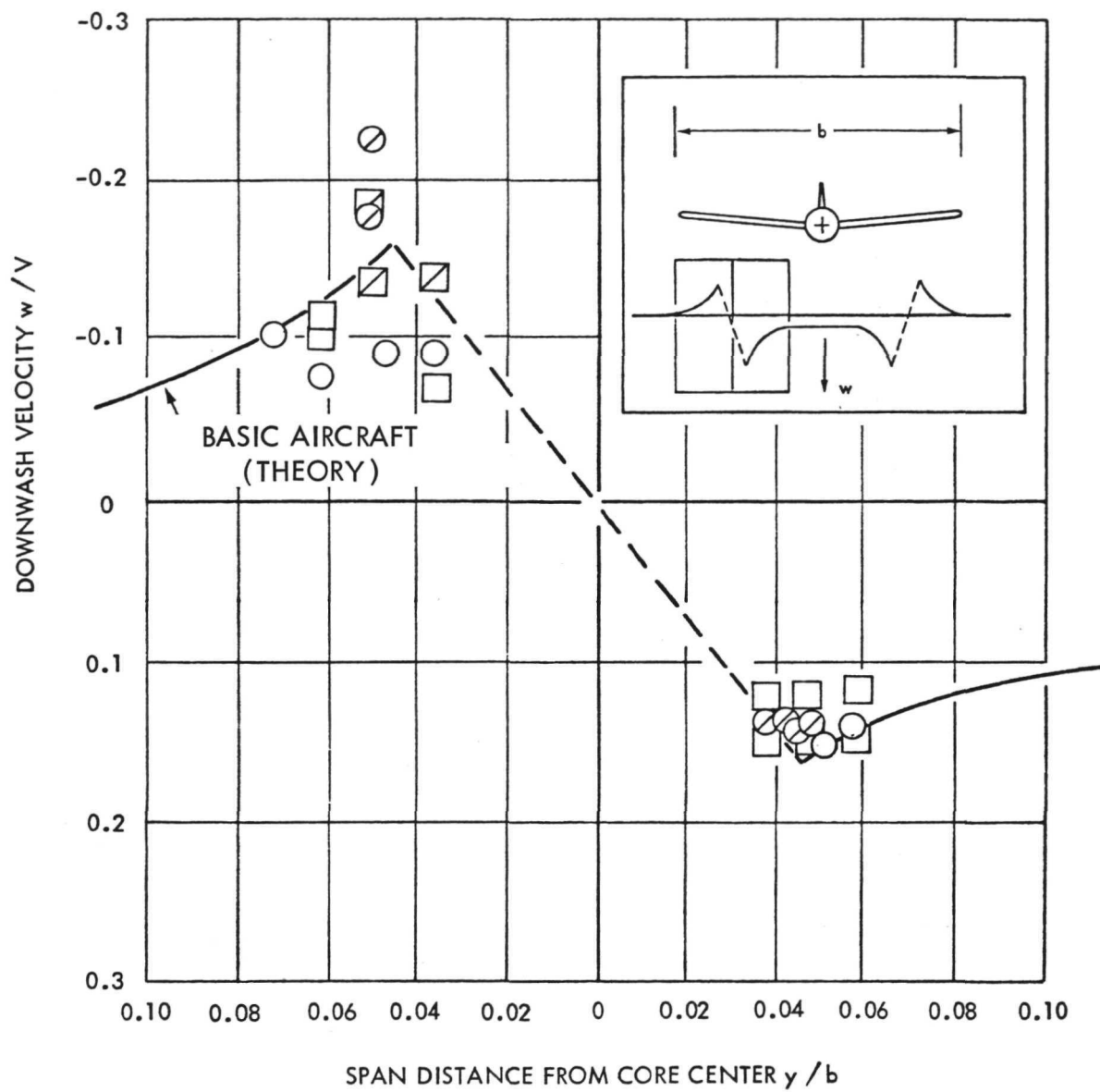


FIGURE 46 - EFFECT OF DEVICE H (SPLINES) ON VORTEX VELOCITY DISTRIBUTION

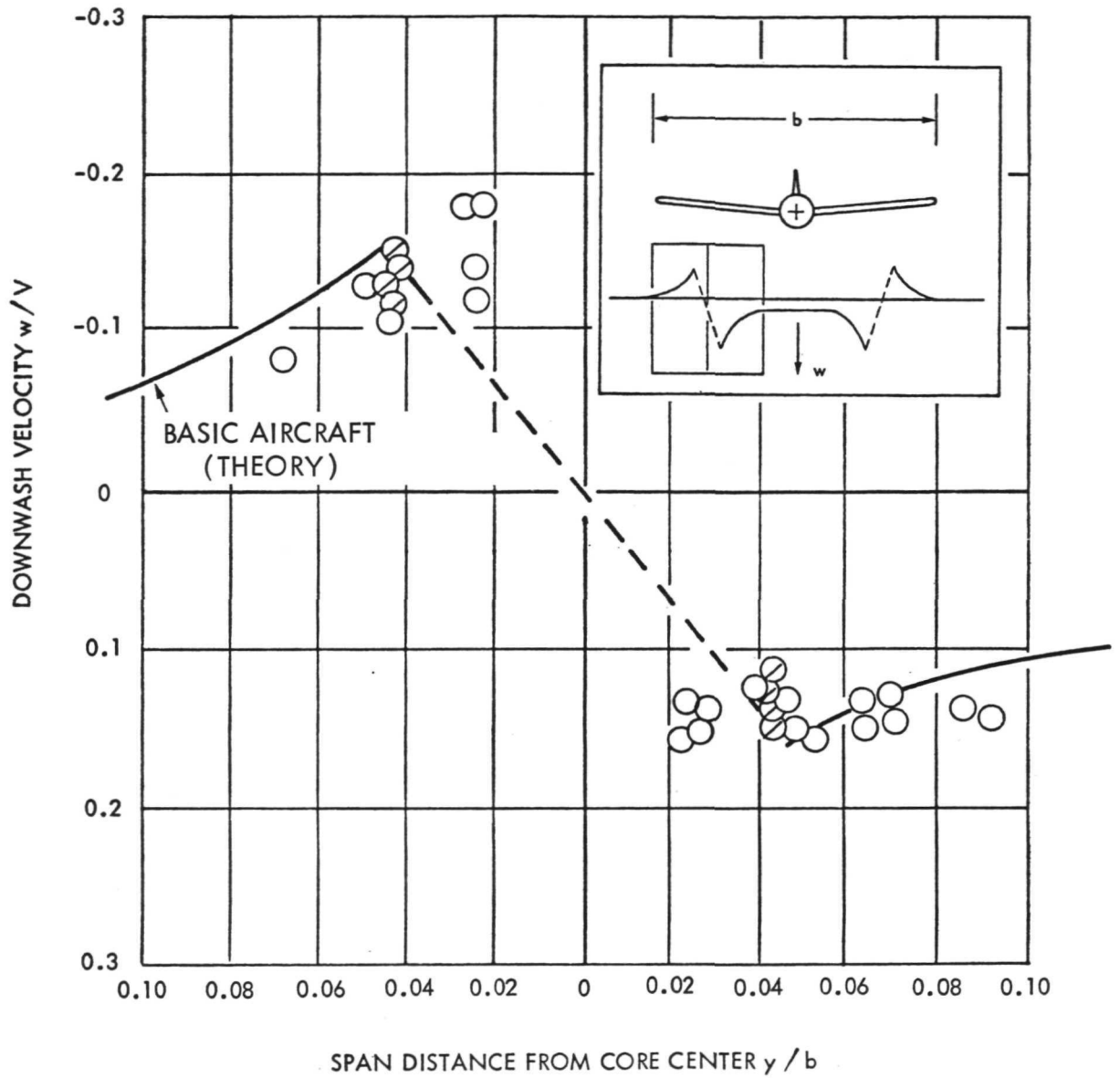


FIGURE 47 - EFFECT OF DEVICE I (VORTEX GENERATOR) ON VORTEX VELOCITY DISTRIBUTION

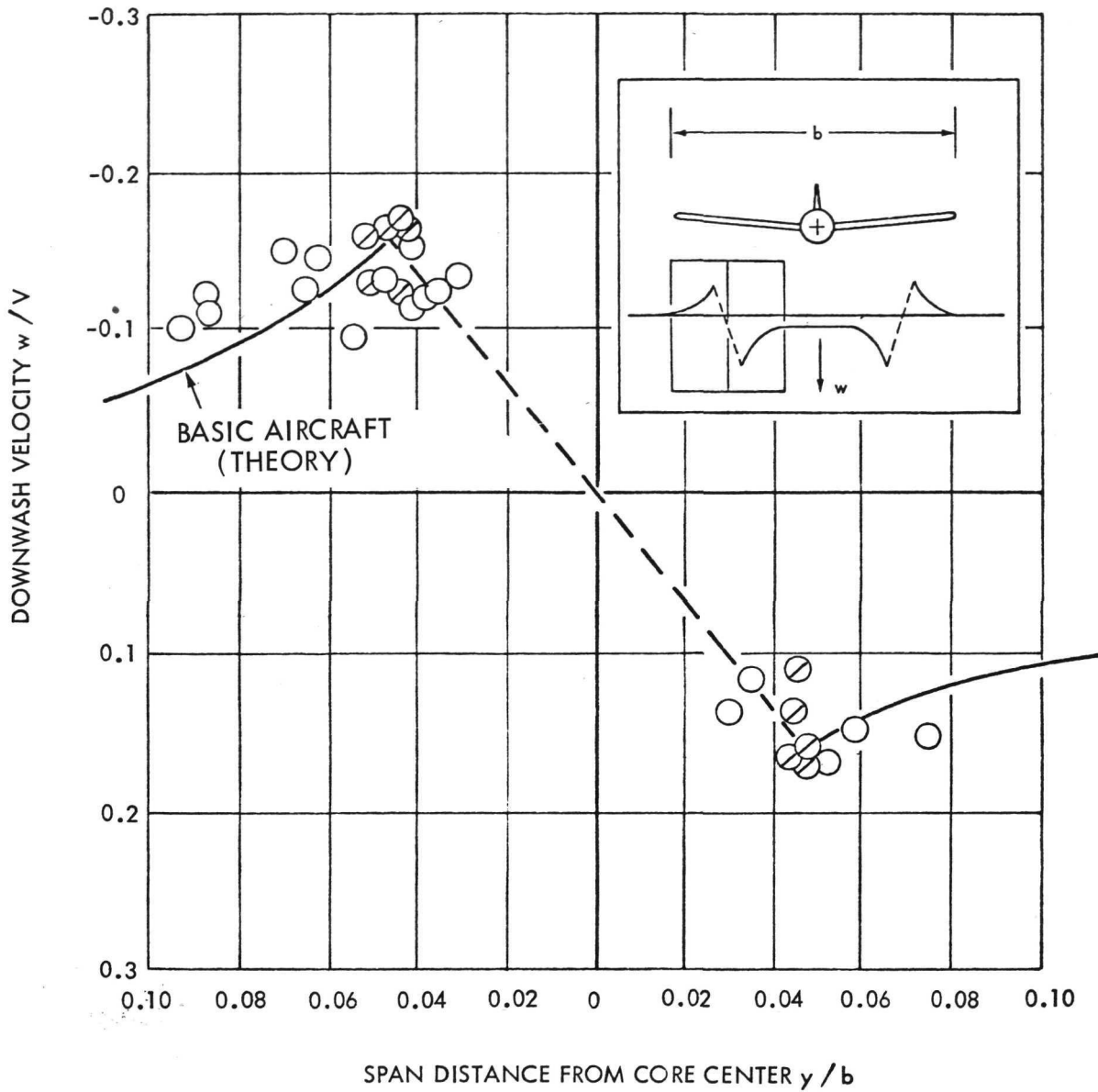


FIGURE 48 - EFFECT OF DEVICE J (SPOILER DISSIPATOR) ON VORTEX VELOCITY DISTRIBUTION

APPENDIX E

TYPICAL TIME-HISTORY RECORDS OF HOT-FILM
VELOCITY MEASUREMENTS FROM TESTS WITH
VARIOUS VORTEX-ATTENUATION DEVICES

(Figures 49 through 59)

Page intentionally left blank

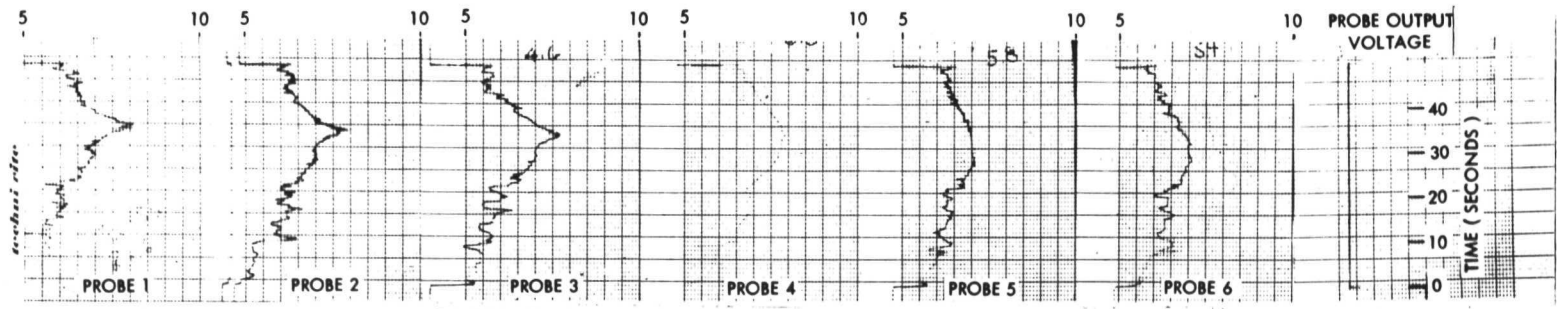


FIGURE 49 - CRUISE CONDITION WITH DEVICE A

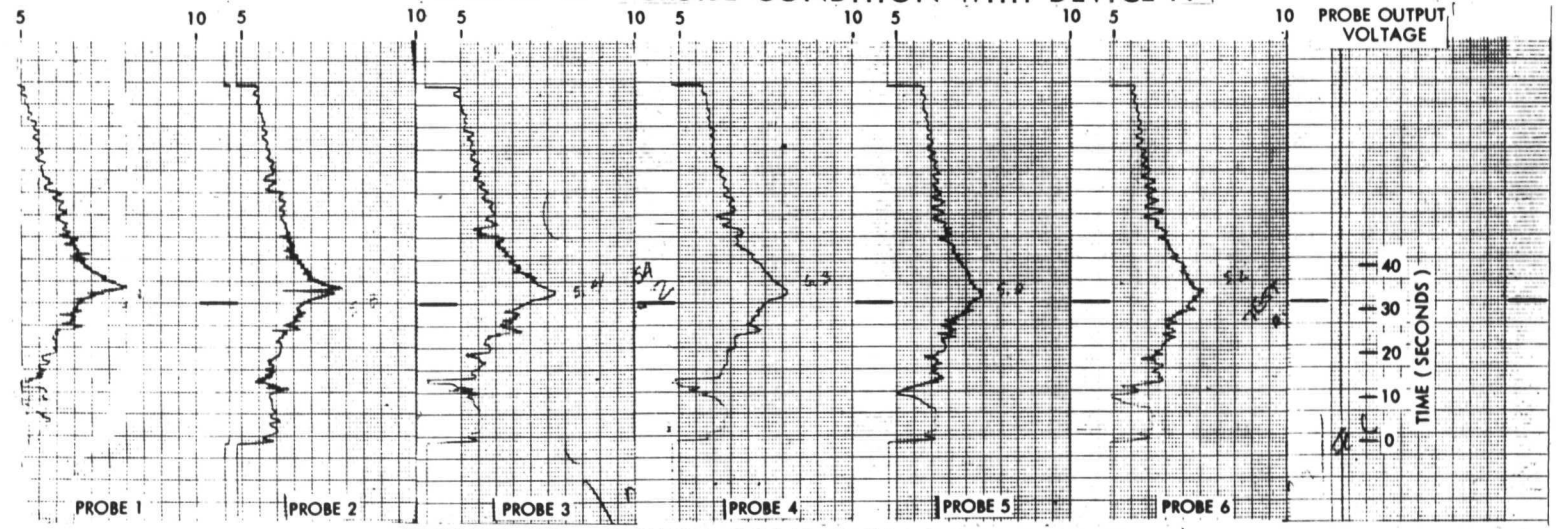


FIGURE 50 - CRUISE CONDITION WITH DEVICE B

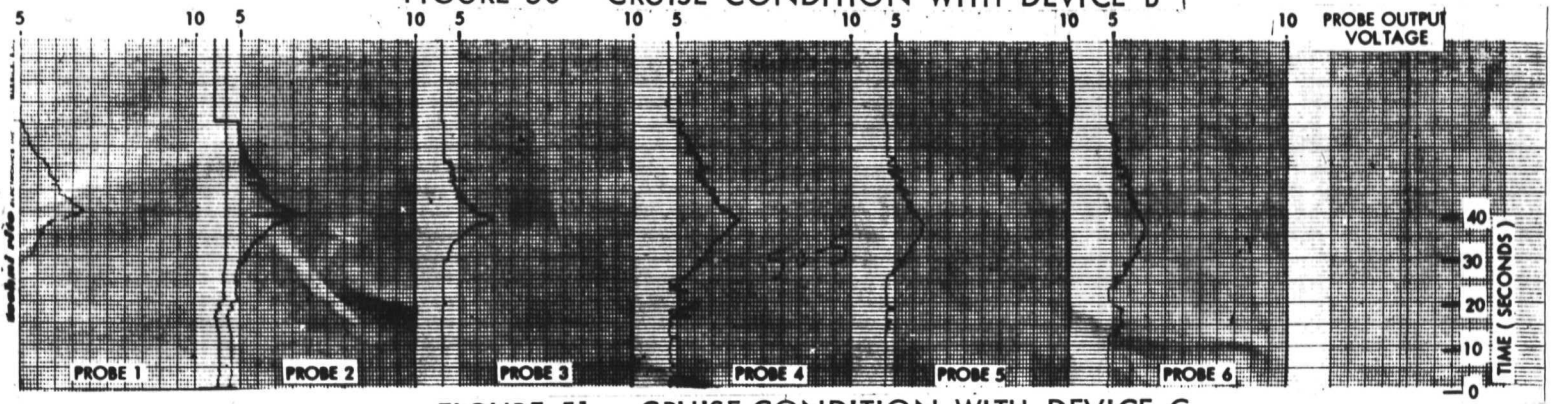


FIGURE 51 - CRUISE CONDITION WITH DEVICE C

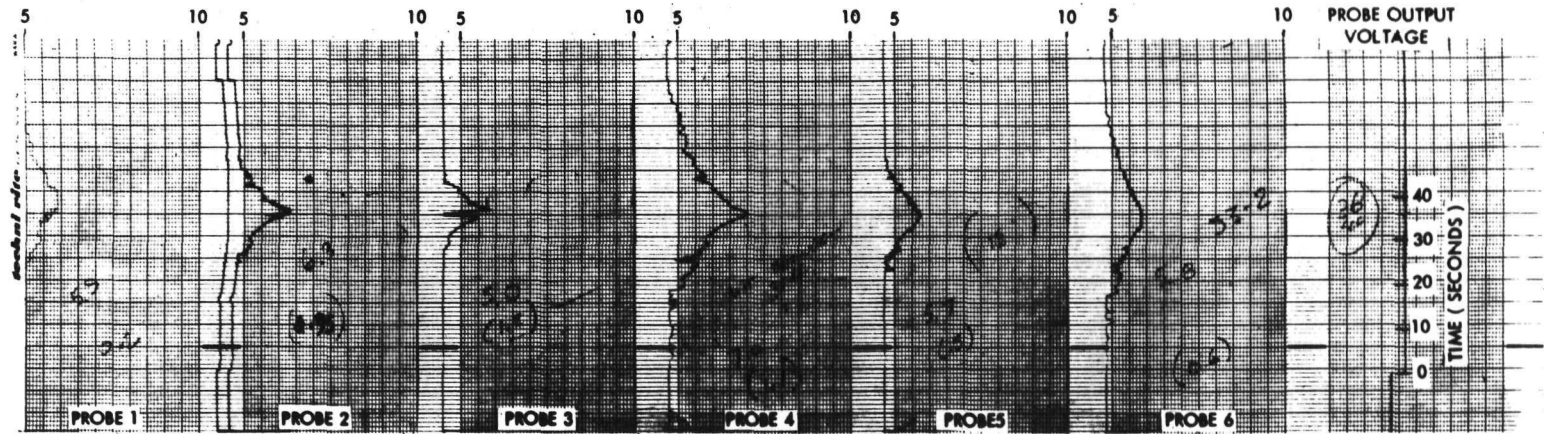


FIGURE 52 - CRUISE CONDITION WITH DEVICE D

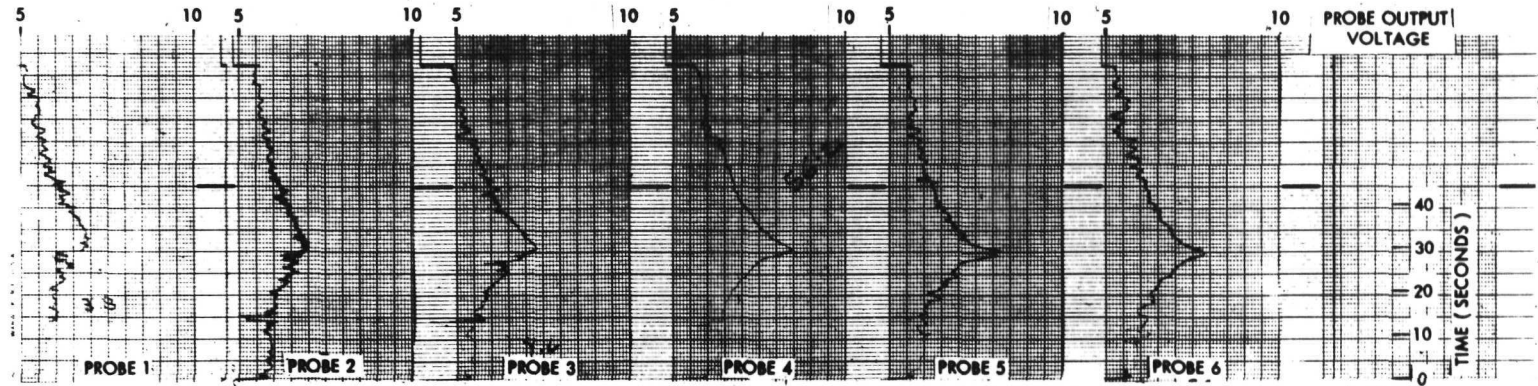


FIGURE 53 - CRUISE CONDITION WITH DEVICE E

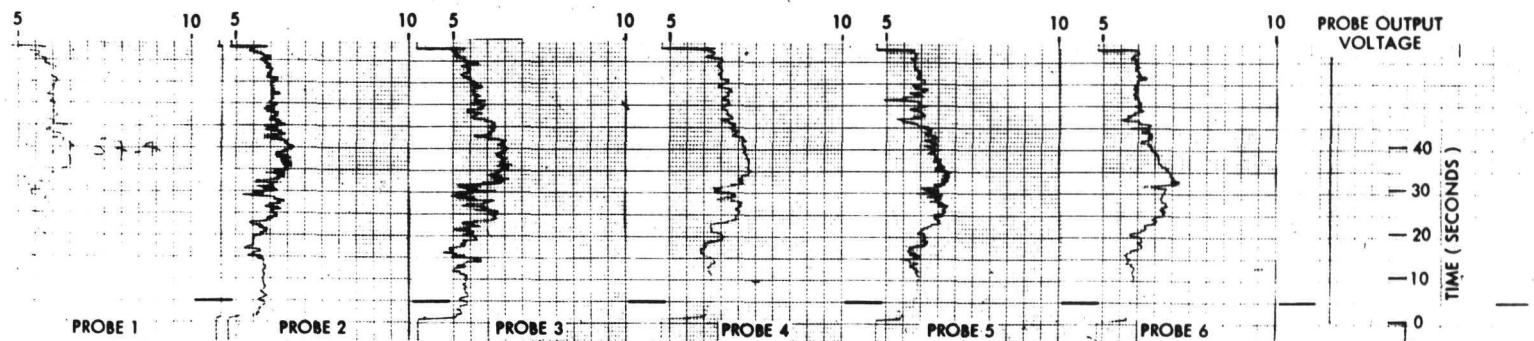


FIGURE 54 - CRUISE CONDITION WITH DEVICE F

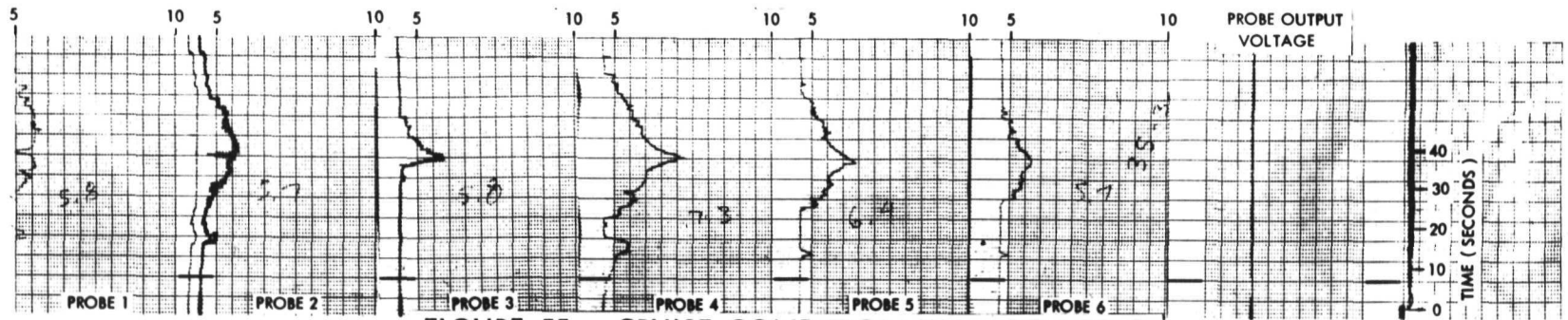


FIGURE 55 - CRUISE CONDITION WITH DEVICE G

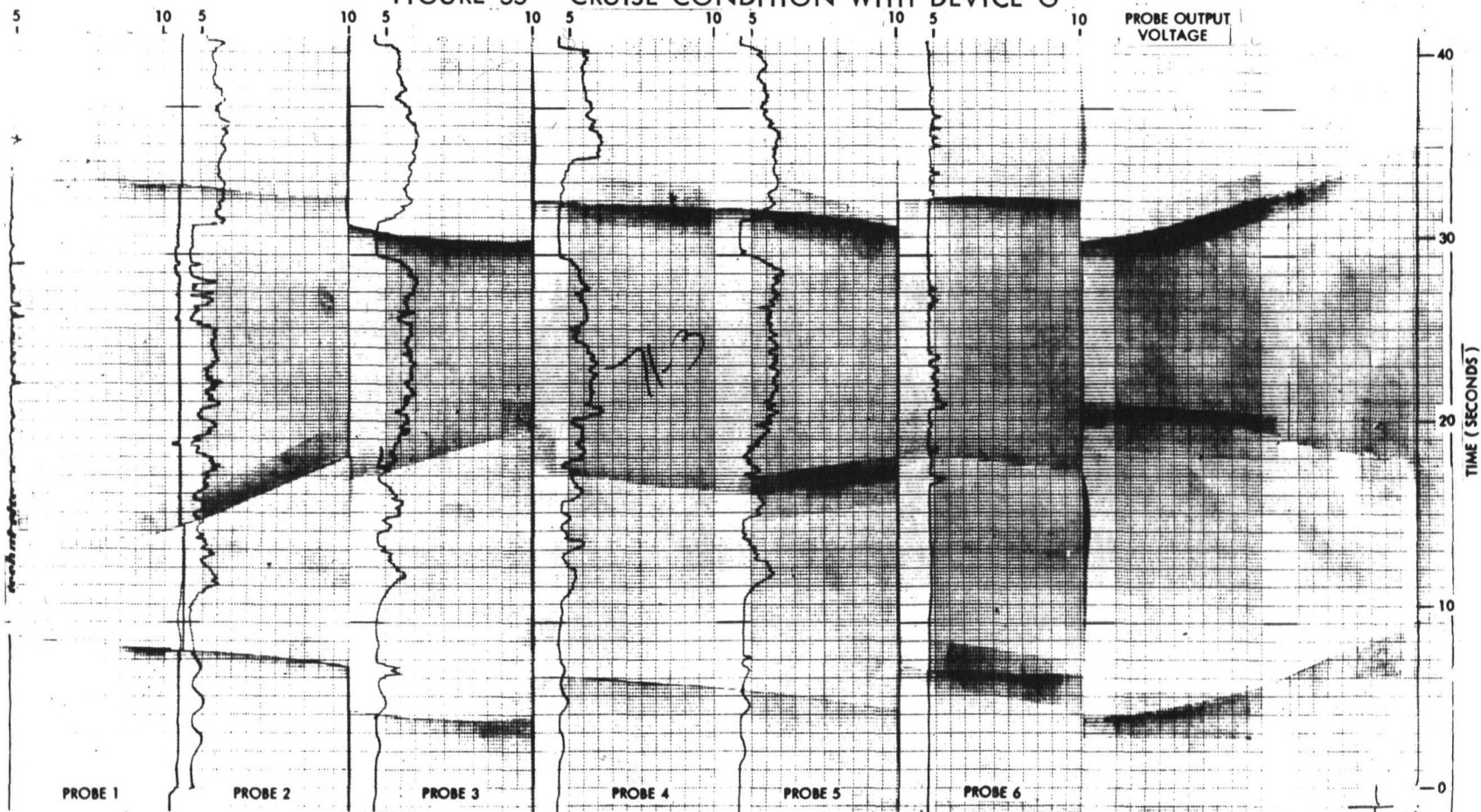


FIGURE 56 - CRUISE CONDITION WITH DEVICE H

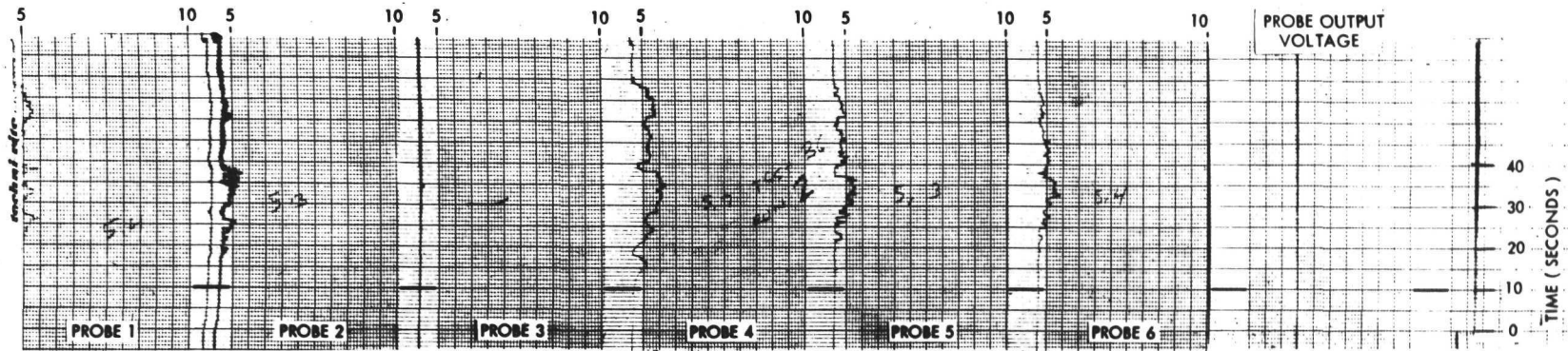


FIGURE 57 - CRUISE CONDITION WITH DEVICE I

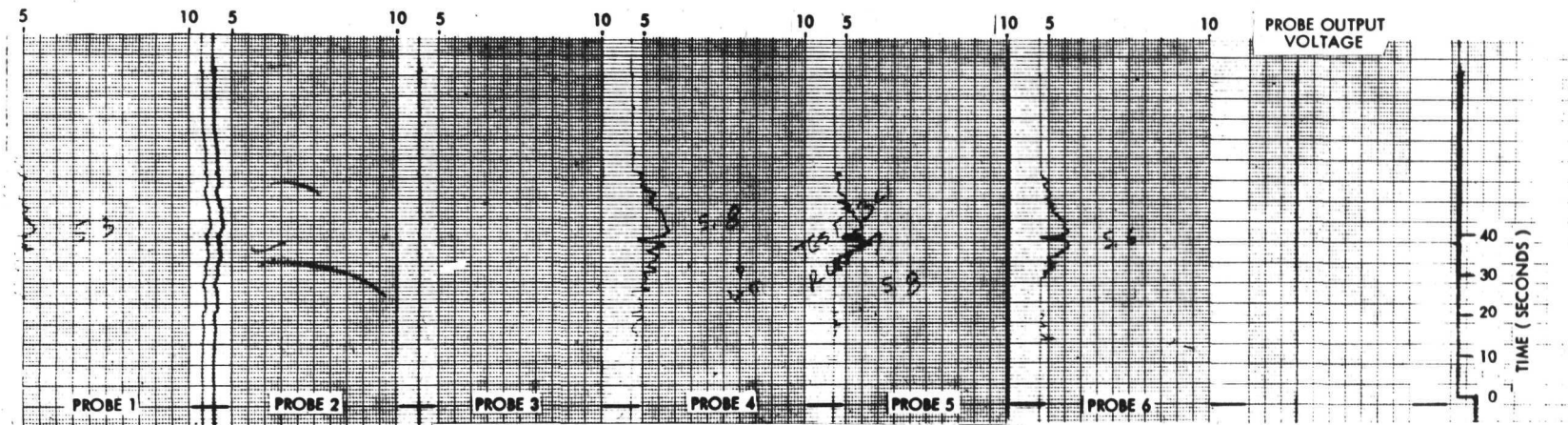


FIGURE 58 - CRUISE CONDITION WITH DEVICE J

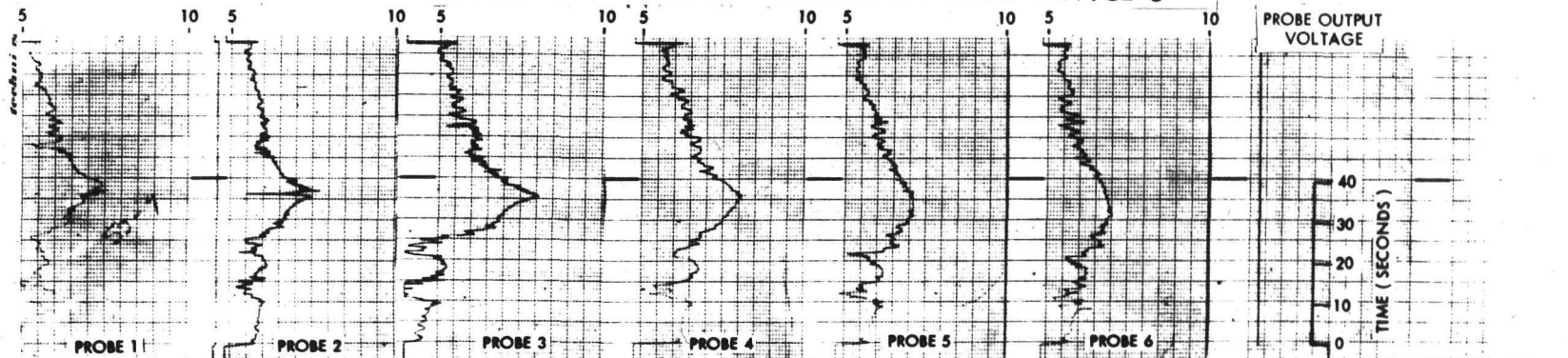


FIGURE 59 - CRUISE CONDITION WITH DEVICE K

APPENDIX F

CALCULATED ROLLING MOMENTS AND ROLLING
VELOCITIES INDUCED ON A SMALL FOLLOWING
AIRCRAFT BY ALTERED TRAILING VORTICES

(Figures 60 through 62)

Page Intentionally Left Blank

As mentioned in the Introduction, the ultimate objective of installing vortex-attenuation devices on wings of large aircraft is to minimize those effects of the vortex wakes which can be hazardous to small following aircraft at significant distances downstream. Accordingly, the most meaningful means for evaluating the effectiveness of such devices from this standpoint would be on basis of force and moment measurements made on the following aircraft itself when it moves through the various altered vortex velocity fields. The purpose of this appendix, therefore, is to calculate some of the effects of the generated vortex wake on the following aircraft. This is accomplished through the use of existing theory in conjunction with the vortex velocity distributions experimentally determined in the subject investigation. The calculation method is first outlined and then the results of calculations are given on the effects of the vortex wakes of the Boeing 747, both without and with selected vortex-attenuation devices, on the span-load distribution, rolling moment, and rolling velocity of a small following aircraft represented by a Gates Learjet.

Outline of Method

The modified lifting-surface method used herein to calculate the contribution of the vortex wake to the span-load distribution and rolling moment of a following aircraft is similar to that developed by Weissinger, Falkner, Campbell, and Zlotnik (Refs. 13, 20, 21 and 22).

In the present method, the following-aircraft wing is represented by a finite number of horseshoe vortices which are distributed spanwise along the quarter-chord line as shown in Figure 60. The downwash induced at the center of each horseshoe vortex along the three-quarter-chord line (control point) is equated to the component of the free-stream velocity normal to the wing chord at each control point. Satisfying this boundary condition at each control point means that there is no flow through the wing. Also, calculating the downwash along the three-quarter-chord line instead of the quarter-chord line (as in the case of lifting-line theory) produces results which are in excellent agreement with experimental data. Application of these conditions results in a set of simultaneous equations which relates the strength of each horseshoe vortex to the angle of attack at each control point located along the three-quarter-chord line. Solution of this set of simultaneous equations provides the span-load distribution, lift-curve slope, lateral center of pressure and rolling moment (if loading is asymmetrical) induced on the wing of the following aircraft.

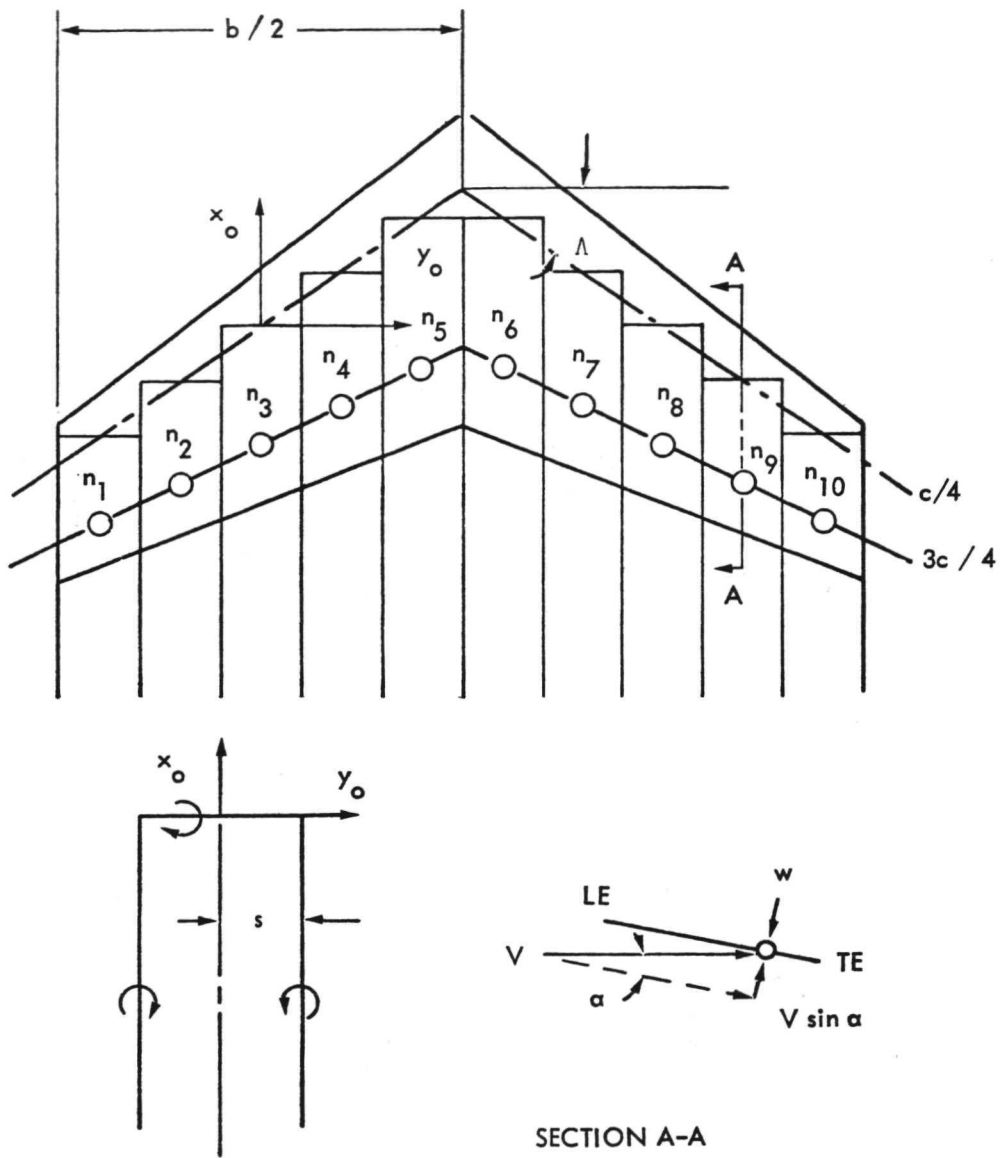


FIGURE 60 - VORTEX PATTERN, SYSTEM OF AXES, AND SUBSCRIPTS USED IN CALCULATION OF SPAN LOADINGS BY MODIFIED-LIFT-SURFACE METHOD

The downwash velocity at any point in the plane of the horse-shoe vortex can be expressed as

$$w(X, Y) = \frac{\Gamma_n}{4\pi s} F(X, Y) \quad [2]$$

From the Biot-Savart law, expressed in Reference 23 (Chapter XII), $F(X, Y)$ is the sum of terms having the form:

$$\begin{aligned} F(X, Y) = & -\frac{1}{X} \left[\frac{(Y+1)}{\sqrt{X^2 + (Y+1)^2}} - \frac{(Y-1)}{\sqrt{X^2 + (Y-1)^2}} \right] \\ & - \frac{1}{(Y-1)} \left[1 - \frac{X}{\sqrt{X^2 + (Y-1)^2}} \right] \\ & + \frac{1}{(Y+1)} \left[1 - \frac{X}{\sqrt{X^2 + (Y+1)^2}} \right] \end{aligned} \quad [3]$$

and the distances X and Y are nondimensionalized by the horseshoe semispan, s . Solutions to Equation [3] for various values of X and Y are given in Reference 24. As shown in Figure 60, ten horse-shoe vortices are used for the present cases. Based on the foregoing, this would imply a set of ten simultaneous equations. However, if the span-load distribution is symmetrical only five simultaneous equations are required.

As shown by Equation [2], the induced velocity is proportional to the circulation, which is related to the lift of the wing by

$$L = C_{L^{\frac{1}{2}}} \rho V^2 S = \rho V \sum_{n=1}^{N/2} 2s\Gamma_n \quad [4]$$

or rearranging terms

$$C_L = 4A(s/b) \sum_n^{N/2} \frac{2\Gamma_n}{bV} \quad [5]$$

If the results of Reference 24 are used in obtaining the values of Γ_n , then Equation [5] becomes (see Equation [2])

$$C_L = 32\pi A(s/b)^2 \sum_{n=1}^{N/2} \frac{2\Gamma_n}{bV} \quad [6]$$

Differentiating Equation [6] with respect to α results in

$$C_{L\alpha} = 32\pi A(s/b)^2 \sum_{n=1}^{N/2} \frac{2\Gamma_n}{bV\alpha} \quad [7]$$

It should be noted that a section lift-curve slope of 2π is assumed in the derivation of Equation [5]. However, the effects of airfoil thickness on the section-lift curve slope can be accounted for by using measured section-lift curve slope data from Reference 25.

In the case of an asymmetrical load distribution, the total rolling moment coefficient can be expressed as

$$C_l = \frac{\text{Rolling Moment}}{qSb} = \frac{l_n}{qS} \frac{y_n}{b} \quad [8]$$

$$= 32\pi A(s/b)^2 \sum_{n=1}^{N/2} \frac{2\Gamma_n}{bV} \frac{y_n}{b} \quad [9]$$

where

l_n is the section lift due to the horseshoe vortex n and y_n is the spanwise distance from the moment reference point to the center of the horseshoe vortex.

It is of interest to determine the maximum rolling-angular velocity that can be overcome by the following aircraft with full-aileron deflection. The steady rolling-angular velocity can be related to the induced rolling moment coefficient in the following manner:

$$C_{l\delta a} = C_{l_p} \frac{pb}{2V} \quad [10]$$

Calculations for Typical Following Aircraft

The principal geometric characteristics of the Gates Learjet (24D) used herein to represent the small following aircraft are given in Table 7. The measured downwash velocity distributions associated with the generating aircraft (Boeing 747 Cruise and Flaps-30 Conditions) are summarized in Figure 34 for the cases of the basic aircraft and for the aircraft equipped with selected vortex-attenuation devices. To accentuate the problem of roll control, the Gates Learjet was assumed for the present calculations to be flying directly along the centerline of one of the tip vortices shed from the Boeing 747 aircraft. The orientation of the wing of the Gates Learjet with respect to the vortex core is shown by the sketch in Figure 61.

The values of w/V presented in Figure 61 were used in the calculations to satisfy the boundary conditions at the selected spanwise control points. Ten horseshoe vortices were used for this calculation. However, because of symmetry, only five simultaneous equations were established. The basic downwash matrix established by this method for the Gates Learjet was checked for the case of uniform velocity ($w/V\alpha = 1.0$). The lift curve slope calculated for this condition using Equation [7] results in a value of $C_{L\alpha} = 0.072$ per degree. This agrees quite well with results presented in Reference 13 for the Gates Learjet wing having the geometric characteristics given in Table 7.

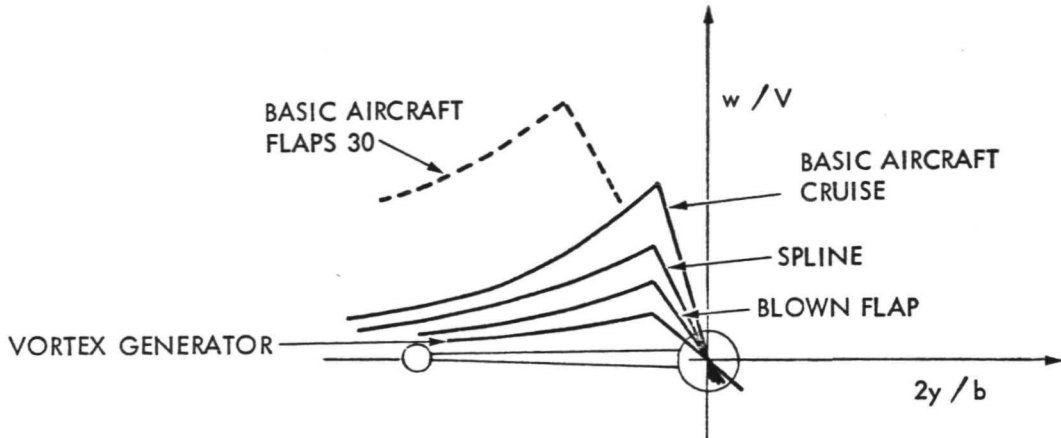
The calculated induced span-load distributions using each of the downwash velocity distributions of Figure 61 are presented in Figure 62. The induced-rolling moment coefficient determined from these span-load distributions using Equation [9] are summarized in Table 8 along with the corresponding rolling-angular velocities obtained using Equation [10].

TABLE 7

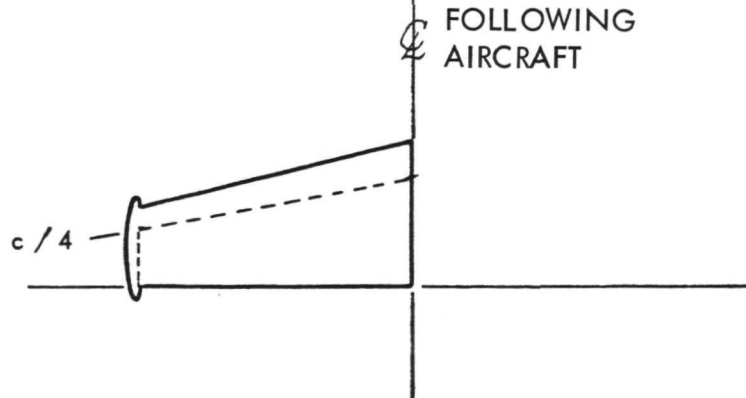
Principal Geometric Characteristics of
Gates Learjet Used in Calculations to
Represent Small Following Aircraft

Wing	
Span (over tip-tanks), m	10.84
Mean aerodynamic chord, m	1.98
Root chord, m	2.74
Tip chord, m	1.39
Area, m ²	21.53
Aspect ratio	5.03
Fuselage	
Length, m	12.49
Tailplane	
Span, m	4.47
Area, m ²	5.01
Aspect ratio	3.98
<p>Note: For other physical characteristics see "Janes All the World's Aircraft 1971-72", pp. 307-308.</p>	

----- FLAPS 30 - 2.25 KILOMETERS DOWNSTREAM
 _____ CRUISE - 4.42 KILOMETERS DOWNSTREAM



(a) DOWNWASH VELOCITY DISTRIBUTION BEHIND GENERATING AIRCRAFT



(b) ORIENTATION OF GATES LEARJET WING WITH RESPECT TO VORTEX CORE

FIGURE 61 - ORIENTATION OF GATES LEARJET WING AND DISTRIBUTION OF DOWNWASH VELOCITIES USED IN CALCULATION

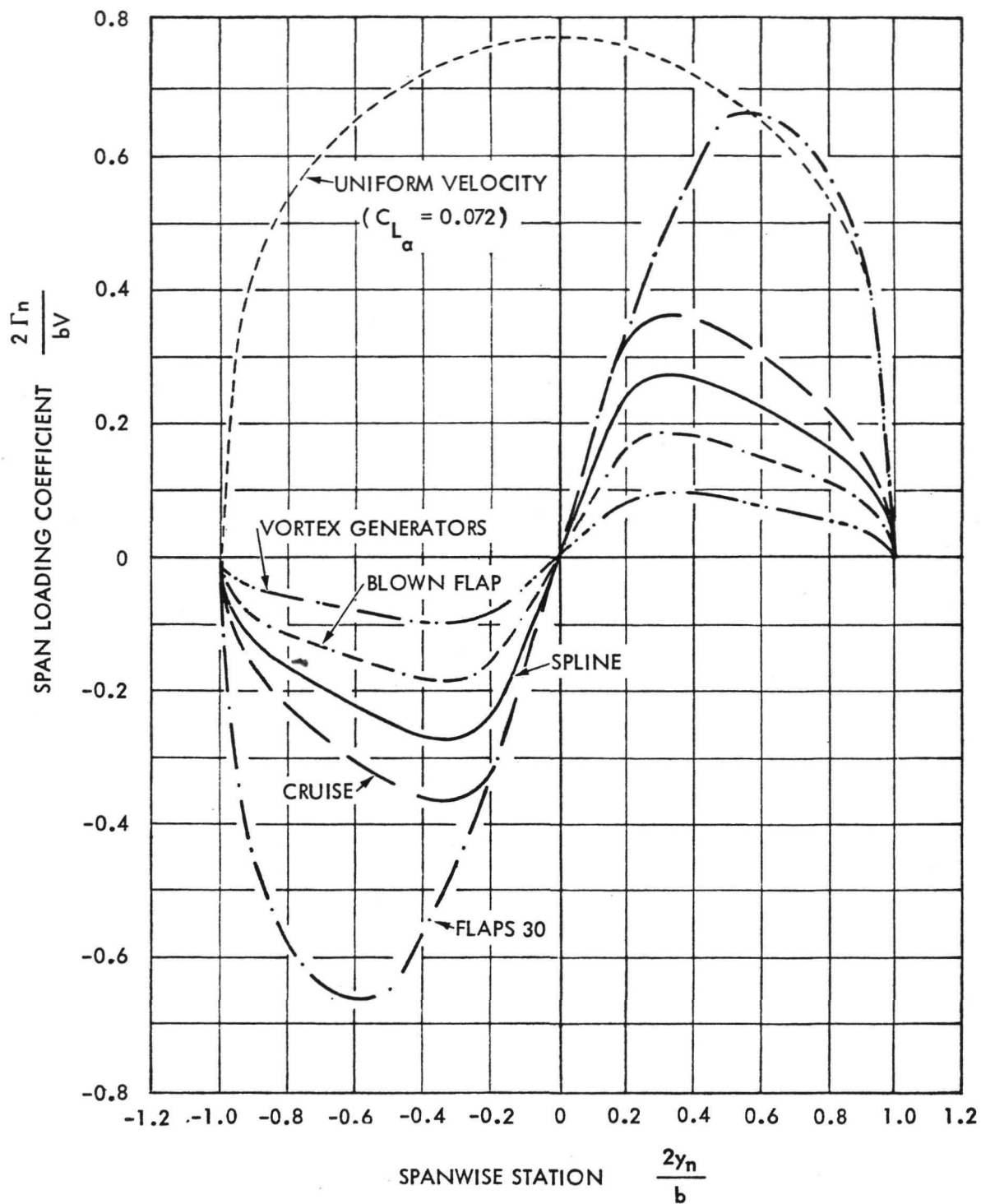


FIGURE 62 - EFFECTS OF VARIOUS DEVICES ON THE CALCULATED INDUCED SPAN LOADING COEFFICIENT FOR THE GATES LEARJET WING

TABLE 8

Calculated Effects of Vortex Wakes of Generating Aircraft on Induced Rolling Moment and Rolling Velocity of Small Following Aircraft

Generating Aircraft (Boeing 747)	Following Aircraft (Gates Learjet)	
Configuration	Induced Rolling Moment Coefficient, C_l	Induced Rolling Velocity, p degrees/second
Cruise-Basic	0.402	1042
Cruise-Vortex Generators (Device I)	0.103	268
Cruise Blown Flap (Device F)	0.202	530
Cruise Spline (Device H-1)	0.304	800
Flaps 30 - Basic	0.845	2200
<p>Note: Maximum rolling-angular velocity corresponding to full aileron deflection on Gates Learjet is 120 degrees per second at an aircraft speed of 120 knots. This corresponds to a rolling moment coefficient $C_l = 0.0463$.</p>		

It may be seen from Table 8 that the rolling moment coefficients and rolling velocities induced on the Gates Learjet are excessively large when operating at the specified location with respect to the vortex wakes generated by the basic Boeing 747 aircraft in both the Cruise and Flaps-30 Conditions. Reductions in these quantities amounting to factors of 4 and 2 are achieved for the Cruise Condition with the Vortex Generators (Device I) and Spline (Device H-1), respectively. However, for the cases investigated, involving distances of up to 4.42 kilometers downstream of the generating aircraft, these reductions may not be adequate when viewed in terms of the aileron control available to the following aircraft. It has been assumed that the maximum rolling-angular velocity corresponding to full aileron deflection for the Gates Learjet is 120 degrees per second at an aircraft speed of 120 knots. For this condition, since $C_{\ell p} = -0.38$ (Ref. 26), the corresponding value for C_{ℓ} obtained from Equation [10] is 0.0463 which is less than half the value shown for Device I in Table 8. Thus it appears that the aileron effectiveness of the Gates Learjet is insufficient to cope with the vortex wake at 2.25 to 4.42 kilometers downstream generated by the Boeing 747 aircraft, particularly in both the basic Cruise and Flaps-30 modes.

The foregoing calculations were performed for the case of the Gates Learjet aligned with the center of the vortex core which should present the worst case from the standpoint of induced rolling moment. It should be noted, however, that the calculation method is equally applicable for any orientation of the following aircraft with respect to the core of the shed vortex. It is conceivable that there are orientations in which direct losses in lift as well as rolling moment induced on the following aircraft can be a serious problem.

REFERENCES

1. Donaldson, Coleman du P., and Sullivan, R. D., "Decay of an Isolated Vortex", Aircraft Wake Turbulence and Its Detection, Plenum Press, New York, 1971, pp. 389-11.
2. Brown, Clinton E., "On the Aerodynamics of Wake Vortices", HYDRONAUTICS, Incorporated Technical Report 7115-1, October 1972.
3. "Vortex Wake Turbulence - Flight Tests Conducted During 1970", Federal Aviation Administration Report FAA-FS-71-1, February 1971.
4. Garodz, Leo J., "Investigation of the Relatively Long Time-History Vortex Characteristics of the Convair CV-880 Airplane in Terminal Area Type Flight Operations (Flight-Test Period July-August 1970)", Federal Aviation Administration Data Report, Project No. 504-303-03X (Special Task No. Three), November 1970.
5. McGowan, William A., "NASA Aircraft Trailing Vortex Research," Presented at the Federal Aviation Administration Symposium on Turbulence, Washington, D. C., 22-24 March 1971.
6. "Aircraft Wake Turbulence and Its Detection", Proceedings of a Symposium on Aircraft Wake Turbulence Held in Seattle, Washington, 1-3 September 1970, Edited by Olsen, John H., Goldberg, Arnold, and Rogers, Milton, 1971.
7. Corsiglia, V. R., Jacobsen, R. A., and Chigier, N., "An Experimental Investigation of Trailing Vortices Behind a Wing with a Vortex Dissipator," Proceedings of Symposium on Aircraft Wake Turbulence, Seattle, Washington, 1971.
8. Rinehart, S. A., Balcerak, J. C., and White, R. P. Jr., "An Experimental Study of Tip Vortex Modification by Mass Flow Injection," Rochester Applied Science Associates Report No. 71-01, 140 Allens Creek Road, Rochester, New York, 146-8, January 1971.
9. Yuan, S. W. and Pisetsky, Y. "Experimental Investigation of Wing Tip Vortices Elimination," 3rd Canadian Congress of Applied Mechanics, Montreal, 17-24 May 1971.
10. Scheiman, J. and Shivers, J. P., "Exploratory Investigation of the Tip Vortex of a Semispan Wing for Several Tip Modifications", NASA TN D-6101, February 1971.

11. Miller, E. R., Jr. and Brown, C. E., "An Experimental Study of Trailing Vortex Wakes Using a Large Towing Tank", HYDRONAUTICS, Incorporated Technical Report 7105-1, August 1971.
12. Betz, A., "Behavior of Vortex Systems," NACA TM 713, June 1933.
13. De Young, John and Harper, Charles W., "Theoretical Symmetric Span Loading at Subsonic Speeds for Wings Having Arbitrary Plan Form," NACA Rep. 921, 1948.
14. Chigier, N. A. and Corsiglia, V. R., "Tip Vortices - Velocity Distributions", 27th Annual National V/STOL Forum of the American Helicopter Society Preprint No. 522, May 1971.
15. Timm, G. K., "Survey of Experimental Velocity Distributions in Vortex Flows with Bibliography," Boeing Sci. Res. Lab. Document D1-82-0683, Seattle, Washington, November 1967.
16. Wadlin, K. L., Ramsen, J. A. and McGehee, J. R., "Tank Tests at Subcavitation Speeds of an Aspect Ratio - 10 Hydrofoil with a Single Strut," NACA RM L9K14a, 20 July 1950.
17. Schlichting, H., "Boundary Layer Theory," McGraw-Hill, New York, pp. 682, 1968.
18. Goodman, Alex, "Description and Operation of Planar-Motion-Mechanism", HYDRONAUTICS, Incorporated Technical Manual 754-1, April 1968.
19. Goodman, Alex, "Description and Operation of Planar Motion Mechanism Instrumentation System," HYDRONAUTICS, Incorporated Technical Report 818-1, February 1968.
20. Falkner, V. M., "The Solution of Lifting Plane Problems by Vortex Lattice Theory," Rep. No. 10, 895, British A.R.C., September 29, 1947.
21. Campbell, George, S., "A Finite-Step Method for the Calculation of Span Loadings of Unusual Plan Forms," NACA RML50L13, July 16, 1951.
22. Zlotnik, M. and Robinson, S. W., Jr., "A Simplified Mathematical Model for Calculating Aerodynamic Loading and Downwash for Wing-Fuselage Combinations with Wings of Arbitrary Plan Form," NACA Technical Note 3057, January 1954.

23. Glauert, H., "The Elements of Aerofoil and Airscrew Theory," Second Edition, Cambridge University Press, 1948.
24. Staff of the Mathematics Division: "Tables of Complete Downwash Due to a Rectangular Vortex," Reports and Memoranda No. 2461, July 21, 1947.
25. Abbott, Ira H., Von Doenhoff, Albert E., and Stevens, Louis, S., Jr., "Summary of Airfoil Data," NACA Rep. 824, 1945.
26. Goodman, Alex and Adair, Glenn H., "Estimation of the Damping in Roll of Wings Through the Normal Flight Range of Lift Coefficient," NACA Technical Note 1924, July 1949.